The Dissertation Committee for Daniel Hayes Fine Certifies that this is the approved version of the following dissertation:

Approaches and Evaluation of Architectures for Chemical and Biological Sensing Based on Organic Thin-Film Field-Effect Transistors and Immobilized Ion Channels Integrated with Silicon Solid-State Devices

Committee:

Ananth Dodabalapur, Supervisor

Sanjay K. Banerjee

Jack C. Lee

Yueh Lin Loo

Wolfgang Frey

Approaches and Evaluation of Architectures for Chemical and Biological Sensing Based on Organic Thin-Film Field-Effect Transistors and Immobilized Ion Channels Integrated with Silicon Solid-State Devices

by

Daniel Hayes Fine B.S.; M.S.E.

Dissertation

Presented to the Faculty of the Graduate School of

The University of Texas at Austin

in Partial Fulfillment

of the Requirements

for the Degree of

Doctor of Philosophy

The University of Texas at Austin

August, 2007

Dedication

To my parents

Mrs. Molly Michaelis Fine and Dr. Ronald Fine

Acknowledgements

During the course of my graduate work I have had the unique opportunity and privilege to work under and with a myriad of highly competent and knowledgeable individuals whose dedication and significant contributions to their chosen fields of research is only outdone by their caring and compassionate dedication to the students they supervise and the colleges with whom they interact. The work presented here is the result of a tremendous interdisciplinary effort which, in some cases, spans multiple universities, institutes, and continents. I would therefore like to enumerate and thank all the people with whom I have worked and without whom much of the results demonstrated in this thesis would not have been possible.

I would first like to thank my advisor, Professor Ananth Dodabalapur, whose guidance and insight has been indispensable. It is through his patience and leadership I have been able to overcome the obstacles which have arisen during the pursuit of my doctorate. I would also like to thank some of the other principle investigators working on the ion channel project, Professor Randolph Duran at the University of Florida and Professor Dr. Wolfgang Knoll at the Max Planck Institute. Their collaboration has opened up new doors and avenues to explore which I did not anticipate upon commencing my Ph.D. Their incredible understanding of their chosen fields in addition

to their abilities to communicate their ideas to others has allowed me to learn about and branch into other areas of science and engineering which will benefit me my entire life.

Next, I would like to thank Professor Sanjay K. Banerjee, Professor Jack C. Lee, Professor Yueh Lin Loo, and Professor Wolfgang Frey for serving on my dissertation committee.

I would also like to thank my coworkers at the University of Texas, Tae-Ho Jung, Debarshi Basu, Deepak Sharma, Suvid Nadkarni, Byungwook Yoo, Yeon Taek Jeong, Chris Lombardo and Lawrence Dunn for lending assistance and support whenever and wherever necessary, as well as the individuals I have worked with at the University of Florida and the Max Planck Institute, Dr. Henk Keiser, Dr. Ingo Köpper, Inga Vockenroth, and Brian Dorvel, for helping to make this cooperative effort very enlightening, enjoyable, and fulfilling. I would further like to thank Professor Dr. Heinz von Seggern whose visit to our laboratory in the formative years of my graduate work was very instructive and educational.

Finally, I would like to thank my compatriot and very dearest friend Liang Wang who has helped to provided all the necessities of any good research environment, a sounding board for discussing ideas, an assistant during processing after fatigue has finally taken its toll, a friend to get meals with in the wee hours of the night, a confidence booster when things didn't seem to be going my way, and perhaps most importantly, a little comic relief.

Thank you all.

Approaches and Evaluation of Architectures for Chemical and Biological Sensing Based on Organic Thin-Film Field-Effect Transistors and Immobilized Ion Channels Integrated with Silicon Solid-State Devices

Publication No._____

Daniel Hayes Fine, Ph.D.

The University of Texas at Austin, 2007

Supervisor: Ananth Dodabalapur

There is significant need to improve the sensitivity and selectivity for detecting chemical and biological agents. This need exists in a myriad of human endeavors, from the monitoring of production of consumer products to the detection of infectious agents and cancers. Although many well established methodologies for chemical and biological sensing exist, such as mass spectrometry, gas or liquid phase chromatography, enzyme-linked immunosorbent (ELISA) assays, etc., it is the goal of the work described herein to outline aspects of two specific platforms which can add two very important features, low cost and portability. The platforms discussed in this dissertation are organic semiconductor field-effect transistors (OFETS), in various architectural forms and chemical modifications, and ion channels immobilized in tethered lipid bilayers integrated with solid state devices. They take advantage of several factors to make these added features possible, low cost manufacturing techniques for producing silicon and organic circuits, low physical size requirements for the sensing elements, the capability to

run such circuits on low power, and the ability of these systems to directly transduce a sensing event into an electrical signal, thus making it easier to process, interpret and record a signal. In the most basic OFET functionality, many types of organic semiconductors can be used to produce transistors, each with a slightly different range of sensitivities. When used in concert, they can produce a reversible chemical "fingerprint". These OFETS can also be integrated with silicon transistors - in a hybrid device architecture - to enhance their sensitivity while maintaining their reversibility. The organic semiconductors themselves can be chemically altered with the use of small molecule receptors designed for specific chemicals or chemical functional groups to greatly enhance the interaction of these molecules with the transistor. This increases both sensitivity and selectivity for discrete devices. Specially designed nanoscale OFET configurations with individually addressable gates can enhance the sensitivity of OFETS as well. Finally, ion channels can be selected for immobilization in tethered lipid bilayer sensors which are already inherently sensitive to the analyte of choice or can be genetically modified to include receptors for many kinds of chemical or biological agents.

Table of Contents

CHAPTER 1 INTRODUCTION

There is significant need for fast, reliable, highly sensitive and highly selective methodologies for detecting a plethora of chemical and biological species that greatly affect the quality of human life, both positively and negatively. From monitoring fermentation during the production of alcoholic beverages [1] to looking for landmines [2] to the early detection of Alzheimer's [3], this need mandates continual improvements and adjustments to the techniques and platforms for low-cost, real-time, portable (on-site), and specific detection of these important chemical and biological agents. Many current technologies for meeting some of these requirements are quite powerful. These include such techniques as mass spectrometry [4], the various types of spectroscopy (infrared, fluorescent, Raman, etc.) [5], liquid or gas phase chromatography [6], enzyme-linked immunosorbent assays (ELISA) [7], etc. It is clear, however, that they presently do not meet all of the aforementioned requirements discussed herein, specifically portability, continuity (continuous sampling), and low cost. In addition, the apparatus needed to utilize these techniques are usually expensive. Thus, the focus of this dissertation is to investigate two such platforms, organic semiconductor field-effect transistors (OFETS), in various architectural forms and chemical modifications, and ion channels immobilized in tethered lipid bilayers. In the case of the immobilized ion channel platforms, an evaluation of promising solid-state devices will be conducted to ascertain which seems the most promising for amplifying the picoampere level currents generated by single ion channels.

There are many reasons for developing highly selective and sensitive artificial chemical and biological detection techniques. Less than 1 μg of anthrax constitutes a fatal dose [8]. Prostate specific antigen, a marker for prostate cancer, is considered

suspiciously elevated when its blood level reaches 2.6 ng/mL [9]. Growing amounts of data on endocrine disruptors, molecules which are similar to and/or mimic the actions of hormones (the chemical messengers of the human endocrine system) [10], have shown that these chemicals can cause significant problems at levels of nanograms per liter [1]. Finally, recent work has shown that it may be possible to enhance early detection of Alzheimer's disease by looking for certain marker proteins in femtomolar concentrations in spinal fluid [3]

1.1 SENSING SYSTEMS IN NATURE

The ability to monitor both its internal and external chemical environments is essential for the survival of all living organism. Highly evolved systems for detecting and distinguishing billions of chemical species, from airborne odorants which give clues to the whereabouts of food, the possibility of nearby predators or social group members, the pathways of migration [11], to invasive viruses and bacteria and their byproducts [12], have been shown to have some of the most efficient, selective, and sensitive chemical detection capabilities known to man. Emulating these biological systems artificially, such as attempting to create an "electronic nose" [13], or isolating and utilizing their components, such as performing assays using immune system protein markers called antibodies to label dangerous foreign invaders called antigens [7], or at least matching their performance, has been and will continue to be an ongoing and sustained area of research for many years to come [1, 14, 15].

The mammalian olfactory system has evolved many distinct features for chemical vapor detection which make it extremely powerful and very hard to duplicate using conventional sensor technology. First, although the individual receptor neurons respond

to a limited range of odorants or classes of odorants, when working as a whole these systems have the ability to distinguish among millions of odors subsequently generating a unique pattern of neuron receptor responses which can be interpreted by the brain [11]. This broad ensemble activity allows for a high degree of sensitivity and selectivity for a myriad of olfactory stimuli which can then be rapidly recorded, processed, and stored directly into memory. The dog, which possesses one of the best examples of a well developed olfactory system, has 220 million receptors with which to detect odors as compared to about 50 million for humans [16].

A second very important aspect of the olfactory system is its ability to process new stimuli quickly. Olfactory systems allows for direct neuronal stimulation of several parts of the brain, such as the area which deals with memory [11]. This means that in addition to allowing higher intelligence areas of the brain to analyze the new odor signature, the stimuli can be instantly recorded in memory and can stimulate certain physical and emotional responses [11]. Some mammals, such as the dog, have a much larger portion of their brains devoted to olfactory signal processing than do humans [17] due to the increased evolutionary importance of scent for finding food, and detecting predators, which requires in many instances more quickly directed responses to olfactory stimuli [11]. In terms of the brain, this requires a more interconnected olfactory system [11]. Figure 1 shows a pattern of responses of individual receptor cells in a frog's olfactory epithelium (the olfactory membrane which provides a substrate for the receptor cells) to various analytes as an example of this pattern recognition [18].

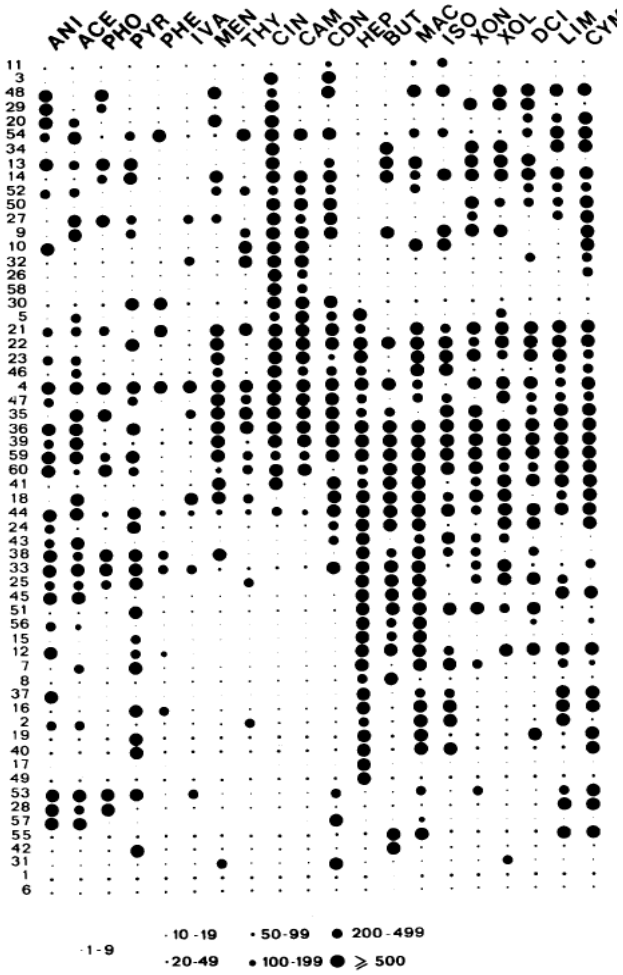

Figure 1. Diagram representing receptor cell activity in a frog olfactory epithelium during stimulation with a variety of analytes. The spot size is roughly proportional to the spike frequency (response intensity). The numbers on the left represent the individual receptors tested. Reprinted from *Brain Researc*h, vol. 292, G. Sicard, and A. Holley, "Receptor cell responses to odorants: Similarities and differences among odorants." pp. 283-296, 1984, with permission from Elsevier [18]

The serial numbers on the left represent the individual receptor cells measured. The analytes are listed on the top and include anisole (ANI), acetophenone (ACE), thiophenol (PHO), pyridine (PYR), phenol (PHE), isovaleric acid (IVA), L-menthol (MEN), thymol (THY), 1,8-cineole (CIN), (±)-camphor (CAM), cyclodecanone (CDN), *n*-heptanol (HEP), *n*-butanol (BUT). Methyl amylketone (MAC), isoamyl acetate (ISO),

cyclohexanone (XON), cyclohexanol (XOL), (+)-citronellol (DCI), (+)-limonene (LIM), and *p*-cymene (CYM). The spot size is roughly proportional to the spike frequency (intensity of response) [18].

A third very attractive feature of the olfaction system is its ability to renew itself. The olfactory neuron is the only type of neuron that can regenerate [11]. This means that individual receptors can rapidly be replaced if damaged or otherwise not properly functioning [11].

Finally, mammalian olfactory perception can follow small odor gradients to their source and can pick up scents which are many hours to days old [19, 20] (some mammals, such as dogs, are better at following gradients than others). These gradients can be caused either by convection, such as scents blown by the wind, or by diffusion, which creates a concentration gradient over time such as the odors left by an escaping convict which can yield directional information [19, 20]. The ability to sniff, or sample the air in defined bursts, is one of the primary ways that animals can achieve this ability [19].

It is these traits which make the mammalian olfactory system so adept at detecting odors. It has been shown that dogs can detect 1 mg of butyric acid (a fatty acid (see figure 2)) in 10^8 m^3 of air, or about .010 parts-per-trillion (ppt) [19].

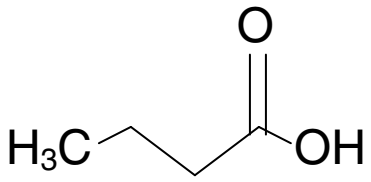

Figure 2. Butyric Acid ($CH_3CH_2CH_2COOH$)

In terms of detecting agents of more immediate interest to humans from a safety standpoint, dogs can detect about 10 ppt of 2,4-dinitrotoluene (DNT), a common explosive [19]. Figure 3 shows the sensitivity of canines for several other explosive chemicals and one drug-related chemical (methyl benzoate) [19].

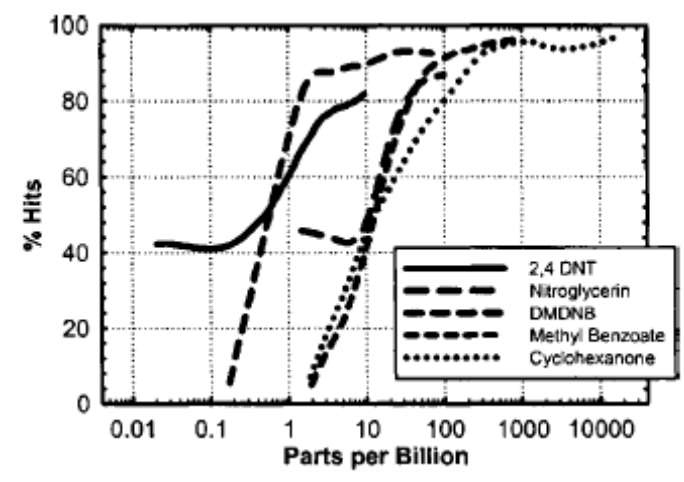

Figure 3. Canine olfaction sensitivity curves. These chemicals are all specific for explosives except methyl benzoate which is a cocaine derivative. "Reprinted with permission from Gary S. Settles, "Sniffers: Fluid-Dynamic Sampling for Olfactory Trace Detection in Nature and Homeland Security – The 2004 Freeman Scholar Lecture." *Journal of Fluids Engineering* vol. 127(2005) pp. 189-218, and the American Society of Mechanical Engineers."

It is for this reason that dogs are still the preferred detection entity used by the military, law enforcement, and border control agents for finding explosives, illicit drugs, and illegally imported animals and produce [16, 19]. Due to their lighter weight, ease of training, faster reproduction, and greater ability to perform highly repetitive tasks, rats are now replacing dogs when it comes to looking for land mines [2]. APOPO, an organization in Africa dedicated to searching for landmines, has demonstrated that rats can detect 0.001 ppt of 2,4,6-trinitrotoluene (TNT) [2]. Dogs have even been used for cancer detection, since there are certain biochemical markers found in the breath of

cancer patients [21]. So far, no man made system has been able to replace these animals in terms of cost effectiveness, ease of use, and world wide applicability.

There are negatives to using animals. Like all mammals, dogs and rats need to sleep, feed, be trained, and reproduce to be effective [19, 22]. They are also living breathing organisms and therefore cannot be exposed to dangerous gasses or aerosols and are at risk when seeking active explosives such as landmines (one reason rats are being used as opposed to dogs to search for landmines is that they are lighter animals and thus won't trigger the mines) [2, 19]. This type of training can be quite resource intensive, since these animals must use nonverbal queues to tell trained personnel where the items in question are located [19]. They cannot be used for 24 hours a day monitoring and may not always cooperative. This limits their ability to be used for continuous real time monitoring [19]. Finally, the biological systems and methodologies animals use to detect various chemical targets are not completely understood and therefore can provide for some degree of uncertainty [23]. It is for these reasons that so much effort over the last 25 years or so has been put into artificial olfactory methodologies [13].

As for biological sensing, the mammalian immune system has evolved a wealth of structures which can be adopted to use in external sensing apparatus. One such structure is a specialized protein, called an antibody (shown in figure 4), which identifies and tags biologically significant chemical or biological intruders, called antigens, with a high degree of specificity [1, 7].

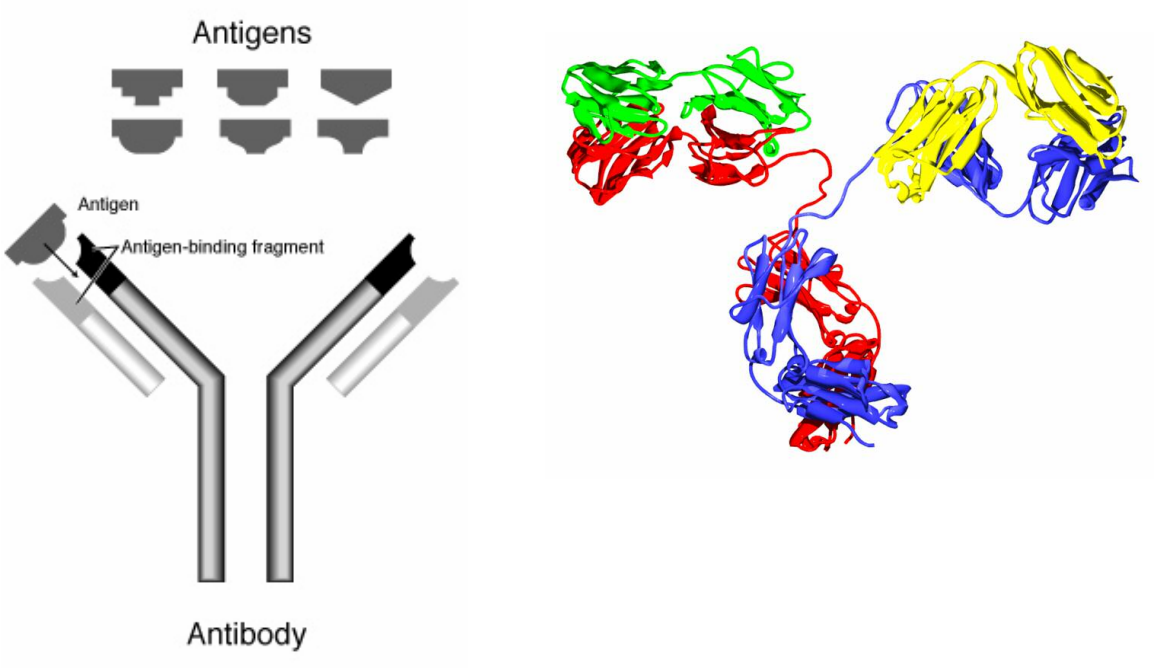

Figure 4. Schematic representation of an antibody (left) [24] and the corresponding molecular model (right) [25]

Once an antibody is isolated and purified for a target antigen of interest, usually by expression of the antibody in an animal system [7], the extreme high degree of specificity means the only obstacle to developing a test is to then find a scheme for demonstrating a positive binding result using as few antibody molecules as possible. One such technique developed at Northwestern University uses nanoparticles, magnetic microparticles, antibodies, and "barcode DNA" to amplify the effect of a single antibody binding event. This approach allows for detection limits down to 30 attomolar concentrations [26]. A single antibody is attached to a gold nanoparticle along with many strands of DNA. The DNA is then hybridized to their complementary strands referred to as the "DNA barcode." Many antibodies sensitive to other regions, or epitopes, of the antigen are also attached to a magnetic microparticle. After the magnetic miroparticle is exposed to and

binds with the antigen, the same mixture is exposed to the nanoparticle. A magnetic field is used to separate the bound nanoparticles from the unbound ones, since the nanoparticles are bound to the magnetic particles. Then the hybridized barcode DNA is released. This released DNA is then assayed by hybridizing part of the barcode DNA to an immobilized complement and the other part to a complement attached to a nanoparticle [26]. The size of this particle is then chemically amplified with another metal and the optical adsorption of the assay area is measured (a single assay area may have a large number of these particles). The larger number of barcode DNA strands than antibodies on the initial nanoparticles gives an instant amplification and thus allows for extremely low detection limits [26].

Antibodies are not the only markers which can be isolated from the mammalian immune system. DNA, with its capability of forming large numbers of hydrogen bonds, can also be used as antigen markers. When DNA is used in this fashion it is referred to as aptamers [27]. Furthermore, enzymes, such as glucose oxidase which breaks down glucose into gluconic acid and hydrogen peroxide, can also serve as sensing elements whose action can be monitored [28].

Thus there are a large number of elements from the mammalian immune system which also demonstrate how exquisitely biological systems are geared towards chemical and biological agent detection. In the case of the immune system, a better understood system than mammalian olfaction, elements are already being used to create highly sensitive and selective sensing techniques.

1.2 THE CASE FOR ORGANIC SEMICONDUCTOR SENSORS

Organic semiconductor field effect transistors are attractive as chemical sensors for several reasons. One is that many types of these semiconductors, unlike silicon, are

inherently quite sensitive to a unique range of chemical analytes [29]. For certain analyte semiconductor combinations, such as NO_2 and copper phthalocyanine, detection limits down to the single digit parts-per-million range can be achieved [30]. Second, many of these semiconductors are soluble in various organic solvents making it possible to drop-cast or spin coat the semiconductors onto preformed source/drain contacts and interconnects [31], or to ink jet print them to make devices and circuits, all of which greatly reduce the cost of fabrication [32]. Finally, they can be incorporated on a variety of substrates, including flexible substrates which can be quite large in area without adding significant complexity to the fabrication process [32]. Figure 5 shows a flexible all polymer humidity sensor.

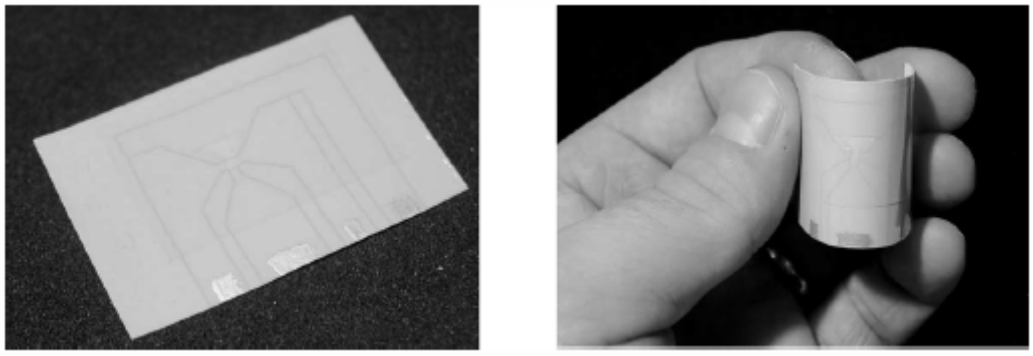

Figure 5. On the left is a printed organic electrochemical transistor humidity sensor which uses Nafion, a proton conductor, as the humidity sensitive layer and is produced on a polyethylene coated fine paper. The dimension of the entire device is 5 cm x 4 cm. The device maintains good electrical performance even while bent at a radius of curvature of approximately 5 cm, shown on the right. Reprinted from *Sensors and Actuators B*, vol. 86, David Nilsson, Thomas Kugler, Per-Olof Svensson and Magnus Berggren, "An all-organic sensor-transistor based on a novel electrochemical transducer concept printed electrochemical sensors on paper." pp. 193-197, 2002, with permission from Elsevier [33].

1.3 THE CASE FOR IMMOBLIZED ION CHANNELS

The primary job of ion channels in the body is to passively translocate ions across the cell membrane which is driven by an ion concentration gradient of a membrane potential [34]. The activation of these ion channels, their opening and closing characteristics, can either be intrinsic or extrinsic. Intrinsic implies random and uncontrolled activation. Extrinsic activation, on the other hand, is activation controlled through voltage gating, ligand gating (something binds to the surface of the channel and blocks it), sensitivity to changes in the mechanical properties of the membrane it resides in, or temporary covalent modification [35]. The fact that the primary job of these channels is to control these ion fluxes naturally yields the ability to directly transduce a chemical sensing event into an electrical signal by measuring conductance changes when the entity of interest interacts with the channel [36]. Thus, there is no need to use optical techniques to read fluorescent dye intensities. This would also yield the ability to provide continuous testing as long as there is a way to periodically cycle out the ions when the potential drop and/or the ion gradient across the membrane equilibrates, in the case of a tethered membrane system, and the biological components can be engineered to have sufficient lifetimes (this is by no means a trivial task). Furthermore, in their natural environments these ion channels are usually sensitive to a host of various biological and chemical analytes but it has been shown that they can be engineered through chemical modification of their surface residues or genetic mutation of their amino acid sequences to be sensitive to a range of new analytes [37]. This surface modification can include the incorporation of a large number of other receptors discussed earlier, such as antibodies and aptamers [36]. High sensitivities have been demonstrated already using tether lipid bilayer systems, but with an ensemble of channels not single ion channels, which can detect picomolar concentrations of proteins [36]. Single ion channels conductances have

been measured using the patch clamp amplifier, which will be discussed later, which can also detect very low concentrations, in the nanomolar range [37]. Being able to see individual ion channel activity can also allow for the ability to better distinguish between small concentrations of analytes which are very similar in size and/or charge characteristics, such as Co^{2+} and Zn^{2+} since the ion channel's response to these species differs in its opening and closing frequency and conductance [37]. The patch clamp amplifier currently being used is not particularly portable, however, and thus the reason for our ongoing attempts to integrate them with single solid-state devices and/or small integrated circuits. Thus, the combination of targeting flexibility, in addition to the direct transduction of these sensing responses into electrical signals, makes this a very promising technology for chemical and biological sensing for various applications ranging from hazardous material detection to targeted drug delivery studies and many more.

1.4 REFERENCES

1. Brian R. Eggins, Chemical Sensors and Biosensors, (John Wiley & Sons, Ltd., 2002) pp. 1-9

2. APOPO, an organization devoted to the detection of land mines in Africa http://www.apopo.org/newsite/content/index.htm

3. Dimitra G. Georganopoulou, Lei Chang, Jwa-Min Nam, C. Shad Thaxton, Elliot J. Mufson, William L. Klein, Chad A. Mirkin, "Nanoparticle-based detection in cerebral spinal fluid of a soluble pathogenic biomarker for Alzheimer's disease." *Proceedings of the National Academy of Sciences* Vol. 102, No. 7 (February 15, 2005) pp. 2273-2276

4. J. Throck Watson, H. Wohltjen, Introduction to Mass Spectrometry, 3rd Edition, (Lippincott-Raven Publishers, 1997)

5. F. Baldini, A. N. Chester, J. Homola, S. Martellucci, Optical Chemical Sensors, (Springer, 2006)

6. James M. Miller, Chromatography: Concepts and Contrasts, (John Wiley & Sons, Inc., 2005)

7. David L. Nelson, Michael M. Cox, Lehninger Principles of Biochemistry, 4th Edition, (W. H. Freeman and Company, 2005) pp. 175-182

8. Federation of American Scientists Anthrax Fact Sheet http://www.fas.org/biosecurity/resource/agents.htm

9. The National Cancer Institute Fact Sheet. The Prostate-Specific Antigen (PSA) Test: Questions and Answers

http://www.cancer.gov/cancertopics/factsheet/Detection/PSA

10. "Endocrine Disruptors", National Institute of Environmental Health Sciences, U.S. Department of Health and Human Services, National Institutes of Health (June 2006) http://www.niehs.nih.gov/oc/factsheets/pdf/endocrine.pdf

11. Michael J. Serby, Karen L. Chobor, Science of Olfaction, (Springer-Verlag, Inc., 1992), pp. 31-119

12. Carol Turkington, Bonnie Lee Ashby, The Encyclopedia of Infectious Diseases, 3rd edition, (Facts on File, Inc., April 30, 2007)

13. Julian W. Gardner, Philip N. Bartlett, Electronic Noses: Principles and Applications, (Oxford University Press, Inc., 1999) pp. 1-6

14. F. Baldini, A.n. Chester, J. Homola, S. Martellucci, Optical Chemical Sensors, (Springer, 2006)

15. D. S. Ballantine, Jr., R. M. White, S. J. Martin, A. J. Ricco, G. C. Frye, E. T. Zellers, H. Wohltjen, Acoustic Wave Sensors: Theory, Design, and Physico – Chemical Applications, (Academic Press, Inc., 1997)

16. Mark Derr, "With Training, a Dog's Nose Almost Always Knows." The New York Times 29 May 2001:

http://www-psych.stanford.edu/~bigopp/Behaviorism.html

17. David Philipps, "Buried alive, waiting for a cheese hound." The Gazette 2004 (published by Gazette Enterprises, a division of Freedom Colorado Information): http://pets.coloradosprings.com/feature_fullstory.jsp?id=4066

18. G. Sicard, and A. Holley, "Receptor cell responses to odorants: Similarities and differences among odorants." *Brain Res.* 292(1984) pp. 283-296

19. Gary S. Settles, "Sniffers: Fluid-Dynamic Sampling for Olfactory Trace Detection in Nature and Homeland Security – The 2004 Freeman Scholar Lecture." *Journal of Fluids Engineering*. 127(2005) pp. 189-218

20. Aud Thesen, Johan B. Steen, Kjell B. Døving, "Behavior of Dogs During Olfactory Tracking." *J. exp. Biol*. 180(1993) pp. 247-251

21. Michael McCulloch, Tadeusz Jezierski, Michael Broffman, Alan Hubbard, Kirk Turner, Teresa Janecki, "Diagnostic Accuracy of Canine Scent Detection in Early - and Late – Stage Lung and Breast Cancer." *Integrative Cancer Therapies*. Vol. 5, Iss. 1(2006) pp. 30-39

22. Julio E. Correa, "The Dog's Sense of Smell." UNP-66, (Alabama A&M and Auburn Universities, Alabama Cooperative Extension System July 2005) http://www.aces.edu/pubs/docs/U/UNP-0066/UNP-0066.pdf?PHPSESSID=899e618c0b54b53ec7ab56f0e314cb54

23. A. Maureen Rouhi, "Detecting Illegal Substances," Chemical & Engineering News, (the American Chemical Society, September 29, 1997) http://pubs.acs.org/hotartcl/cenear/970929/detect.html

24. National Human Genome Research Institute, National Institutes of Health http://www.genome.gov//Pages/Hyperion//DIR/VIP/Glossary/Illustration/antibody.cfm referenced from a Wikipedia article on antibodies http://en.wikipedia.org/wiki/Antibodies

25. Research Collaboratory for Structural Bioinformatics (RCSB), Protein Data Bank http://www.rcsb.org/pdb/explore.do?structureId=1IGT

referenced from Wikipedia

http://en.wikipedia.org/wiki/Image:Antibody_IgG.png

26. Jwa-Min Nam, C. Shad Thaxton, Chad A. Mirkin, "Nanoparticle-Based Bio-Bar Codes for the Ultrasensitive Detection of Proteins." *Science* 301(26 september 2003) pp. 1884 – 1886

27. Scott E. Osborne, Ichiro Matsumura, Andrew Ellington, "Aptamers as therapeutic and diagnostic reagents: problems and prospects." *Current Opinion in Chemical Biology* Vol. 1, Iss. 1 (June 1997) pp. 5-9

28. Mirtha Umaña, Jess Waller, "Protein – Modified Electrodes. The Glucose Oxidase/Polypyrrole System." *Anal. Chem.* 58 (1986) pp. 2979-2883

29. B. Crone, A. Dodabalapur, A. Gelperin, L. Torsi, H. E. Katz, A. J. Lovinger, Z. Bao, "Electronic sensing of vapors with organic transistors." *Applied Physics Letters*, Vo. 78, No. 15(April 9, 2005) pp. 2229-2231

30. Q. Zhou, R. D. Gould, "A study of the response rate to nitrogen dioxide exposure in metal phthalocyanine thin film sensors." *Thin Solid Films*, 317(1998) pp. 436-439

31. Yanming Sun, Yunqi Liu, Daoben Zhu, "Advances in organic field effect transistors." *Journal of Materials Chemistry*, 15(2005) pp. 53-65

32. Daniel R. Gamota, Paul Brazis, Krishna Kalyanasundaram, Jie Zhang, Printed Organic and Molecular Electronics, (Kluwer Academic Publishers, 2004) pp. 56-75

33. David Nilsson, Thomas Kugler, Per-Olof Svensson and Magnus Berggren, “An all-organic sensor-transistor based on a novel electrochemical transducer concept printed electrochemical sensors on paper.” *Sensors and Actuators B*, vol. 86(2002) pp. 193-197

34. Frances M. Ashcroft, Ion Channels and Disease, (Academic Press, 2000) pp. 1-3

35. Adrea Vescovi, Adrea Knoll, Ulrich Koert, “Synthesis and functional studies of THF-gramicidin hybrid ion channels.” *Organic & Biomolecular Chemistry*, vol. 1, iss. 16 (August 21 2003) pp. 2983-2997

36. B. A. Cornell, V. L. B. Braach-Maksvytis, L. G. King, P. D. J. Osman, B. Raguse, L. Wieczorek, R. J. Pace, “A biosensor that uses ion-channel switches.” *Nature* 387(June 5 1997) pp. 580-583

37. Hagan Bayley, Charles R. Martin, “Resistive-Pulse Sensing—From Microbes to Molecules.” *Chemical Reviews* vol. 100, iss. 7(July 2000) pp. 2575-2594

CHAPTER 2 ORGANIC THIN-FILM FIELD-EFFECT TRANSISTORS (OTFTS)

The electrical properties of organic materials have been studied for nearly a century [1, 2]. In the last thirty years, major breakthroughs in the synthesis of organic and polymeric electronic grade materials, the fabrication of devices such as field-effect transistors, light emitting diodes and photovoltaics, and the physical understanding of the properties of these materials has progressed to the point where large scale commercialization of products using organics is on the horizon. Organic radio frequency identification tags [3], emissive displays and back planes [4, 5], chemical sensors [6], and electronic paper [7] have already reached the initial capital investment stage [8, 9]. The following chapter deals with some of the history of organic electronics development and then goes into a discussion of the origin of the conductive properties of these materials, the fabrication of organic transistors, and an overview of the transport properties and injection effects which dominate their electrical characteristics. This is of crucial importance if one is to better understand their chemical sensing behavior.

2.1 THE HISTORY OF OTFTS

The beginnings of the study of organic compounds capable of conducting electrical current can be traced back to the early 20th century [1]. In 1906, an Italian scientist named Pochettino first investigated the photoconductivity of anthracene, pictured in Figure 1 [1, 2]. This was shortly followed by an investigation of anthracene's dark current in 1910 by Konigsberger and Schilling at the University of Freiburg/Brg. in Germany [2]. The first organic photovoltaic prototype was then demonstrated in 1913 by Vollmer at the University of Leipzig [2]. In the 1940's, further impetus for looking into

organic materials as conductors and semiconductors was provided by Robert S. Mulliken and Albert Szent-Gyorgi when they put forth the concept of donor-acceptor charge transfer complexes and the possibility that proteins might not be insulators [10]. In the 1960's, it was discovered that anthracene displayed the ability of electroluminescence when it was shown that it could emit blue light when carriers were injected into it from external electrodes [1].

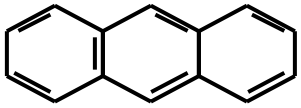

Figure 6. Anthracene [1]

The first organic metal, a combination of two small organic molecules tetrathiofulvalene and tetracyanoquinodimethane or TFF-TCNQ (see Figure 2), to approach the conductivity of inorganic metals was synthesized in 1973 and had a conductivity of 8000 S/cm (inorganic metals have conductivities around 10,000 S/cm) [1].

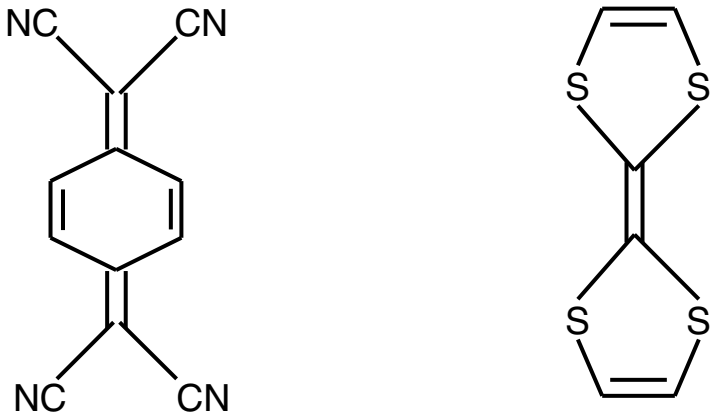

Figure 7. Tetracyanoquinodimethane (left) and tetrathiofulvalene (right) [1]

In 1977, Alan J. Heeger, Alan G. MacDiarmid and Hideki Shirakawa discovered that by doping polyacetylene (see figure 3) with chlorine, bromine, or iodine vapor, they could adjust its conductivity by eleven orders of magnitude [11]. For this discovery they won the Nobel Prize in 2000 [12].

After the seminal work by MacDiarmid *et al* in the late 1970s, which demonstrated that organics materials could be very interesting due to the amazing range over which their conductive properties could be tuned, the 1980s marked a period when significant efforts were launched to determine what kinds of electronic structures could be produced with these molecules [1, 13]. One of the first electrical devices produced which demonstrated that conductivity could be modulated by the presence of an external electric field, as opposed to chemical doping, was fabricated in 1983 by Ebisawa [1]. This earliest example of a thin-film transistor made from an organic material was built on glass with a patterned gate followed by a dielectric layer made from polysiloxane, a semiconductor layer consisting of polyacetylene and metallic source/drain contacts (see figure 3) [1]. Due to significant amounts of impurities, however, this device had limited conductivity modulation [1].

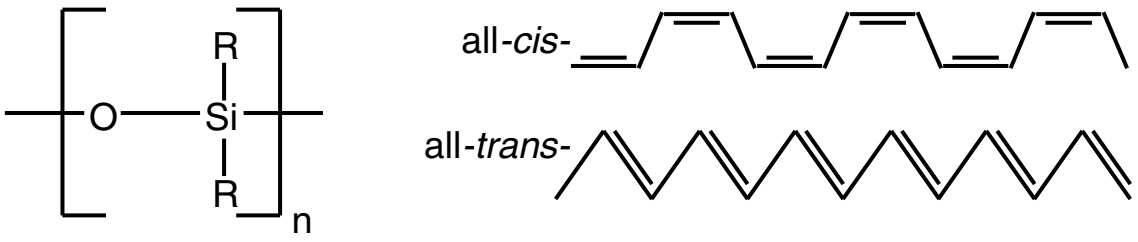

Figure 8. The chemical formula of the monomer unit of polysiloxane can be seen on the left [14]. On the right is the *cis* and *trans* isomers of polyacetylene [12].

In 1986, Tsumura, Koezuka, and Ando produced a device with significantly better transistor characteristics, such as many times better gate modulation of channel

conductivity, than the aforementioned polyacetylene device [1]. The device was built using an n-type silicon wafer as the substrate (resistivity of 4-8 •·cm) which was covered with a thermally grown 300 nm thick oxide layer which served as the gate insulator [15]. Gold coated chromium source/drain electrodes spaced 10 μm apart and 2 mm long came next, patterned using photolithography with the metals vacuum deposited [15]. Finally a layer of polythiophene, shown in Figure 4, was electrochemically deposited [15]. This device was able to achieve a mobility of 10^{-5} cm^2/Vs and had an on/off ratio of about 100-1000 [15]. By 1996, a polythiophene derivative would achieve a mobility as high as 0.045 cm^2/Vs and an on/off ratio of greater than 1000 [16].

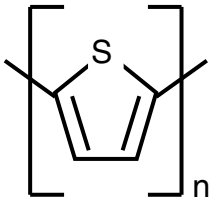

Figure 9. Polythiophene [15]

That same year, 1986, C. W. Tang reported a photovoltaic device from a heterojunction of copper phthalocyanine and a derivative of perylene tetracarboxylic dianhydride (copper phthalocyanine and the perylene tetracarboxylic derivative are shown in Figure 5) [17]. It demonstrated a charge generation efficiency which was independent of the bias voltage leading to a high fill factor [17]. The fill factor is the ratio of the actual maximum output power to the power which would result from the maximum possible output voltage (the open circuit voltage) and the maximum output current (the short circuit current) [18]. This device was capable of a power conversion efficiency of 1%, an order of magnitude higher than any previously recorded organic photovoltaic device [17, 19]. Later, also using an organic heterojunction made from 8-

hydroxyquinoline aluminum and an aromatic diamine, shown in figure 6, C. W. Tang *et al* reported an organic light emitting diode with an external quantum efficiency of 1%, a luminous efficiency of 1.5 lm/W and a brightness of >1000 cd/m^2, all while using a driving voltage of 10 V [20].

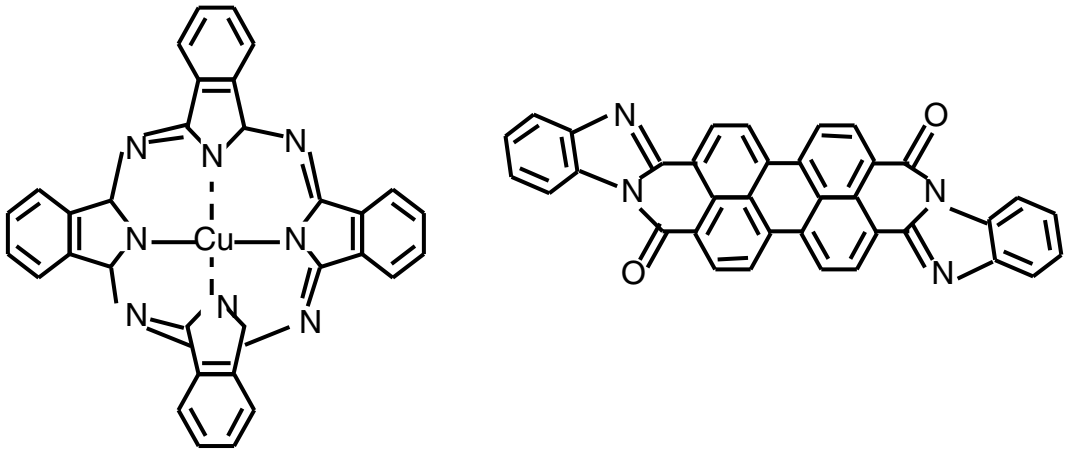

Figure 10. The structure of copper phthalocyanine on the left and a perylene tetracarboxylic derivative on the right [17].

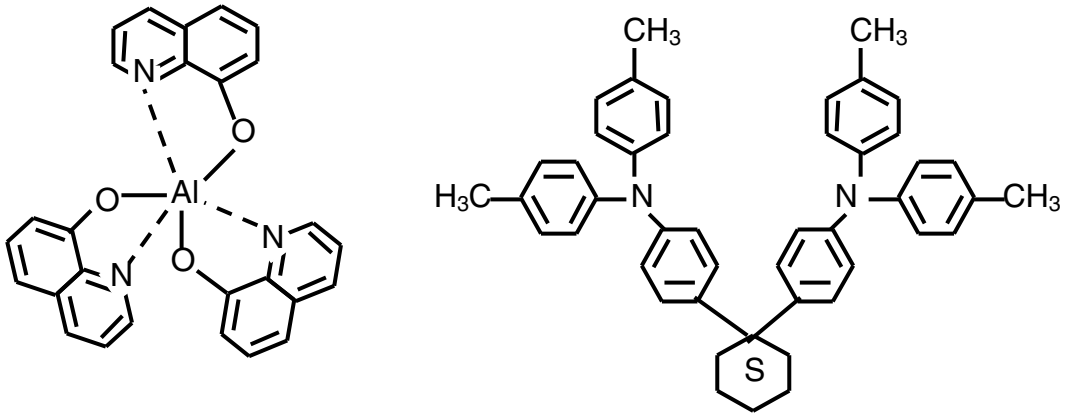

Figure 11. The structure of 8-hydroxyquinoline aluminum is shown on the left and the aromatic diamine is shown on the right [20]

One of the first small organic molecule thin-film transistors which also demonstrated appreciable gate modulation and carrier mobilities was created in 1988 by Clarisse *et al* [1]. This device was made from two forms of phthalocyanine, whose

structure is similar to the copper phthalocyanine shown in Figure 5 but with a different metal ion at the center [1, 21]. In the case of diphthalocyanine, two phthalocyanine molecules coordinate to the central metal atom. The device structure was similar to that produced by Tsumura *et al*, mentioned above, whereby n-type doped silicon was used as the substrate covered with 100 nm of thermally grown oxide as the gate dielectric [21]. The combination of 300 Å of scandium diphthalocyanine ($ScPc_2$) deposited on top of 1000 Å of nickel phthalocyanine (NiPc) acted as the semiconductor layer, which was followed by the deposition of gold that served as the source drain electrodes [21]. The scandium diphthalocyanine's thickness had to be carefully controlled to prevent the device from becoming a resistor. It was the mixing of the two organic molecules at the interface which yielded the semiconductor properties. Too much $ScPc_2$ and its conductivity would dominate and eliminate the possibility for channel conductance modulation [21]. This thin-film transistor had a mobility of 10^{-3} cm^2/Vs, one to two orders of magnitude higher than comparable polymer thin-film transistors that were being produced at the time [1, 21].

This decade of groundbreaking research into novel organic and polymeric electronic devices was capped off in 1990 with the unveiling of the first polymer light emitting diode (LED) by Burroughes *et al* [22]. The device was based on poly(p-phenylene-vinylene) (see figure 7) and several combinations of metal and metal oxide contacts, one with a high work function and one with a low work function. One contact was also required to be semi transparent [23]. It could achieve a photoluminescence (PL) quantum yield of ~8% [23] (this is the ratio of excitons which decay radiatively to the total number of decaying excitons [24]). The PL quantum yield is due to nonradiative recombination at defect sites [23].

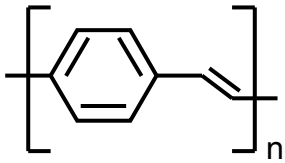

Figure 12. Poly(p-phenylene-vinylene) [23]

The 1990s was another explosive period for organic and polymeric electronics. Devices made with pentacene, similar to anthracene but including five fused benzene rings as opposed to three (see Figure 8), were demonstrated to have mobilities as high as 1.5 cm^2/Vs [25] and on/off ratios greater than 10^8 [26]. This meant that they now approached and, in some cases, exceeded the mobility of amorphous silicon, the form in which silicon appears when deposited as a thin film. These films had to be vacuum evaporated. Recently, the same group which generated these results was able to realize a device made from a soluble form of pentacene with a mobility greater than 1.5 cm^2/Vs and an on/off ratio of ~10^6 [27]

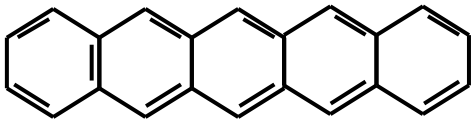

Figure 13. Pentacene [26]

Most of the semiconductors described above are p-type. Development of n-type organic semiconductors had not been as straightforward due to the normally increased reactivity to oxygen of molecules with extra electrons [28]. One of the first n-type semiconductors, demonstrated in 1993, was C_{60} which had a mobility of 10^{-4} cm^2/Vs (shown in figure 9) [29]. This was increased two years later by another group, Haddon *et al*, to 0.08 cm^2/Vs [30]. These devices were some of the most susceptible to reaction with oxygen and subsequent loss of stable characteristics [28].

Figure 14. C_{60} [31]

In 1994, another n-type material was presented by Brown *et al*, tetracyanoquinodimethane (TCNQ) [32]. This material had a fairly low mobility, $3x10^{-5}$ cm^2/Vs, but actually had an improved on/off ratio of 450 upon exposure to air due to oxidative dedoping [32].

There were several other n-type materials presented in the 1990s culminating in the presentation of fluorinated copper phthalocyanine, depicted in figure 10 [33]. This obtained one of the highest n-type mobilities of the decade for an air stable n-type semiconductor material, 0.03 cm^2/Vs [33].

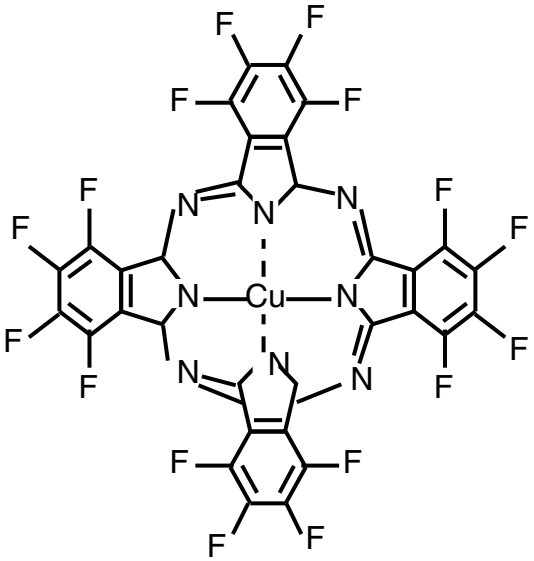

Figure 15. Hexadecafluorinated copper phthalocyanine [33]

The middle of this decade also saw the beginnings of applications such as early prototypes of organic LED emissive displays [34]. Some of these displays were in full color, had good resolution, and could achieve video level refresh rates but were fairly small in area [34].

The beginning of the 21st century saw continued improvement of organic semiconductor electronic properties and stability [31] (this reference is also a good, recent review of many different organic semiconductors including tables of their mobilities). Devices made from single crystal, mainly p-type, began to become more prevalent such as rubrine, with a mobility that approaches 20 cm^2/Vs (see figure 11) [31]. Until this point, most thin film transistors had active materials which had a polycrystalline morphology and therefore suffered from substantial disorder at the domains between grains [35]. N-type devices also continued to make steady improvements towards higher mobilities and better stability [31].

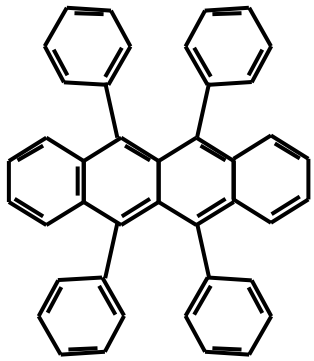

Figure 16. Rubrene [13]

The big emphasis now switched to realizing the real potential of organic electronics, low cost manufacturing. The major problem so far with organic and polymer semiconductors was that if the material had good carrier mobility it needed to be vacuum evaporated, such as with pentacene [25]. Solution processable materials usually had

pretty bad mobility or at least not as high as was necessary to compete with amorphous silicon [36]. Therefore a large amount of focus went to finding solution processable materials which could be inkjet printed [37], drop cast or spun [38]. Attempts are underway to achieve this by either trying to make small organic molecules soluble [27] or improving the properties of polymers [31].

Finally, the end of the 20th, beginning of the 21st Century saw significant attempts at using the inherent sensitivity of many organic semiconductors to their surrounding environments to create organic transistor chemical and biological sensors [39]. Many of the phthalocyanine derivatives had been used as chemiresistors with very good detection limits for such gases as NO_2 [40]. Concentrations as low as 1 part-per-billion (ppb) were detected in 1984 with such resistive sensors [40]. Phthalocyanine derivatives had also been used as the sensitizing layer for silicon chemical field-effect transistors (CHEMFETs) [41, 42]. CHEMFETS are silicon transistors where the gate medal has been replaced by a sensitizing layer. This sensitizing layer interacts with the analyte of choice to produce a change in the charge on the gate or a change in the work function of the sensitizing material and thus changes the transistor channel conductance [41, 42, 43]. The mechanism by which the phthalocyanine can so effectively measure nitrogen dioxide is that the gas adsorbs to the surface of phthalocyanine at specific sites on the film and then diffuses [41]. The gas then oxidizes the phthalocyanine molecule and creates more excess holes which either affects the conductivity of the phthalocyanine, in the case of a chemresistor, or the charge state in the case of a CHEMFET [41]. In 2000, Torsi *et al* showed that organic transistors have a major advantage over chemiresistors since more device parameters could be probed, such as shifts in threshold voltages and changes to the field induced mobility and conductivity in addition to adjustments to the bulk conductivity and mobility [44]. Crone *et al* later demonstrated an array of organic thin

film transistors which were sensitive to a host of organic vapors [39]. The devices could easily and quickly be refreshed by reverse biasing the gate [39]. These devices could then reproduce the same responses to chemical vapors many times very accurately [39]. Organic devices have also been demonstrated which can detect biologically important analytes, such as glucose, or use biological components as a functioning part of their structure. Transistors utilizing poly(3-hexylthiophene) and glucose oxidase were used to detect glucose concentrations [45]. Bernards *et al* demonstrated a device which used a bilayer lipid membrane as the gate for an organic electrochemical transistor (OECT) [46]. A reservoir was created above a layer of poly(3,4-ethylenedioxythiophene) doped with poly(styrene sulfonate) (PEDOT:PSS) by use of polydimethylsiloxane (PDMS) [46]. The OECT was gated by the addition of gramicidin ion channels which allowed ions to flow into the reservoir [46]. These ion channels, and thus the sensor itself, could distinguish between monovalent and divalent ions due to the inherent properties of the gramicidin [46]. The important consideration for most biological sensors is that the sensors usually must be able to operate under aqueous conditions, an ability which has been demonstrated for organics by many groups over the last few years [45].

2.2 ORGANIC SEMICONDUCTORS REALIZED FROM PI-CONJUGATED MATERIALS

The origin of the conductive and semiconductive properties of organic and polymeric materials is their high level of conjugation, or alternating single and double bonds [13]. Carbon has an atomic number of 6 which indicates six protons, six electrons, and in its most common isotope, six neutrons. This means that in order to have a stable octet carbon requires four more electrons in its valence electron shell [47]. This could be satisfied by forming a combination of single, double and triple covalent bonds with other

atoms. Looking at the energy level filling of carbon, there would be two electrons in its 2*s* orbital and two electrons in its 2*p* orbitals [48]. In the case of four single, or , bonds, these bonds do not differ in energy nor are the electrons delocalized over the whole molecule [48]. The 2s and 2p orbitals do not reside at the same energy but the four bonds have the same bond energy and bond length. The highest probability of finding the electrons, the area of highest electron density, in one of these bonds will be between the bonded nuclei, not symmetrically surrounding the atomic nuclei (as is the case for *s* orbitals, a sphere surrounding the nucleus, and *p* orbitals, a dumbbell shape with two lobes centered around the nucleus, as seen in figures 12a and 12b) [48]. To satisfy these criteria, the orbitals of the carbon hybridize (this is similar for most period 2 elements other than the alkali metals in groups 1 and 2 which tend to form ionic compounds), as shown in figure 12c [47, 48]. In their lowest energy state, called the bonding state, the *s* and *p* orbitals combine in such a way as to heavily favor having the highest electron density between the two nuclei of the bonding atoms and not symmetrically distributed around a single nuclei [48]. In higher energetic states, the area of highest electron density can exist in line with the two nuclei but outside of them, not between them [47]. This is referred to as an antibonding state. The nature of how these bonding and antibonding states, called bonding and anti bonding molecular orbitals, fill with electrons from the two bonding components, either atoms or molecules, determines whether the molecule is stable [48]. The bond angles between the bonds arrange to maximize the distance between them [47]. The number of hybrid orbitals depends on the number of bonds in the molecule. When four atoms are bonded to carbon, there are four bonds and thus four hybrid orbitals and the molecule is said to be sp^3 hybridized (see figure 12d) [47]. When three bonds are required, there are three hybridized orbitals and the molecule is sp^2 hybridized (see Figure 12e). Finally, when two bonds are present, there are two

hybridized orbitals which are then referred to as sp hybridized (see figure 12f) [47]. There must be the same number of hybrid orbitals in the molecule as the total of combined *s* and *p* orbitals required to form bonds [48]. Thus, if three bonds are required, then two *p* orbitals (such as p_x and p_y) must hybridize with the *s* orbital to make an sp^2 hybridized molecule [48]. When discussing nitrogen or oxygen, which have nonbonding paired electrons, the electrons can be treated the same as if they were bonding electrons and still reside in a hybrid orbital [47, 48].

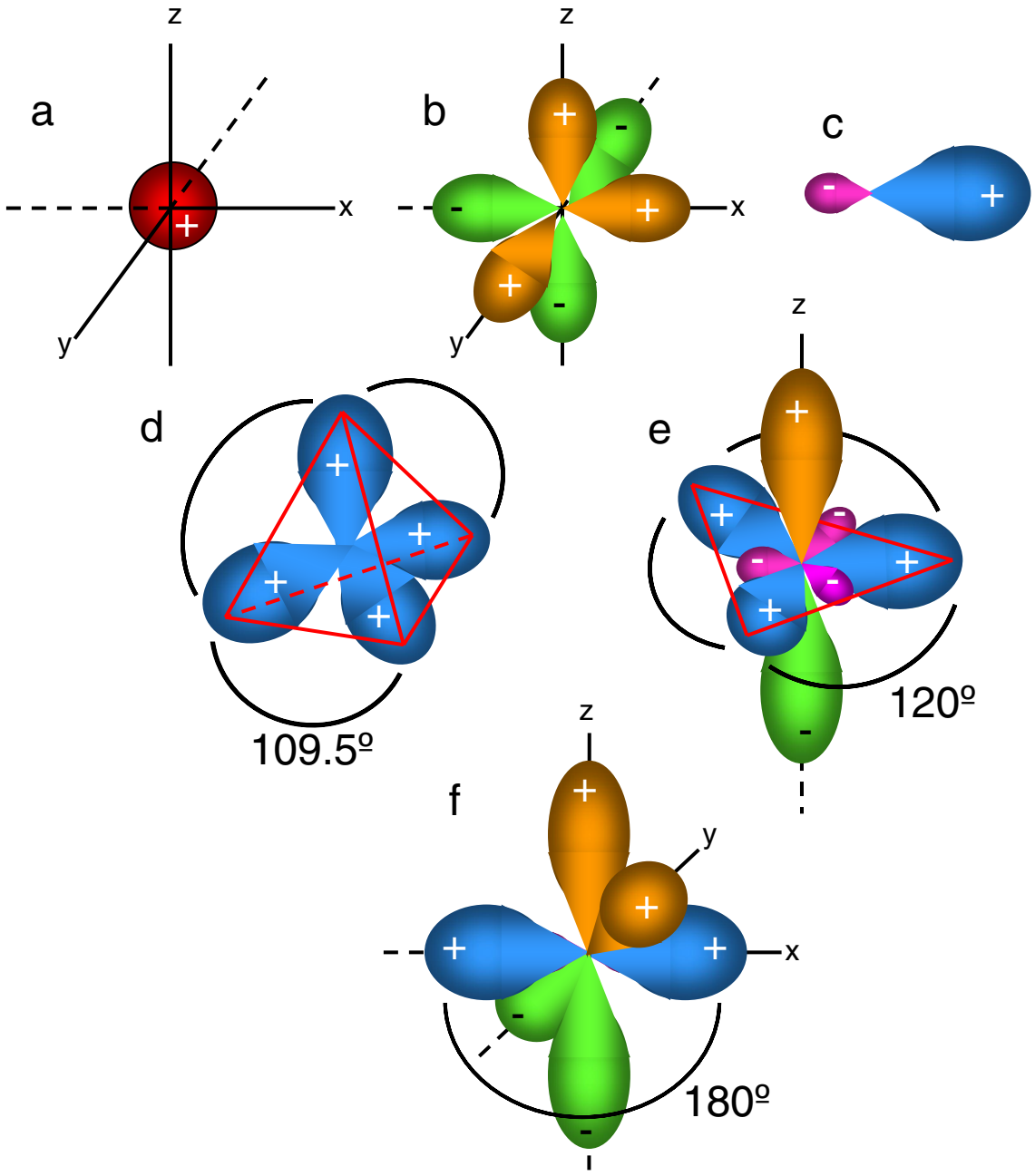

Figure 17. a) A representation of an *s* orbital where the nucleus resides in the middle of the orbital. b) The three pairs of lobes of the three *p* orbitals with the nucleus also residing at the origin (one orbital includes both an orange and green lobe on the same axis). c) A hybridized orbital showing the unequal lobe sizes which yields the directional nature of the covalent bond with the nucleus residing between the lobes. d) The sp^3

hybridization (small lobes not shown for clarity). The bond angles are all 109.5º. e) The sp^2 hybridization showing the unhybridized *p* orbital mutually perpendicular to the sp orbitals. The bond angles for the sp orbitals are all 120º and they are all in the same plane. f) The sp hybridization with a bond angle of 180º. This diagram also shows the two unhybridized *p* orbitals which are at right angles to the sp orbitals. For all the diagrams, the signs indicate positive and negative phases of the electron wave functions which are vital to determining whether molecular orbitals are bonding or antibonding and thus whether the molecule is stable. The colors in a), b), and c) also indicate the same as the signs, green and magenta being negative phases and red, orange, and blue representing positive phases. These color differences then help to distinguish the various orbitals in d), e), and f) [47, 48].

The other bonds which are formed, in the case of double bonds and triple bonds, are called bonds and do not require hybridization to explain them [47, 48]. They are bonds formed off the axis which directly connect the two nuclei [47]. These bonds have lower bond energies than bonds and, in their bonding (or lowest energy) state, can be delocalized over the entire molecule provided there is more than one bond in close molecular proximity (see figure 13c) [48]. This means that electrons can be withdrawn or added to bonding orbitals much easier than to bonding orbitals [48]. Furthermore, once the molecule has been ionized, the normally reactive ionic state can be stabilized, made less reactive, by diffusing or delocalizing the effects of the added or subtracted electron wave functions over the whole molecule. When a lot of double bonds or triple bonds exist near each other on a molecule, either right next to each other or alternating with single bonds, the molecule is called a -conjugated system [48]. Molecules with a high degree of -conjugation can act as good organic conductors and semiconductors because carriers can easily be added and removed and passed to the next molecule without a significant increase in the molecule's reactivity [1, 2, 13]. Figure 14 shows three such molecules, copper phthalocyanine, pentacene, and regioregular poly(3-hexylthiophene). All three are normally p-type semiconductors. The focus of much of

the experimental work described in Chapter 3, and the following discussions of thin-film transistor characteristics and physics, will focus on copper phthalocyanine and pentacene. There will be a very brief description of an experiment with regioregular poly(3-hexylthiophene) also described in Chapter 3 within the context of small molecule receptors. Procedures for synthesizing these molecules can be found in [1, 49, 50] for pentacene, in [51] for copper phthalocyanine and in [52] for poly(3-hexylthiophene).

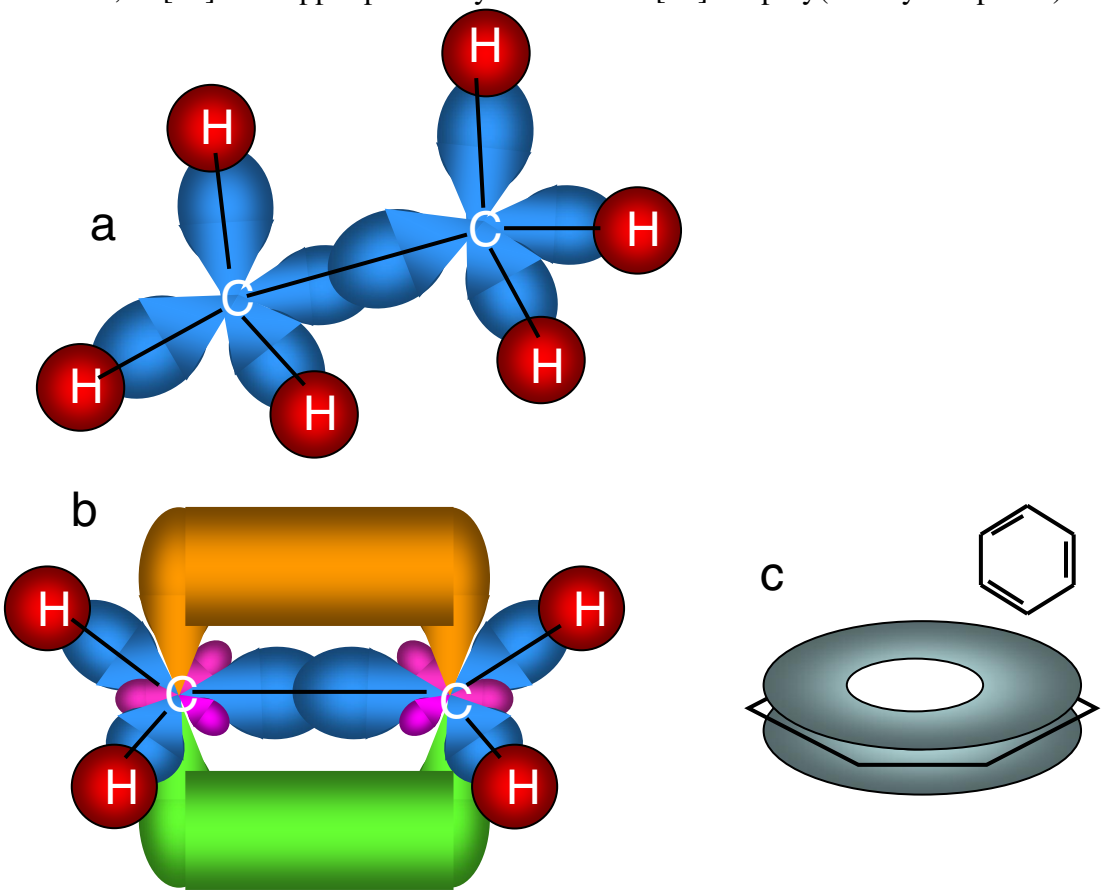

Figure 18. a) The structure of ethane showing the bonds aligned on the axis between the nuclei of the hydrogens (whose *s* orbitals are represented by red circles) and the carbons and between the two carbons. b) The structure of ethene showing the bonds which all lie in the same plane and the bonds located out of the plane. c) The delocalized orbitals of the conjugated benzene ring whose chemical structure is shown above [47, 48].

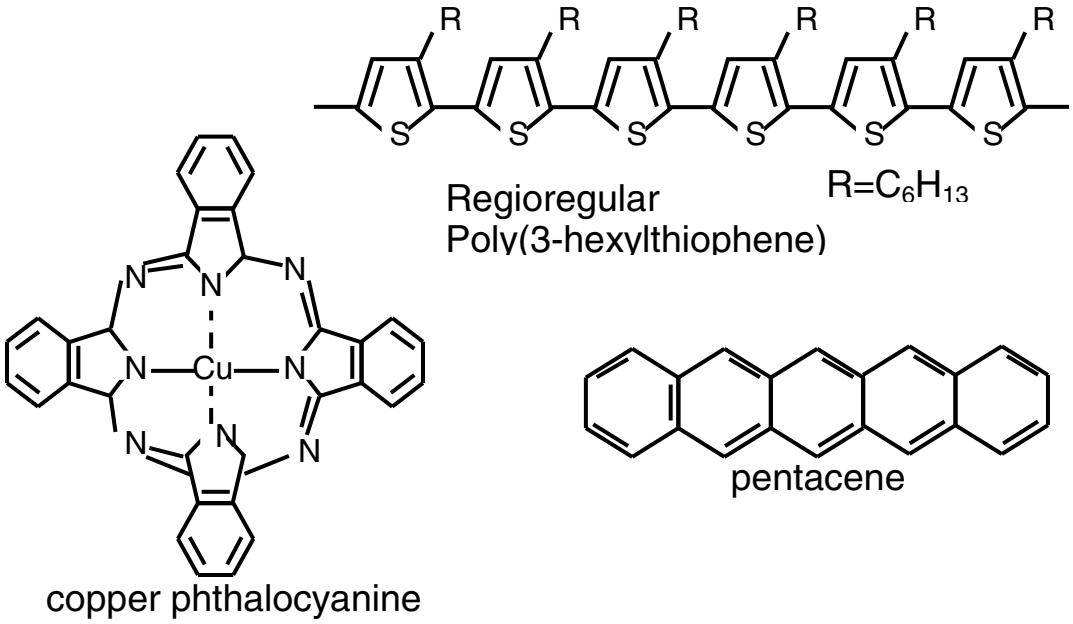

Figure 19. Chemical structures of Copper phthalocyanine (CuPc), regioregular poly(3-hexylthiophene) (P3HT), and pentacene [15, 17, 26].

2.3 FABRICATION OF OTFTS FROM MICROSCALE TO NANOSCALE

The methodologies used to fabricate devices for the chemical sensing studies described in Chapter 3 are some of the very same used to pattern and process silicon devices. Since most of these experiments were designed to demonstrate the chemical sensitivity of the organic transistors and not to test novel techniques for creating them, silicon processing on heavily doped silicon wafers (used as the gate) was the easiest way to produce high performance micro and nanoscale devices [53, 54]. The two basic device geometries used in these studies was the bottom contact and the top contact device structures shown in Figure 15 (there are two cases in Chapter 3 where device processing techniques differ from these more generic techniques described in this Section which will also be elucidated in Chapter 3).

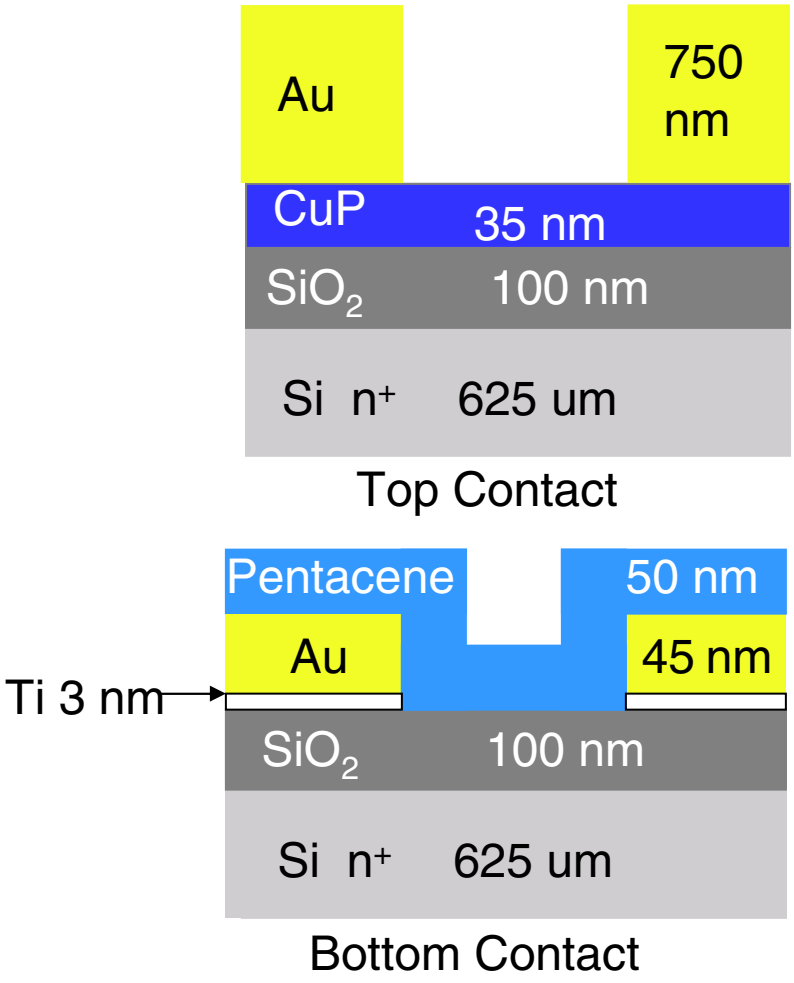

Figure 20. The top and bottom contact device geometries [53, 54].

Heavily doped silicon was used as both the substrate and the gate. 1000 Å of thermally grown silicon dioxide served as the gate dielectric. In a few studies, an additional dielectric, glass resin which is a molecule with a silicon oxygen back bone but alkane side chains, was spun on top of the silicon dioxide. This dielectric is more hydrophobic then silicon dioxide [55]. In the case of the top contact geometry, some amount of semiconductor, in most cases pentacene or CuPc, was thermally evaporated. Poly(3-hexylthiophene) was drop cast onto the surface. The thermally evaporated

semiconductors were deposited to a thickness usually between 30 and 50 nm (it is difficult to control the thickness of drop cast films). The deposition rate had to be very carefully controlled to achieve optimal molecular alignment [26]. To reduce gate leakage current, the semiconductor could be patterned through a shadow mask. This would then reduce the surface area of the substrate covered by the semiconductor which would allow for fewer pinholes to be accessed when biasing the device. Pinholes are defects in the dielectric which allow leakage current to flow through. Spin coating was rarely used at this stage due to the large amount of semiconductor needed. Gold was then thermally evaporated through a shadow mask to form source and drain contacts [53]. Gold was chosen due to its high work function (•5.2 eV) which should match well with (is greater than) the energy levels of the highest occupied molecular orbitals (HOMO) (the ionization energy) of both CuPc (•5.0 eV) and pentacene (•4.9-5.1eV) [1, 13, 56] (for reasons discussed later, this simple matching of energy levels is not completely accurate). In the case of the bottom contact geometry, gold source and drain contact areas were defined by either photolithographic or electron beam lithographic techniques. These techniques use a UV light or electron sensitive polymer called resist. It comes in the form of positive or negative resist which distinguishes between whether the polymer is made soluble by exposure to light or electrons (positive) or insoluble (negative). To form the contacts, a thin layer of about 3 nm of titanium was deposited first, for purposes of better gold adhesion to the silicon dioxide, followed by 50 nm of gold in an electron beam evaporator [54]. Afterwards, the resist was removed using acetone or another type of solvent. What was left was only the gold that had been in contact with the surface of the thermal oxide and not the gold that had been on top of the resist. This procedure is called liftoff. Liftoff is most effective when the edge profile of the resist is either perpendicular or has a negative slope (the top of the resist wall overhangs the bottom).

With electron beam lithography, the resists are normally designed to have very perpendicular walls, and the electron beam is very carefully focused to achieve this. With photolithography, negative sloped walls could be realized by performing image reversal (a capability with AZ 5214 made by Clariant Corporation). Image reversal is used when the resist is switched from positive to negative after exposure, which usually yields very nice negative edge profiles due to the shadows cast by the contact mask which prevents a perpendicular profile upon initial exposure [57]. This was followed by the deposition of the semiconductor in a similar fashion to that described for the top contact devices [54]. In several studies, nanoscale transistors were utilized. Some of these devices had source to drain spacing of 5 to 10 nm (see figure 16) [54].

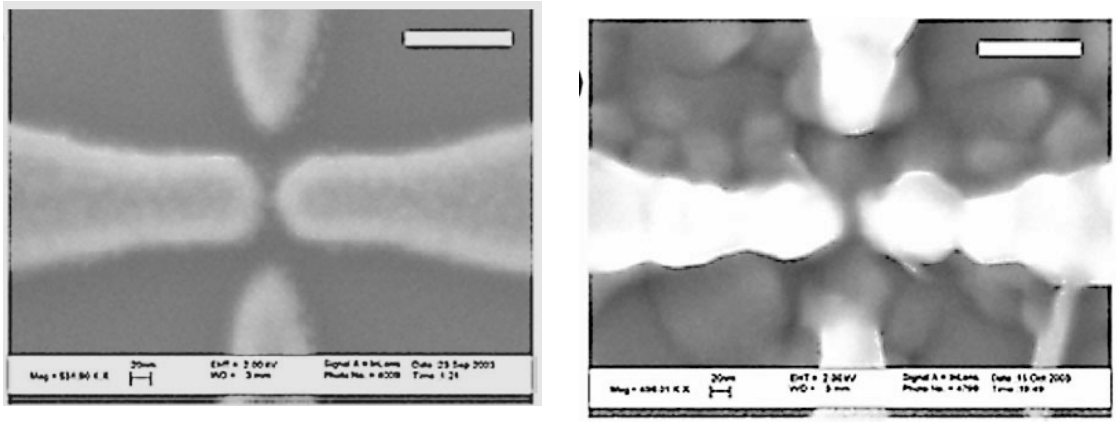

Figure 21. On the left is an SEM of source/drain electrodes, the horizontal pair of electrodes, of a bottom contact nanoscale device prior to semiconductor deposition with a source to drain spacing around 5-10 nm. On the right is a similar nanoscale device after semiconductor has been deposited and after the device's electrical characteristics have been measured. This device also has a horizontal source to drain spacing of less then 10 nm. The outside guarding electrodes, the vertical pair of electrodes, are designed to reduce spreading current to allow the true nanoscale behavior of the electrodes to be investigated. They are typically biased to the same potential as the drain. This is necessary due to the very poor width to length ratio. The scale bars for both devices are 100 nm [54].

To produce devices with these nanoscale characteristics a JEOL JBX-6000FS/E Electron Beam Lithography system was used. At its maximum acceleration voltage, this tool is capable of a minimum spot size of 5 nm, with a minimum accurate beam deflection capability of 1.25 nm [58]. With this tool, in addition to the extremely small gaps shown in figure 16, we have been able to write gold lines which are 25 nm wide (see figure 17).

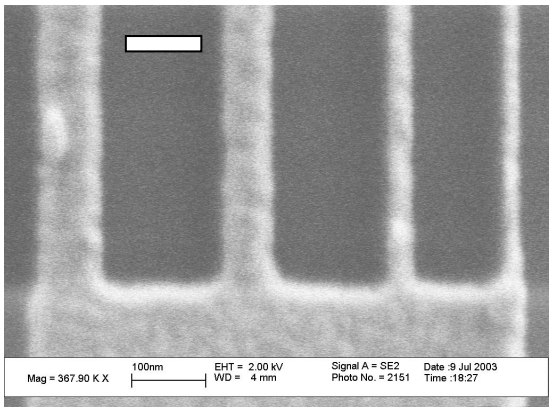

Figure 22. A set of gold wires created using a lift off procedure with the JEOL JBX-6000Fs/E. The right most wire is 25 nm in width. The scale bar is 100nm.

Achievement of this kind of source drain spacing requires a significant amount of dose testing and the inclusion of a range of gap sizes in the design. The dose is the amount of charge used to expose a certain area of resist, usually given in C/cm^2. The equation for the dose is $Q= I*T/P^2$ (as quoted from JEOL) [58]. Q is the dose requirement for the particular resist and is usually predetermined by the company which produces it. I is the electron beam current, T is the dwell time, or shot time, of the beam on a particular spot and P is the pitch, the spacing between adjacent spots where the electron beam will expose the resist. As mentioned earlier, the minimum pitch for this tool is 1.25 nm. It is important to do at least one trial exposure on any new type of substrate or substrate coating on which the resist will reside to insure that the proper dose is realized. Usually

this is accomplished by using a representative pattern, such as a large number of dots of different sizes or small parallel lines with small interstitial spacing. In our case, we simply dose tested with our nanogaps. Many copies of these patterns are exposed with different doses to see which dose will produce the best results. It may also be necessary to include a small range of doses on the actual sample wafer to insure that the desired gap is achieved. This is due to the fact that 5 nm are gaps are below what is considered to be reproducible with this machine. The other important aspect of achieving small gaps is to design several source-to-drain gap sizes into the exposure pattern to insure that at least a few will develop properly. To create the electrodes, the liftoff procedure described above was used. One of the main reasons dose testing and multiple gaps designs are necessary is due to surface charging [59]. Since we are creating these devices on an insulator, cannot etch the electrodes effectively with a dry process due to the fact we are using gold (gold is a very bad contaminant in silicon the processing of which most of the etchers in the clean room are intend for), and do not want any residues between the electrodes and the silicon dioxide, we are forced to pattern the devices directly on the dielectric. This means that the effect of surface charging must be factored into our design since surface charging causes over exposure of the pattern.

When we design a particular source to drain spacing, we usually must make the designed gap much larger than the final desired gap size. We also have to worry about surface curvature [60]. Since the thermal oxide causes surface stress to the silicon wafer due to a difference in thermal expansion coefficients, the wafer bends slightly such that a focus point obtained for writing patterns in the middle of the wafer may not be accurate for the edge of the wafer. This can be compensated for by either focusing at many different points on the wafer before exposing that area, or by making sure the range of designed gap sizes can accommodate for any shifting focus. Focusing with the electron

beam, however, causes exposure of the resist. A contamination spot must be created by allowing the beam to expose one point of the resist continuously which leaves a small blemish. This blemish can then be used for focusing. However, the constant scanning of the beam over the blemish area also exposes the resist. It is therefore not necessarily advantageous to have to perform the focusing procedure a large number of times. Instead, one can use successive exposures to determine how much the focus shifts and plan accordingly. The shift is not large but neither is the feature being written.

2.4 MORPHOLOGY AND CRYSTAL STRUCTURE OF THE THIN ORGANIC FILMS

Once deposited, the thin films of pentacene and CuPc can assume a variety of morphologies. The films are usually polycrystalline, which is the case for all devices described in Chapter 3 (see figure 18), although there are now reports of devices made with single crystal pentacene with high mobility [61]. The size and conformation of the crystalline domains in these films is substrate temperature and deposition rate dependent [26]. They are also dependent on the type of substrate [62] and whether the substrate surface is more polar (silicon dioxide) or nonpolar (glass resin) (which will come into play in sensing as well). The morphology of any organic semiconductor can thus be altered by preparing the surface with various self assembled monolayers (SAMs), such as octadecanethiol, which can change the polarity of the surface, in this case making it more nonpolar [63]. Pentacene, however, arranges quite well on silicon dioxide [26]. Device performance is largely dependent on how well and how closely packed the molecules in the film can arrange themselves in their molecular lattices, maximizing molecular overlap of their conjugated orbitals [26, 64]. These materials also do not form well on gold (see figure 19). This does not matter when fabricating top contact devices as the gold is deposited on top of the semiconductor. This can make a large difference, however, when

the devices are scaled down to the nanoscale. Poor morphology of the organic material at the contact such as a high amount of disorder or a region next to the contact with no semiconductor present, due to geometry considerations, can substantially affect charge injection into the material and reduce device performance. To reduce this problem, the gold can be covered by a second SAM called nitrobenzenethiol which can present a gold surface more friendly to organic semiconductor crystal formation without yielding good electrical connection between the contact and the organic semiconductor [65].

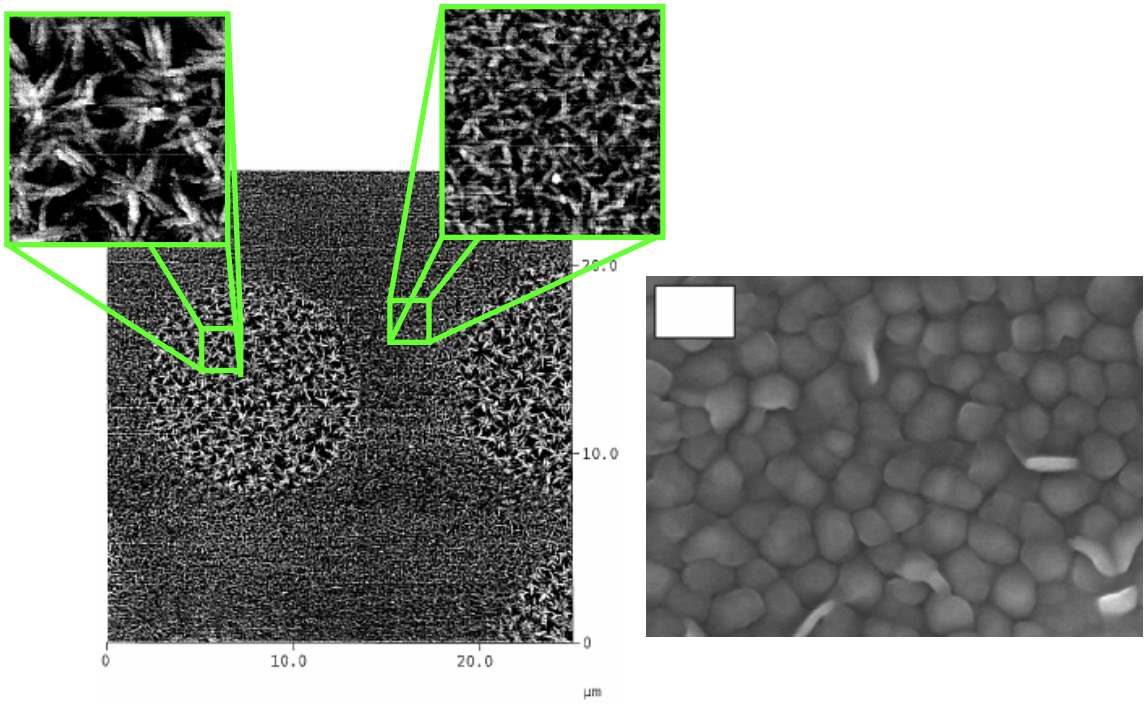

Figure 23. On the left are three atomic force microscopy (AFM) images of CuPc deposited on polyimide which has been spun on ITO covered glass. The crystalline domains are spindle-like in appearance and show two different phases, large spindles and small spindles. This is almost certainly influenced by the morphology of the underlying material. ITO covered glass is usually very rough compared to silicon. The scans in the insets are of equal area, 5 um by 5 um (these AFM images of CuPc were provided by Dr. Andre Gesquiere). The image on the right is a scanning electron micrograph (SEM) of pentacene grains deposited without substrate heating. The scaling bar is 200 nm.

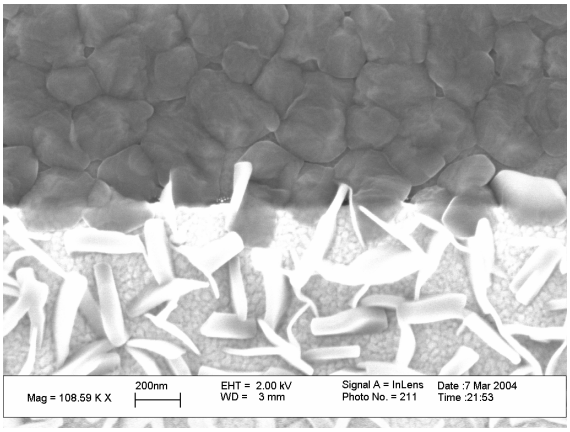

Figure 24. Pentacene grains on silicon dioxide (darker areas) and on gold source/drain electrodes (brighter areas) without nitrobenzenethiol.

Both pentacene and copper phthalocyanine tend to form a herring bone molecular crystal lattice with the individual molecules standing close to perpendicular to the surface when deposited on silicon dioxide (see figure 20 for pentacene with copper phthalocyanine not shown but whose crystal structure and molecular orientation is similar) [13, 66]. As can be seen from figure 20, the molecular overlap is much better in the horizontal than vertical directions [13, 66].

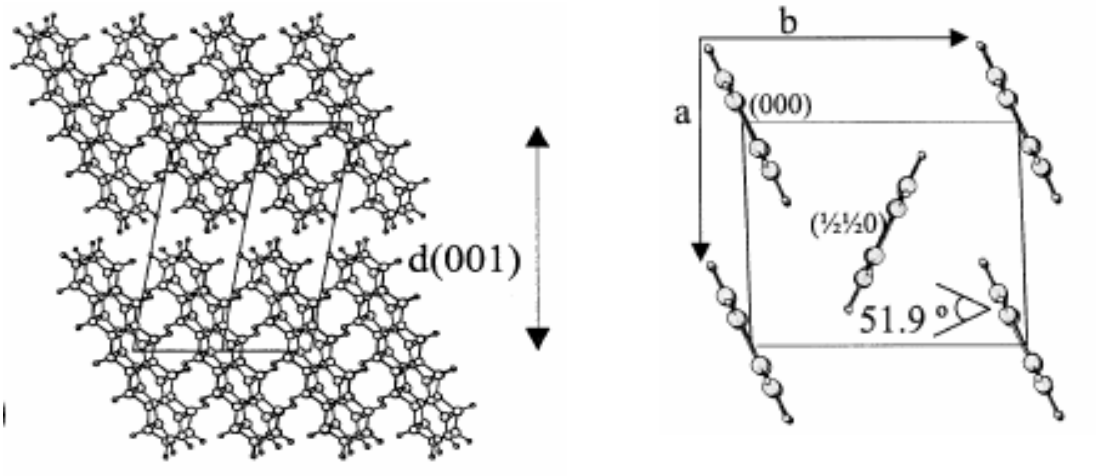

Figure 25. On the left is the pentacene crystal lattice as seen parallel to the dielectric interface. This shows the layered arrangement whereby the

molecular overlap is much better in the horizontal than vertical directions. The geometrical shape shown in the picture is the unit cell. On the right is a representation looking into the unit cell perpendicular to the dielectric surface showing the herring bone structure. [66] This molecular arrangement is similar for copper phthalocyanine [13]. "Reprinted in part with permission from Christine C. Mattheus, Gilles A. de Wijs, Robert A. de Groot, Thomas T. M. Palstra, "Modeling the Polymorphism of Pentacene." *Journal of the American Chemical Society* vol. 125, no. 20 (2003) pp. 6323-6330. Copyright 2003 American Chemical Society."

2.5 ELECTRICAL CHARACTERIZATION OF OTFTS

Once the OTFTs had been fabricated, it was necessary to characterize their performance. To do this, an HP 4145B or Agilent 4155C parameter analyzer was used. Source to drain current was measured for a series of gate voltages. A typical set of curves are shown in Figure 21 for both a CuPc and a pentacene transistor.

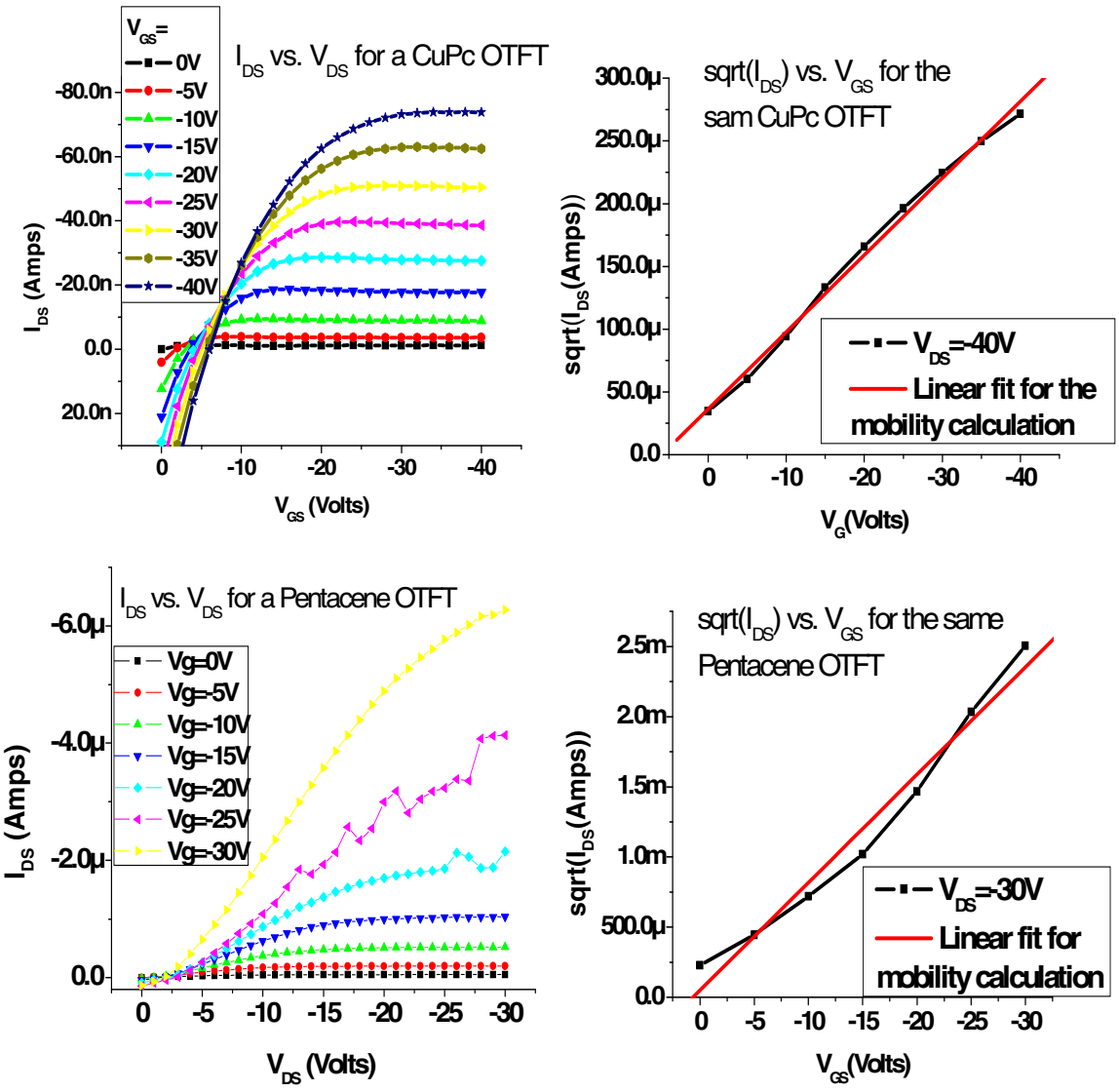

Figure 26. On the top left and bottom left are plotted I_{DS} vs. V_{DS} for a CuPc and a pentacene transistor, respectively. On the top right and bottom right are plotted $\bullet I_{DS}$ vs. V_{GS} for the same set of devices. The leakage current through the gate dielectric is quite apparent for the CuPc device as can be seen from the high positive current at low V_{DS}. Gate leakage is not as big a problem with the pentacene device as there is little positive current at low V_{DS}. Both materials are p-type and thus have their drain and gate biased negatively with respect to the source in accumulation mode.

OTFTs are accumulation mode devices in that they are not doped and so do not have to drive away majority carriers to create a channel. The selection between using holes or electrons as charge carriers is made through the intrinsic properties of the material and not through doping. Conduction is known to occur in the first few monolayers from the gate dielectric/semiconductor interface [67]. Plots of I_{DS} vs. V_{DS} and $\bullet I_{DS}$ vs. V_{GS} were generated to extract important parameter values to determine if the OTFT was a fully operational device. These important parameters can be extracted by the use of equations similar to those used with transistors made from inorganic materials [13]. The relationships between current and voltage in the linear region of device operation and the saturation region are shown in equations I and II, respectively [13].

$$I_{DS} = \frac{W}{L} C_i \mu (V_{GS} - V_t) V_{DS} \qquad \text{I}$$

$$I_{DS} = \frac{W}{2L} C_i \mu (V_{GS} - V_t)^2 \qquad \text{II}$$

I_{DS} is the source to drain current, V_{DS} is the source to drain voltage, V_{GS} is the source to gate voltage, W is the device width (length of source and drain electrodes), L is the device length (distance from source to drain electrodes), C_i is the capacitance per unit area of the gate insulator, μ is the mobility and V_t is the threshold voltage which can be extracted from the plot of I_{DS} vs. V_{GS} (not shown). To enter the saturation regime requires the following criteria to be met (seen in equation III) [1].

$$V_{DS} \geq (V_{GS} - V_t) \qquad \text{III}$$

$$V_{GS} > V_t \qquad \text{IV}$$

Rearranging equation II. yields an expression for the mobility shown in equation V.

$$\mu = \frac{2L}{WC_i} \left(\frac{\partial \sqrt{I_{DS}}}{\partial V_{GS}} \right)^2 \qquad \text{V}$$

From this equation, the calculated saturation region mobilities for the devices above are 0.00016 cm^2/Vs for CuPc and 0.025 cm^2/Vs for pentacene. These values are both low for what has been reported in the literature (0.02 cm^2/Vs for CuPc [68] and 1.5 cm^2/Vs for pentacene [25]). For chemical sensing, however, it is not as important to have the highest mobility devices possible, just to have devices that operate consistently. Since both CuPc and pentacene are p-type semiconductors (primary charge carrier is holes), they have their gates and drains biased negatively with respect to the source in accumulation mode (these are accumulation mode devices, not inversion mode devices like silicon transistors). There are other important parameters which can also be extracted. One such parameter is the on/off ratio, which for these devices is 42 for the CuPc OTFT and 121 for the pentacene OTFT at a gate voltage of -30 volts and a drain voltage of -40V, also significantly lower than reported literature ($4x10^5$ for CuPc [68] and greater than 10^8 for pentacene [69]). This is also not a significant problem since we are running our sensors in steady state in most of these studies. The high off currents may be due to impurities and can be alleviated by purification of the semiconductor before deposition [69]. There is also the subthreshold swing, not identified for these devices. This is a measure of how easy it is to turn the device off. Below the threshold voltage, the I_{DS} vs. V_{GS} relationship is usually exponential (although the absolute current is quite small by comparison). Plotting the log of the source to drain current versus the gate voltage can allow this slope to be extracted. For single crystal silicon, it is usually around 60 mV/decade [69]. Amorphous silicon is around 0.3-1.5 V/decade [69]. Reports for pentacene yield around 1.6 V/decade, close to amorphous silicon [69]. Figure 22 shows current vs. voltage characteristics for a nanoscale pentacene transistor [54]. In this particular device, the current does not saturate due to the inability to raise the source to drain voltage to high

enough levels to satisfy the criteria from equation III due to the high electric fields generated at nanoscale source/drain geometries and the dielectric thickness which is larger than the gap size.

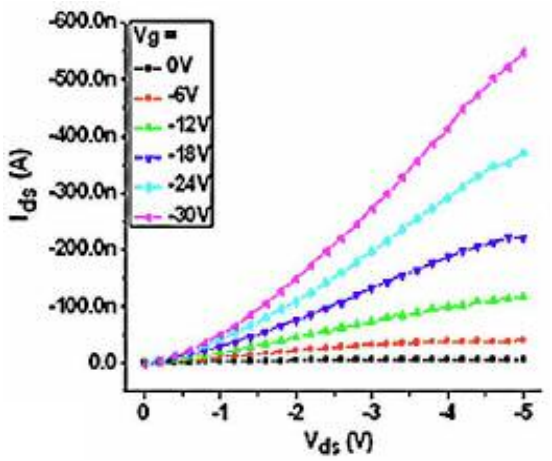

Figure 27. I_{DS} vs. V_{DS} for the device pictured on the right in figure 16 with a source to drain spacing of less than 10 nm. The guarding electrodes are biased to the same potential as the drain [54]. "Reprinted with permission from Liang Wang, Daniel Fine, Taeho Jung, Debarshi Basu, Heinz von Seggern, Ananth Dodabalapur, "Pentacene field-effect transistors with sub-10-nm channel lengths." *Applied Physics Letters* vol. 85, no. 10 (September 6, 2004) pp. 1772-1774 and the American Institute of Physics."

2.6 CHARGE TRANSPORT IN OTFTS

Understanding exactly how these carriers move through these materials can be quite complex. Adding to this complexity is the nature of how charges are introduced into organic materials, which will be discussed in the next Section. It is, however, imperative that an understanding of these phenomena be obtained so that device performance can be improved allowing for their integration into architectures designed for many modern applications.

The organic molecules, as discussed, have their electrons distributed in molecular orbitals at different energies, the energy levels for each orbital corresponding to the amount of energy required to remove the electron from that orbital to the vacuum level (off the molecule) [70]. The highest molecular orbital in the molecule which is filled with electrons is referred to as the highest occupied molecular orbital or HOMO. The lowest unoccupied molecular orbital is called the LUMO [70]. When these molecules form solid phases, either crystalline, polycrystalline or amorphous, the HOMO and LUMO rearrange themselves to form concentrated bands of energy states [70]. In a highly conductive polymer (similar to a metal), the HOMO and LUMO levels are very close to each other or overlapping and there is a large number of empty energy states in the LUMO level so that electrons previously confined to a particular state in the HOMO level can now easily find new states to occupy and become mobile. In a semiconductor these two energy levels are separated by a forbidden gap which is usually low enough in energy to allow electrons to be excited into the LUMO level with a moderate amount of added energy (either thermal or optical). When an electron is excited like this it leaves a hole in the HOMO level. An insulator has a very wide forbidden gap and therefore is unlikely to have any mobile carriers in the LUMO level. Another way to get carriers, holes and electrons into the HOMO and LUMO level is to inject them from an outside source like a metal contact.

When carriers are excited or added to organic molecules in the crystal, they exist as ionic states on a particular molecule [70]. Transport occurs by transitioning these states from one molecule to the other [70]. Due to the relatively weak intermolecular interactions between molecules in organic crystals, which are governed primarily by van der Waals forces (a blanket term for various attractive forces between atoms and molecules which include dipole-dipole interactions, induced dipole-dipole interactions,

and induced dipole-induced dipole interactions which are also called dispersion forces [47]), HOMO and LUMO levels can be further stabilized (indicating a reduction in the energy of the HOMO and LUMO levels and thus their energy separation) by the fact that organic materials can be polarized upon formation of these ionic states [70]. A molecular ion in the crystal lattice deforms the other molecules around them by inducing a dipole, i.e., a polarization, which lowers the energy of the ionic state [70]. The carrier combined with its polarized lattice distortion is called a polaron. Small polarons are those in which this lattice polarization does not extend beyond a single lattice site. Large polarons extend to many lattice sites within the crystal [70]. The polarization causes the carrier to become localized on that crystal site, reducing its mean free path and making movement to the next site more difficult (mean free path of most polyacenes is on the order of the intermolecular spacing at room temperature) [70]. In an inorganic semiconducting crystal, such as germanium, there is significantly less polarization of the lattice due to the crystals strong covalent inter-atomic bonds, and thus the carrier is delocalized over a large portion of the crystal (the mean free path of Ge at room temperature is 1000Å while the inter-atomic spacing is 2.45Å) [70].

Polaron transport can occur through three predominant mechanisms depending on whether the polarization energy is larger than the interaction energy of a lattice site to its neighbor [70]. The first is band transport which is similar to the case of inorganic semiconductors. Band transport dominates when carriers move as highly delocalized waves in a wide carrier band with a large mean free path (Ge has a valence band (holes) • 3eV, a relatively high scattering time of 10^{-3} seconds, and a mean free path discussed earlier) [70]. It is characterized by a power law dependence of mobility to temperature shown in equation VI:

$$\mu \propto T^{-n}, n > 1 \qquad \text{VI}$$

Band transport puts the most emphasis on the collective nature of conduction states [70].

The second is thermally activated hopping which involves highly localized carriers which move by hopping from one site to another at the same energy level [70] (energy levels can be adjusted and brought into coincidence by phonon coupling [71]). In materials where this mechanism dominates, there is a narrow carrier band, very low time between scattering events, and low mean free paths [70]. The relationship between mobility and temperature in this type of transport is characterized in equation VII:

$$\mu \propto e^{(\frac{-E}{kT})} \qquad \text{VII}$$

where E is the activation energy, k is Boltzmann's constant [70]. Thermally activated hoping puts the most emphasis on the molecular nature of conduction states [70]. Hopping transport is dependent on intermolecular overlap [72]. The polaron binding energies for most polyacenes are in the range of 21-35 meV [70]. There are two theories to describe the hopping transport of small polarons, the theories of correlated and uncorrelated hopping [70]. Uncorrelated hopping occurs when the lattice polarization relaxes faster than the mean time between hops so that future hops can be considered independent of past hops [71]. Correlated hopping occurs when the lattice polarization does not relax faster than the time until the next hop, so that hopping to a new site is influenced by the site on which the carrier was previously due to a transfer of the relaxation energy [71]. This form of hopping actually has a reduced activation energy and thus the temperature dependence of this mode of transport is significantly reduced [71]. Correlated hopping is considered when the mobility of the organic material approaches 1 cm^2/Vs [71]. There are examples of organic semiconductors which

demonstrate both hopping and band-like transport, such as in some of the polyacenes, with a transition from one to the other occurring at low temperatures [70].

The third transport mechanism is carrier tunneling between one site and another through the barrier between them [73]. This mechanism is temperature independent.

These transport mechanisms occur in pristine crystals. The transport in most OTFTs, however, is largely governed by traps [13]. Traps, or impurities or physical deformities in the crystal lattice, can create energy levels in the forbidden gap into which carriers can fall energetically [70]. These carriers can then not participate in normal conduction and are stuck in position spatially. When there is a vacancy in the crystal lattice, the extent of the polarization of the surrounding material will be reduced by the fact that there will be a portion of the material which will not participate in polarization. This effect is even more pronounced at the surface where surface molecules are missing a significant number of their neighbors (there are no dangling bonds in organic materials since each lattice site is composed of a full molecule) [70]. This reduction in polarization increases the energy of that state since the polarization energy is less and can now act as a scattering center for those materials exhibiting band transport [70]. Conversely, compression to the lattice increases polarization energy and thus forms a trap since this energy can push the energy state of that lattice site into the forbidden gap [70]. Both trapping and scattering are detrimental to obtaining high mobilities. Large amounts of disorder in the crystal can create a situation where the polarization energies of the different lattice sites within the crystal are not all the same [70]. This disparity creates a spreading of the bands at the HOMO and LUMO levels [70]. This energy level spreading has been modeled as either a Gaussian distribution of energy states or an exponentially decaying distribution of energy states from the edge of the HOMO (for holes) or LUMO (for electrons) bands with the tails of the distributions extending into the band gap [70].

As these distributions tail off, the density of states close enough in energy and space for a carrier to hop to becomes significantly reduced, and thus these energy levels can act as traps [13].

Depending on the organic semiconductor deposition conditions, even in transistors made from highly purified materials (low impurity concentrations), the boundaries between grains can be highly disordered [74]. It is thus these grain boundaries which dominate transport in these devices [74]. The hopping mechanism in this case is between disorder-induced localized states with activation energies much larger than the polaron binding energy, around 130 meV (depending on deposition conditions) and follows a Poole-Frenkel relationship with Coulomb potential barriers which can be lowered by the longitudinal electric field (electric field from source to drain) [74]. This is influenced by the amount of charge accumulated by the gate field [74]. Figure 23 shows mobility (μ) versus longitudinal electric field (•(V_{DS}/L), where L is the channel length) for transistors fabricated with several different channel lengths [74]. The graph show fits for the Poole-Frenkel model and the polaron model for two different temperatures. It is clear from this data that the Poole-Frenkel model fits that data more closely [74]. The Poole-Frenkel relationship predicts a dependence of mobility to temperature as seen in equation VIII as opposed to the dependence seen in equation VII [74].

$$\mu \propto e^{(\frac{-\beta\sqrt{E}}{kT})} \qquad \text{VIII}$$

where is the field dependent coefficient as proposed by Gill in an empirical relation [75].

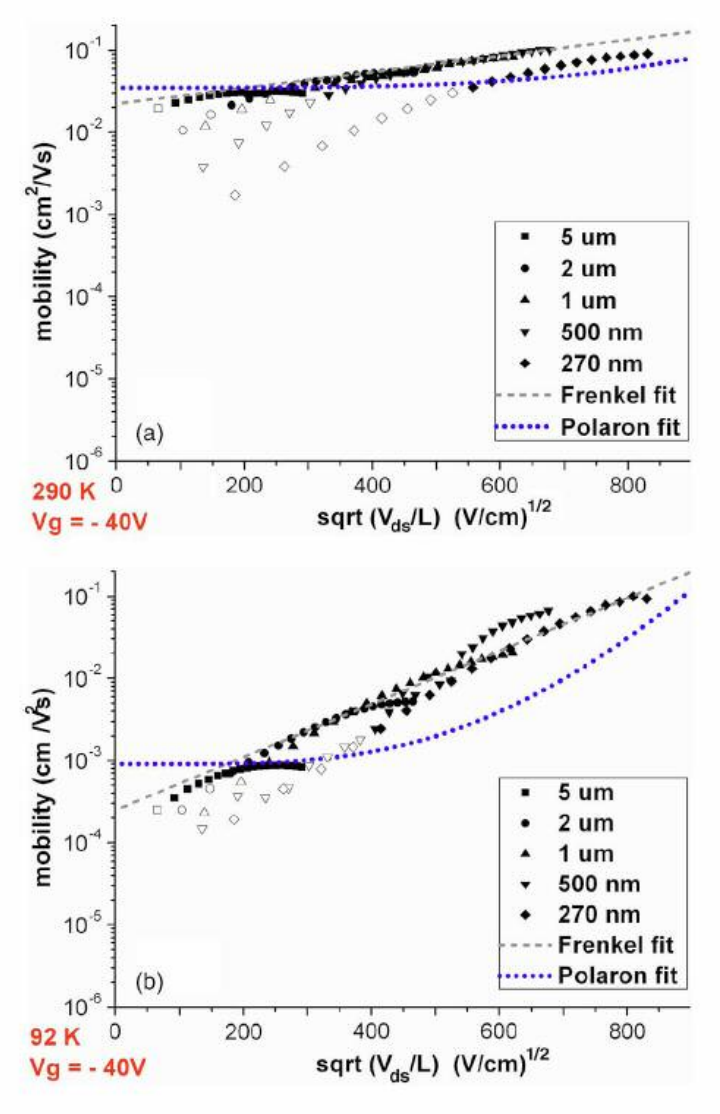

Figure 28. Mobility (μ) vs. longitudinal electric field (•(V_{DS}/L)) for OTFTs of several channel lengths. The gray dotted line and the purple dotted line are the fits for the Poole-Frenkel model and the polaron model respectively. It is clear the Poole-Frenkel model for transport in a disordered system fits the data more accurately. "Reprinted with permission from Liang Wang, Daniel Fine, Debarshi Basu, Ananth Dodabalapur, "Electric-field-dependent charge transport in organic thin-film transistors." *Journal of Applied Physics* vol. 101, article # 054515 (2007) pp. 1-8 and the American Institute of Physics."

2.7 INJECTION EFFECTS IN OTFTS

In addition to considering how carriers move through the semiconductor, it is also important to understand how they are injected into the semiconductor. Unlike silicon, where the use of doping can shield the channel from the metal contacts by adjusting the energy level difference between the silicon Fermi level and the metal work function to make the contacts ohmic (an indication that charge transport is not limited by the nature of the contact), organic transistors usually have metal contacts deposited directly on to the active material. There are reports of using doped regions directly adjacent to the metal contact [76] or self assembled monolayers chemically attached onto the contact to improve the injection characteristics [77]. Careful consideration must be made as to what types of metals to use and whether to chemically modify the contacts in order to get the most efficient charge injection.

The typical choice of metal for many p-type materials, such as pentacene, is gold due to the close alignment of the work function of gold to many p-type organic semiconductors' ionization energies (the amount of energy to take an electron from the HOMO level to the vacuum level) (•5.1 eV for both) [1, 56], and the fact that gold is inert. Investigations into contact resistances using scanning-probe potentiometry have shown that large resistances can be associated with Schottky barriers caused by the work function of the metal being significantly lower than the ionization energy of the semiconductor (this is for p-type semiconductors) [78]. This energy mismatch also produces reduced (in terms of noninjection limited current), super linear current at low source to drain potentials [78]. By changing metals (and thus work function) Bürgi *et al* demonstrated that the contact resistance varies exponentially with the Schottky barrier height after a certain threshold, depending on the semiconductor (their study used

polymers) [78]. The barrier height that was measured, however, was lower than that predicted by previous reports of diffusion limited thermionic emission [78]. Furthermore, they suggested that below this Shottky barrier threshold, the contact resistance is dominated not by injection but by transport through the depleted layer of the semiconductor adjacent to the contact [78]. In this region, there is no channel formation induced by the gate either because an ionization energy/work function difference has created a reverse electric field which opposes the source to drain electric field (dominant at the source), or the drain potential is too close to the gate potential which precludes accumulation near the drain [78]. This would be alleviated by increasing the gate potential [78].

As was mentioned earlier, the surfaces of most organics usually have lower polarization energies due to lattice sites which have incomplete numbers of neighbors [70]. When the metal is deposited on the surface, however, the polarization of the organic lattice sites just inside the contact can be much higher because metals are usually quite polarizable in that they can produce image charges [70]. HOMO and LUMO bands could then be adjusted or split at the metal/organic interface since the polarization energy is larger at the interface and thus the forbidden energy gap, E_g, would be expected to get smaller. This has been demonstrated for pentacene and gold by F. Amy *et al* using ultra-violet photoemission spectroscopy (UPS) and inverse photoemission spectroscopy (IPES) [79]. There studies have quantified the band gap narrowing of pentacene at the contact [79]. They have also shown an interface dipole forming at the pentacene/gold contact which has also been shown by Diao *et al* and increases the injection barrier by about 0.5-0.6 eV [79, 80]. Diao *et al* used sandwiches of various metals around pentacene to measure their Schottky barrier behavior and extract the dipole shift from the diode reverse bias currents [80]. This dipole is represented as a shift of the vacuum level in the

organic so that the metal and organic vacuum levels are no longer aligned (see figure 24) [81, 82].

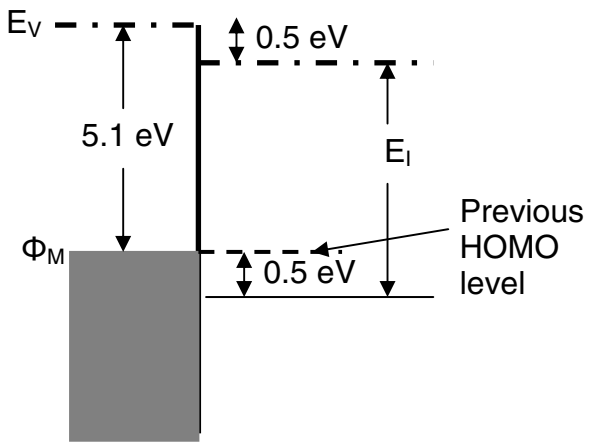

Figure 29 Schematic of the interface dipole for pentacene/gold showing the vacuum level shift (LUMO level is not shown) [80].

Injection issues usually get worse as devices are scaled. Work by Wang *et al* demonstrated that nanoscale devices usually suffer from significant injection limitations [54]. This may be due to a significant amount of disorder near the contact from morphology differences between the semiconductor deposited on the dielectric to the semiconductor deposited on the metal [78]. Furthermore, shadowing effects can occur from the metal contacts which are deposited first in the bottom contact configuration [78]. These problems seem to become much worse as the channel size is scaled down. Wang *et al* also demonstrated, however, that in some of these devices, when considering the high electric fields present at these small source/drain geometries, Fowler-Nordheim tunneling is possible [54]. This tunneling occurs through a triangular potential barrier at the source when the barrier width is thinned by the high electric field. Instead of needing enough thermal energy to surmount the entire barrier height, carriers now need only to reach an energy level from which they can tunnel, thus effectively reducing the injection barrier height [54]. This barrier height can be further reduced by applying a gate bias.

Further data from the studies demonstrating the Poole-Frenkel relationship depicted in the previous section (see Figure 30) show a departure from normal semiconductor limited transport when the channel sizes get sufficiently small [81].

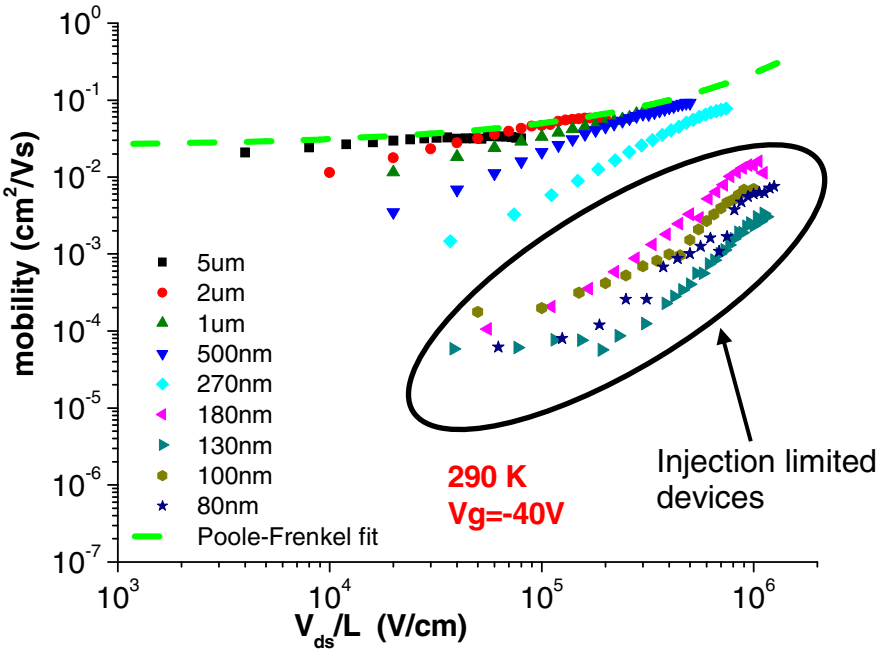

Figure 30. Mobility (μ) vs. longitudinal electric field (•(V_{DS}/L)) for OTFTs of several channel lengths. The dashed green line is a fit for the Poole-Frenkel model. The circled data indicate devices which due not fit the Poole-Frenkel model and therefore constitute injection limited devices [81].

Understanding injection limitations is crucial to improving the design and fabrication for better organic devices. It is also crucial to being able to evaluate the potential of new materials. As we will see in Chapter 3, it is vital to understanding the chemical sensing response of OTFTs to many classes of analytes.

2.8 REFERENCES

1. Daniel R. Gamota, Paul Brazis, Krishna Kalyanasundaram, Jie Zhang, Printed Organic and Molecular Electronics, (Kluwer Academic Publishers, 2004) pp. 1-36

2. R. Farchioni, G. Grosso, Organic Electronic Materials,(Springer-Verlag, 2001) pp. 215-219

3. P. F. Baude, D. A. Ender, T. W. Keller, M. A. Haase, D. V. Muyres, S. D. Theiss, "Organic semiconductor RFID transponders." *Electron Deivces Meeting, 2003, IEDM '03 Technical Digest, IEEE International* (December 8-10, 2003) pp. 8.11-8.14

4. Yoshinori Fukuda, Teruichi Watanabe, Takeo Wakimoto, Satoshi Miyaguchi, Masami Tsuchida, "An organic LED display exhibiting pure RGB colors." *Synthetic Metals* vol. 111-112 (2000) pp. 1-6

5. Lisong Zhou, Sungkyu Park, Bo Bai, Jie Sun, Sheng-Chu Wu, Thomas N. Jackson, Shelby Nelson, Diane Freeman, Yongtaek Hong, "Pentacene TFT Driven AM OLED Displays." *IEEE Electron Device Letters* vol. 26 no. 9 (September 9, 2005) pp. 640-642

6. Jefrey T. Mabeck, George G. Malliaras, "Chemical and biological sensors based on organic thin-film transistors." *Analytical and Bioanalytical Chemistry* vol. 384 (2006) pp. 343-353

7. John A. Rogers, Zhenan Bao, Kirk Baldwin, Ananth Dodabalapur, Brian Crone, V. R. Raju, Valerie Kuck, Howard Katz, Karl Amundson, Jay Ewing, Paul Drzaic, "Paper-like electronic displays: Large-area rubber-stamped plastic sheets of electronics and microencapsulated electrophoretic inks." *Proceedings of the National Academy of Science* vol. 98 no. 9 (April 24, 2001) pp. 4835-4840

8. Organic Electronics Conference and Exhibition 2007, “Organic semiconductors: What’s it all about?” Display Technology Investor (October 2005) http://www.oec-europe.com/persp_overview.htm

9. David L. Margulius, “WHAT’S NEXT; With an Organic Sensor, a Food Wrapper Sniffs Out Trouble.” The New York Times 4 April 2002: http://query.nytimes.com/gst/fullpage.html?res=9907E6D8103AF937A35757C0A9649C8B63

10. Noel S. Hush, “An Overview of the First Half-Century of Molecular Electronics.” *Molecular Electronics III, Annals of the New York Academy of Sciences* vol. 1006 (December 2003) pp. 1-20

11. H. Shirakawa, C. K. Chiang, C. R. Fincher, Jr., Y. W. Park, E. J. Louis, S. C. Gau, A. J. Heeger, Alan G. MacDiarmid, “Electrical Conductivity in Doped Polyacetylene.” *Physical Review Letters* vol. 39, no. 17(October 24, 1977) pp. 1098-1101

12. Bengt Nordén, Eva Krutmeijer, Nobel Prize Advanced Information, “The Nobel Prize in Chemistry, 2000: Conductive Polymers” Kungl. Vetenskapsakademien The Royal Swedish Academy of Sciences http://nobelprize.org/nobel_prizes/chemistry/laureates/2000/chemadv.pdf

13. Wolfgang Brütting, Physics of Organic Semiconductors, (WILEY-VCH Verlag GmbH & Co. KGaA, 2005) pp.1-13, 273-276, 396-400

14. Norman R. Mowrer, “Polysiloxanes.” *Ameron International Performance Coatings and Finishes* (November 2003) pp. 1-11 http://www.ameronpsx.com/docs/presentation_polysiloxanes.pdf

15. A. Tsumura, H. Koezuka, T. Ando, “Macromolecular electronic device: Field-effect transistor with a polythiophene thin film.” *Applied Physics Letters* vol. 49, iss. 18 (November 3, 1986) pp. 1210-1212

16. Zhenan Bao, Ananth Dodabalapur, Andrew J. Lovinger, “Soluble and processable regioregular poly(3-hexylthiophene) for thin film field-effect transistor applications with high mobility.” *Applied Physics Letters* vol. 69, iss. 26(December 23, 1996) pp. 4108-4110

17. C. W. Tang, “Two-layer organic photovoltaic cell.” *Applied Physics Letters* vol. 48, no. 2(January 13, 1986) pp. 183-185

18. The Encyclopedia of Alternative Energy and Sustainable Living, A resource of *The Worlds of David Darling*
http://www.daviddarling.info/encyclopedia/F/AE_fill_factor.html

19. Holger Spanggard, Frederik C. Krebs, “A brief history of the development of organic and polymeric photovoltaics.” *Solar Energy Materials & Solar Cells* vol. 83(2004) pp. 125-146

20. C. W. Tang, S. A. VanSlyke, “Organic electroluminescent diodes.” *Applied Physics Letters* vol. 51, no. 12(September 21 1987) pp. 913-915

21. C. Clarisse, M. T. Riou, M. Gauneau, M. Le. Contellec, “Field-Effect Transistor with Diphthalocyanine Thin Film.” *Electronic Letters* vol. 24, no. 11(May 26, 1988) pp. 674-675

22. Ana C. Arias, Joaquim R. de Lima, Ivo A. Hümmelgen, “Tin Oxide as a Cathode in Organic Light-Emitting Diodes.” *Advanced Materials* vol. 10, no. 5(1998) pp. 392-394

23. J. H. Burroughes, D. D. C. Bradley, A. R. Brown, R. N. Marks, K. Mackay, R. H. Friend, P. L. Burns, & A. B. Holmes, "Light-emitting diodes based on conjugated polymers." *Nature* vol. 347(October 11 1990) pp. 539-541

24. Hedi Mattoussi, Hideyuki Murata, Charles Merritt, Yasuhiro Iizumi, Junji Kido, Zakya H. Kafafi, "Photoluminescence quantum yield of pure and molecularly doped organic solid films." *Journal of Applied Physics* vol. 86, no. 5 (September 1, 1999) pp. 2642-2650

25. S. F. Nelson, Y. Y. Lin, D. J. Gundlach, T. N. Jackson, "Temperature-independent transport in high-mobility pentacene transistors." *Applied Physics Letters* vol. 72 no. 15 (April 13, 1998) pp. 1854-1856

26. D. J. Gundlach, Y. Y. Lin, T. N. Jackson, S. F. Nelson, D. G. Schlom, "Pentacene Organic Thin-Film Transistors—Molecular Ordering and Mobility." *IEEE Electron Device Letters* vol. 18, no. 3(March 1997) pp. 87-89

27. Sung Kyu Park, Chung-Chen Kuo, J. E. Anthony, T. N. Jackson, "High mobility solution-processed OTFTs." *Electron Devices Meeting, 2005 IEDM Technical Digest, IEEE International* (December 5-7, 2005) pp. 4-7

28. Joyce G. Laquindanum, Howard E. Katz, Ananth Dodabalapur, Andrew J. Lovinger, "n-Channel Organic Transistor Materials Based on Napthalene Frameworks." *Journal of the American Chemical Society* vol. 118(1996) pp. 11331-11332

29. J. Kastner, J. Paloheimo, H. Kuzmany, in Solid State Sciences, edited by H. Kuzmany, M. Mehring, J. Fink (Springer, New York, 1993) pp. 512-515

30. R.C. Haddon, A. S. Perel, R. C. Morris, T. T. M. Palstra, A. F. Hebard, R. M. Fleming, "C_{60} thin film transistors." *Applied Physics Letters* vol.67, iss. 1(July 3, 1995) pp 121-123

31. Antonio Facchetti, "Semiconductors for organic transistors." *Materials Today* vol. 10, no. 3 (March 2007) pp. 28-37

32. A. R. Brown, D. M. deLeeuw, E. J. Lous, E. E. Havinga, :Organic n-type field-effect transistor.", *Synthetic Metals* vol. 66, iss. 3 (October 1994) pp. 257-261

33. Zhenan Bao, Andrew J. Lovinger, Janelle Brown, "New Air-Stable n-Channel Organic Thin Film Transistors." *Journal of the American Chemical Society* vol. 120 (1998) pp. 207-208

34. C. Hosokawa, M. Eida, M. Matsuura, K. Fukuoka, H. Nakamura, T. Kusumoto, "Organic multi-color electroluminescence display with fine pixels." *Synthetic Metals* vol. 91(1997) pp. 3-7

35. Liang Wang, Daniel Fine, Debarshi Basu, Ananth Dodabalapur, "Electric-field-dependent charge transport in organic thin-film transistors." *Journal of Applied Physics* vol. 101, article #054515(2007) pp. 1-8

36. Reji Hattori, Tsutomu Tsukamizu, Ryusuke Tsuchiya, Kazunori Miyake, Yi He, Jerzy Kanicki, "Current-Writing Active-Matrix Circuit for Organic Light-Emitting Diode Display using a-Si:H Thin-Film-Transistors." *IEICE Trans. Electron* vol. E83-C, no. 5 (May 2000) pp. 779-782

37. H. Sirringhaus, T. Kawase, R. H. Friend, T. Shimoda, M. Inbasekaran, W. Wu, E. P. Woo, "High-Resolution Inkjet Printing of All-Polymer Transistor Circuits." *Science* vol. 290 (December 15, 2000) pp. 2123-2126

38. Yanming Sun, Yunqi Liu, Daoben Zhu, "Advances in organic field effect transistors." *Journal of Materials Chemistry*, 15(2005) pp. 53-65

39. B. Crone, A. Dodabalapur, A. Gelperin, L. Torsi, H. E. Katz, A. J. Lovinger, "Electronic sensing of vapors with organic transistors." *Applied Physics Letters* vol. 78, no. 15 (April 9, 2001) pp. 2229-2231

40. B. Bott, T. A. Jones, "High sensitivity NO sub(2) sensor based on electrical conductivity changes in phthalocyanine films." *Sensors and Actuators* vol. 5, no. 1 (1984) pp. 43-53

41. R. Zhou, F. Josse, W. Göpel, Z. Z. Öztürk, Ö. Bekaro lu, "Phthalocyanines as Sensitive Materials for Chemical Sensors." *Applied Organometallic Chemistry* vol. 10 (1996) pp. 557-577

42. A. Oprea, U. Weimar, E. Simon, M. Fleischer, H. P. Frerichs, Ch. Wilbertz, M. Lehmann, "Copper phthalocyanine suspended gate field effect transistors for NO_2 detection." *Sensors and Actuators B* vol. 118 (2006) pp. 249-254

43. Luisa Torsi, Ananth Dodabalapur, "Organic Thin-Film Transistors as Plastic Analytical Sensors." *Analytical Chemistry* vol. 77, iss. 19 (October 1, 2005) pp. 380A-387A

44. L. Torsi, A. Dodabalapur, L. Sabbatini, P. G. Zambonin, "Multi-parameter gas sensors based on organic thin-film-transistors." *Sensors and Actuators B* vol. 67 (2000) pp. 312-316

45. Jeffrey T. Mabeck, George G. Malliaras, "Chemical and biological sensors based on organic thin-film transistors." *Analytical and Bioanalytical Chemistry* vol. 384(2006) pp. 343-353

46. Daniel A. Brenards, Gilman E. S. Toombes, George G. Malliaras, Sol M. Gruner, "Gating of an organic transistor through a bilayer lipid membrane with ion channels." *Applied Physics Letters* vol. 89 article no. 053505 (2006) pp. 1-3

47. William H. Brown, Christopher S. Foote, Organic Chemistry, 2nd Edition, (Saunders College Publishing, 1998) pp.30-40

48. David W. Oxtoby, H. P. Gillis, Norman H. Nachtrieb, Principles of Modern Chemistry, 4th Edition, (Saunders College Publishing, 1999) pp. 581-600

49. Jihmei Luo, Harold Hart, "Linear Acene Derivatives. New Routes to Pentacene and Naphthacene and the First Synthesis of a Triptycene with Two Anthracene Moieties." *The Journal of Organic Chemistry* vol. 52, no. 22 (October 30, 1987) pp. 4833-4836

50. William J. Bailey, Milton Madoff, "Cyclic Dienes. II. A New Synthesis of Pentacene." *New Synthesis of Pentacene* [Contribution from the Department of Chemistry, Wayne University] (November 20, 1953) p. 5603

51. B. I. Kharisov, U. Ortiz, Méndez, L. A. Garza-Rodríguez, H. M. Leija Gutiérrez, A. Medina Medina, S. S. Berdonosov, "Use of various activated forms of elemental nickel

and copper for the synthesis of phthalocyanine at low temperature." *Journal of Coordination Chemistry* vol. 59, iss. 15(October 15, 2006) pp. 1657-1666

52.Tian-An Chen, Xiaoming Wu, Reuben D. Rieke, "Regiocontrolled synthesis of Poly(3alkylthiophenes) Mediated by Rieke Zinc: Their Characterization and Solid-State Properties." *Journal of the American Chemical Society* vol. 117 (1995) pp. 233-244

53. Maria Cristina Tanese, Daniel Fine, Ananth Dodabalapur, Nicola Cioffi, Luisa Torsi, "High Performance Organic Thin Film Transistor Sensors." Organic Field-Effect Transisoros III *Proceedings of SPIE* vol. 5522 (October, 2004) pp.22-26

54. Liang Wang, Daniel Fine, Taeho Jung, Debarshi Basu, Heinz von Seggern, Ananth Dodabalapur, "Pentacene field-effect transistors with sub-10-nm channel lengths." *Applied Physics Letters* vol. 85, no. 10 (September 6, 2004) pp. 1772-1774

55. Zhenan Bao, Valerie Kuck, John A. Rogers, Mark A. Paczkowski, "Silsesquioxane Resins as High-Performance Solution Processible Dielectric Materials for Organic Transistor Applications." *Advanced Functional Materials* vol. 12, no. 8(August 2002) pp 526-531

56. Lei Diao, Dominic D. Schroepfer, C. Daniel Frisbie, P. Paul Ruden, "Electrical characterization of metal/pentacene contacts." *Journal of Applied Physics* vol. 101, article #014510 (2007) pp. 1-8

57. Product Data Sheet, "AZ 5214 E Image Reversal Photoresist" Clariant Corporation http://groups.mrl.uiuc.edu/dvh/pdf/AZ5214E.pdf

58. JEOL Ltd. Instruction manual (IEB6FSE-GS-1 (1720)), JBX-6000FS/E: General Statement, (JEOL, Ltd., 2002)

59. V. Jaubert, P. Lucas, L. Mollard, S. Tedesco, B. Dal'zotto, S. Landis, "Characterization of charging effect on 8" wafer during e-beam lithography exposure." *Microelectronic Engineering* vol. 67-68(2003) pp 149-156

60. J. Laconte, F. Iker, S. Jorez, N. André, J. Proost, T. Pardoen, D. Flandre, J. P. Raskin, "Thin films stress extraction using micromachined structures and wafer curvature measurements." *Microelectronic Engineering* vol. 76(2004) pp. 219-226

61. V. Y. Bulko, X. Chi, D. V. Lang, A. P. Ramirez, "Field-effect transistor on pentacene single crystal." *Applied Physics Letters* vol. 83, no. 23 (December 8, 2003) pp. 4773-4775

62. D. Knipp, R. A. Street, A. VöLkel, J. Ho, "Pentacene thin film transistors on organic dielectrics: Morphology, structural properties, and electronic transport." *Journal of Appied Physics* vol. 93, no. 1(January 1, 2003) pp. 347-355

63. Byungwook Yoo, Brooks A. Jones Taeho Jung, Debarshi Basu, Antonio Facchetti, Michael R. Wasielewski, Tobin Marks, Ananth Dodabalapur, "High-mobility bottom-contact *n*-channel organic transistors and their use in complementary ring oscillators." *Applied Physics Letters* vol. 88, article # 082104 (2006) pp. 1-3

64. J. L. Brédas, J. P. Calbert, D. A. Da Silva Filho, J. Cornil, "Organic semiconductors: A theoretical characterization of the basic parameters governing charge transport." *Proceeding of the National Academy of Sciences* vol. 99, no. 9(April 30, 2002) pp. 5804-5809

65. Siddharth Mohapatra, Michelle Grigas, Robert Wenz, Robert Rotzoll, Viorel Olariu, Oleg Shchekin, Klaus Dimmler, Ananth Dodabalapur, "High Mobility Pentacene Field

Effect Transistors on Plastic." *Materials Research Society Symposium Proceedings* vol. 870E (Materials Research Society, 2005) pp. H3.2.1-H3.2.6

66. Christine C. Mattheus, Gilles A. de Wijs, Robert A. de Groot, Thomas T. M. Palstra, "Modeling the Polymorphism of Pentacene." *Journal of the American Chemical Society* vol. 125, no. 20 (2003) pp. 6323-6330

67. A. Dodabalapur, L. Torsi, H. E. Katz, "Organic Transistors: Two-Dimensional Transport and Improved Electrical Characteristics" *Science* vol. 268 (April 14, 1995) pp. 270-271

68. Zhenan Bao, Andrew J. Lovinger, Ananth Dodabalapur, "Organic field-effect transistors with high mobility based on copper phthalocyanine." *Applied Physics Letter* vol. 69, iss. 20(November 11, 1996) pp. 3066-3068

69. Yen-Yi Lin, David J. Gundlach, Shelby F. Nelson, Thomas N. Jackson, "Pentacene-Based Organic Thin-film Transistors." *IEEE Transactions on Electron Devices* vol. 44, no. 8(August 1997) pp. 1325-1331

70. Martin Pope, Charles E. Swenberg, Electronic Processes in Organic Crystals and Polymers, (Oxford University Press, 1999) pp. 202-369

71. David Emin, "Correlated Small-Polaron Hopping Motion" *Physical Review Letters* vol. 25, no. 26 (December 28, 1970) pp.1751-1755

72. J. L. Brédas, J. P. Calbert, D. A. Da Silva Filho, J. Cornil, "Organic semiconductors: A theoretical characterization of the basic parameters governing charge transport" *Proceedings of the National Academy of Sciences* vol. 99, no. 9 (April 30, 2002) pp. 5804-5809

73. S. Jeyadev, J. R. Schrieffer, “Interchain polaron tunneling in *trans*-polyacetylene” *Physical Review B* vol. 30, no. 7 (October 1, 1984) pp. 3620-3624

74. Liang Wang, Daniel Fine, Debarshi Basu, Ananth Dodabalapur, “Electric-field-dependent charge transport in organic thin-film transistors.” *Journal of Applied Physics* vol. 101, article # 054515 (2007)

75. W. D. Gill, “Drift mobilities in amorphous charge-transfer complexes of trinitrofluorenone and poly-*n*-vinylcarbazole” *Journal of Applied Physics* vol. 43, no. 12 (December 12, 1972) pp. 5033-5040

76.Yulong Shen, Ahmad R. Hosseini, Man Hoi Wong, George G. Malliaras, “How To Make Ohmic Contacts to Organic Semiconductors” *ChemPhysChem* vol. 5 (2004) pp. 16-25

77. David J. Gundlach, Thomas N. Jackson, “Pentacene TFT With Improved Linear Region Characteristics Using Chemically Modified Source and Drain Electrodes” *IEEE Electron Device Letters* vol. 22, no. 12 (December 2001) pp. 571-573

78. L. Bürgi, T. J. Richards, R. H. Friend, H. Sirringhaus, “Close look at charge carrier injection in polymer field-effect transistors” *Journal of Applied Physics* vol. 94, no. 9 (November 1, 2003) pp. 6129-6137

79. F. Amy, C. Chan, A. Kahn, “Polarization at the gold/pentacene interface” *Organic Electronics* vol. 6 (2005) pp. 85-91

80. Lei Diao, Dominic D. Schroepfer, P. Paul Ruden, C. Daniel Frisbie, “Electrical characterization of metal/pentacene contacts” *Journal of Applied Physics* vol. 101, article# 014510 (2007) pp. 1-8

81. Liang Wang, Daniel Fine, Debarshi Basu, Ananth Dodabalapur (unpublished)

CHAPTER 3 ORGANIC THIN-FILM TRANSISTORS (OTFTS) AS CHEMICAL SENSORS

Organic thin-films, such as the various forms of the phthalocyanines, have been shown to sensitively detect certain gases, such as electron withdrawing NO_2, when utilized as either chemically sensitive resistors (chemiresistors) or sensitizing layers for silicon chemical field-effect transistors (CHEMFETs) [1, 2]. These devices have achieved detection limits in the 50 parts-per-billion (ppb) range [1]. There have also been reports of organic thin-film field-effect transistors which have been used to detect organic vapors which do not chemically react with the sensing material, such as vapors composed of polar organic molecules [3]. These transistor sensors have been measured achieving detection limits of 10 ppm, but they are predicted to be able to go as low as 1 ppm for many types of these organic vapors [3].

It is the goal of this Chapter to explore the interaction between organic vapors and organic semiconductor thin-film transistors in order to understand how these sensors produce their responses to these analytes. Furthermore, interesting changes to these sensor responses occur as these devices are scaled down to nanometer dimensions which shall also be described. Finally in Chapter 3, device architectures which can further exploit these interactions to produce even lower detection limits and enhance vapor selectivity will be detailed.

3.1 THE CHEMICAL CHARACTERISTICS OF TARGET ANALYTES

The analytes chosen for the studies outlined in Chapter 3 consisted of high vapor pressure organic molecules. These organic molecules are shown in Figure 34 and include

alkanes, alcohols, ketones, esters, ethers, aldehydes, aromatic compounds or some combination thereof.

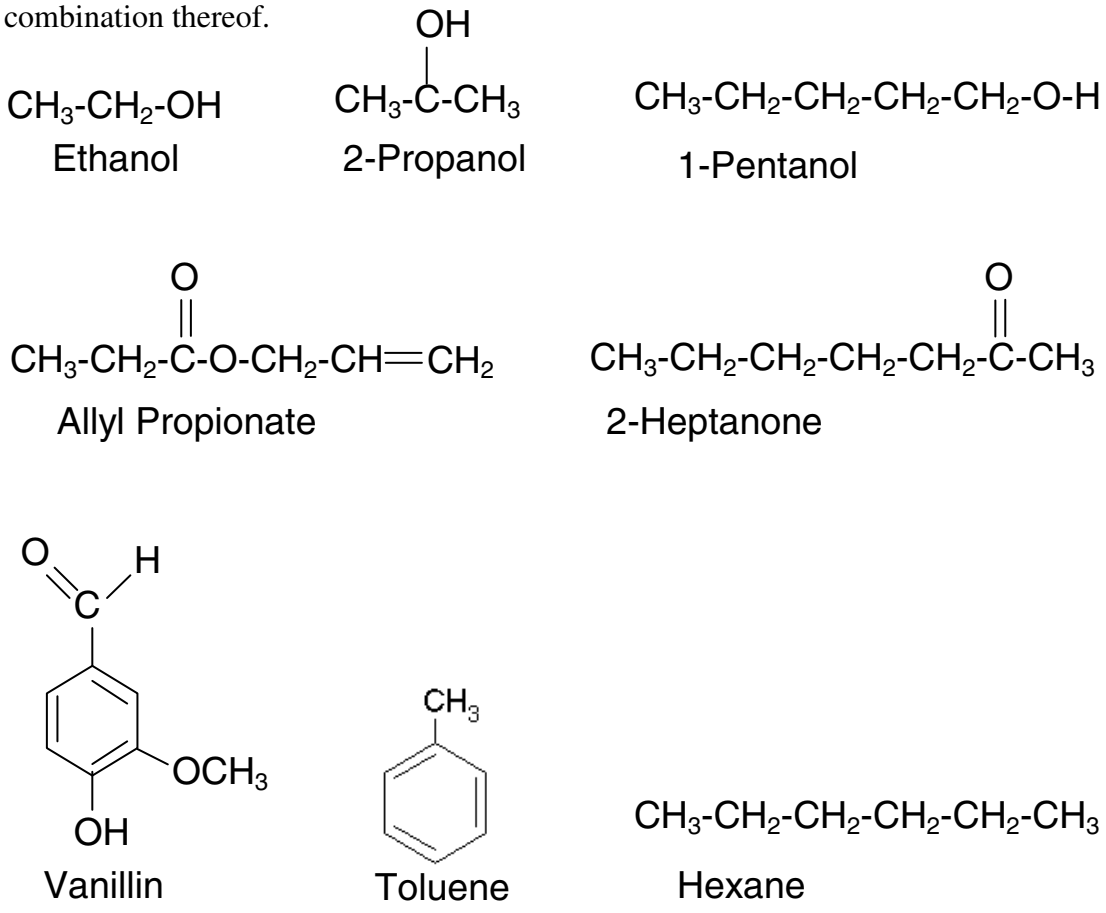

Figure 34. A list of the organic analytes used in the studies outlined in this Chapter with their molecular formulas [4].

The important aspect to notice is that almost all of these substances have moieties which are either polar, such as the carbonyl group in heptanone (C=O), or conjugated, such as the aromatic ring in toluene. The length of the alkane chain in these molecules also plays a role as well as the position of the polar functional group on the molecule, although, to first order, these considerations are not as important as the presence and dipole strength of the polar or aromatic moiety. Hexane, for example, was tried in a few experiments

utilizing copper phthalocyanine (CuPc) based OTFTs but produced no electrical response in any of them. Torsi *et al* have demonstrated the importance of alkyl chain length in the electrical responses of a pair of polythiophene derivatives to two organic alcohols, ethanol and 1-hexanol [5]. The reason for the importance of the polar or aromatic functional groups will be discussed in later Sections. Tanese *et al* have also demonstrated polymer thin films with the ability to distinguish analytes based on chirality [6], although this property of the molecules or the organic thin films will not be discussed in this thesis. It is important to remember that water vapor is also polar. Several groups have reported using organic transistors as humidity sensors [7, 8]. The importance of this property of water will also be discussed in a later Section as it relates to the polar functional groups in the organic analytes.

3.2 MEASURING THE SENSING RESPONSE OF AN OTFT TO AN ANALYTE

In order to measure the response of the OTFTs to the analytes, three experimental apparatus were used. The first apparatus is illustrated in Figure 35 and shall be referred to hereafter as experimental apparatus number 1. A peristaltic pump is used to blow air through an irrigation syringe which contains a section of filter paper saturated with one of the high vapor pressure organic analytes shown in Figure 34. The peristaltic pump is used to allow for the movement of air without exposing the pumping apparatus to the analyte being investigated. A rubber stopper with a hole in it is placed into the back of the syringe into which Tygon tubing is fed. The tip of the irrigation syringe is positioned over the active area of the OTFT using a micromanipulator.

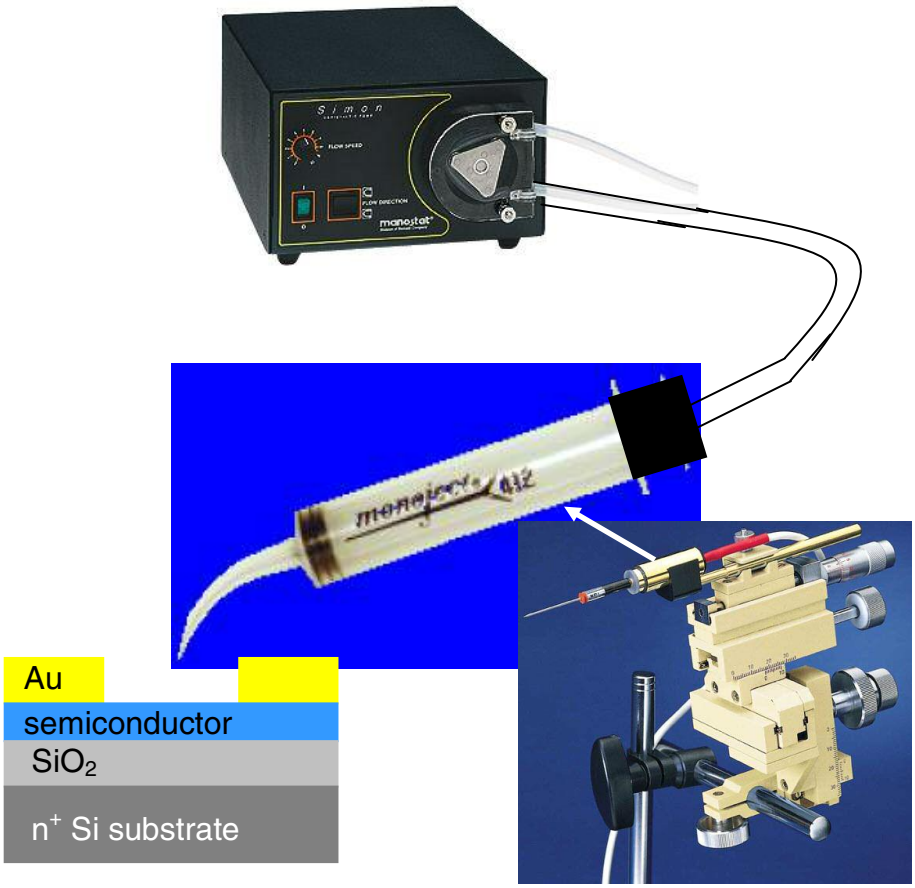

Figure 35. One experimental apparatus used for measuring the electrical response of the OTFTs to the organic analytes. A peristaltic pump was used to blow air through the irrigation syringe which contained a piece of filter paper saturated with the organic analyte. The syringe was positioned using the micromanipulator.

The apparatus shown in Figure 35 was useful in studying how the organic semiconductor would respond to the analyte. It was not as useful in determining the lower detection limits of the OTFTs since it was only capable of presenting saturated vapors to the devices. The only way to change the concentration at the surface of the transistor was to adjust the height of the tip off the surface and let the concentration adjust through diffusion. Thus, it was hard to determine precisely what the concentration was at the

surface if the tip wasn't at its closest point when it approached the known partial pressure of the organic liquid (even though it may not have been exactly that depending on whether the filter paper remained fully saturated).

In order to achieve more quantitative data, i.e., the exact concentration which the device was detecting, a second experimental apparatus was used as shown in Figure 36, which will be referred to as experimental apparatus number 2.

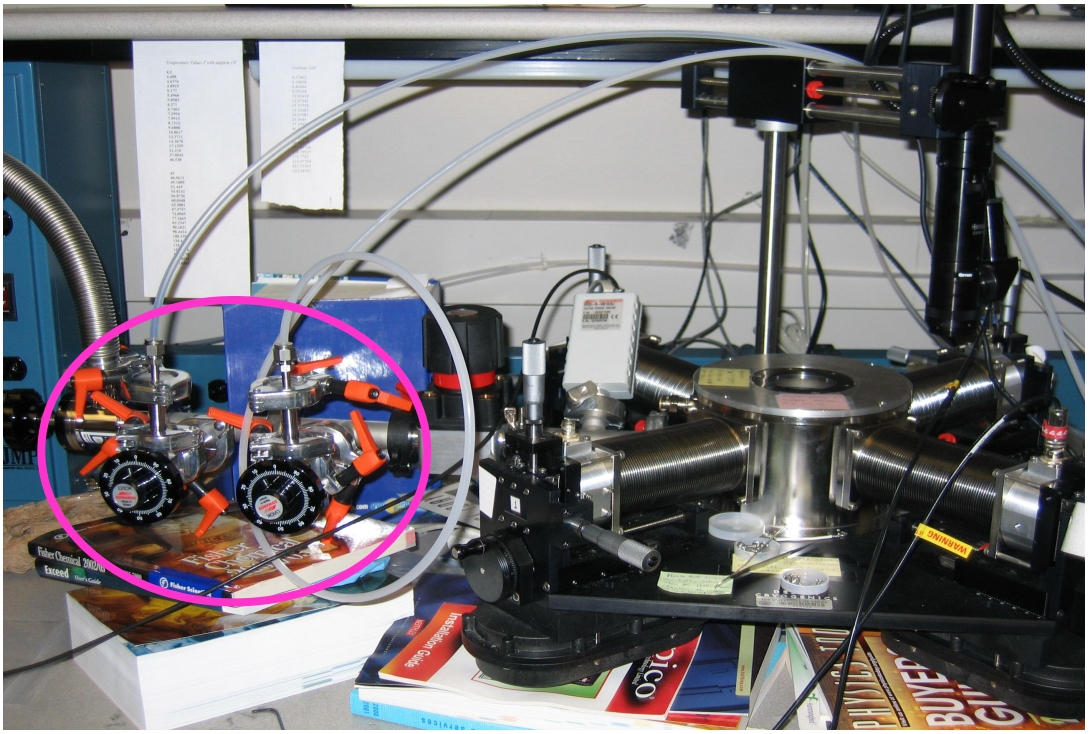

Figure 36. A second experimental apparatus used to measure OTFT sensing responses. It consists of a vacuum probe station (on the right) connected to two valves used to bleed in analyte/nitrogen mixtures and pure nitrogen (circled on the left) to further dilute the mixture.

The OTFT was loaded into a vacuum probe station which was subsequently pumped out using a turbo pump to around 10^{-4} Torr. Two valves were used to then bleed into the chamber controlled amounts of a nitrogen/ethanol mixture (5 ppm of ethanol in nitrogen) and pure nitrogen. The pure nitrogen was used to dilute the 5 ppm of ethanol to lower

concentrations. Ethanol was the only analyte used with experimental apparatus number 2 because ethanol would not condense on the surface of the apparatus and is not caustic at the low concentrations used for this experiment (which might have contaminated or damaged the vacuum probe station). The final concentration of ethanol in the chamber is shown in equation IX [9].

$$C_{Final} = C_{ethanol} \frac{P_{ethanol}}{P_{ethanol} + P_{nitrogen}} \qquad \text{IX}$$

A draw back to experimental apparatus number 2 is that it is difficult to test repeated exposures due to the fact that the entire overhead space of the device must be returned to low vacuum, a process which takes a considerable amount of time. In order to be able to rapidly expose the devices repeatedly while maintaining knowledge of the exact analyte concentration, a third apparatus is currently being developed, which will be referred to as experimental apparatus number 3. This apparatus consists of a series of mass flow controllers which feed into a small Teflon chamber in which the transistor is secured. As of now, however, it has only been used for some preliminary testing. An example of a response which can be measured using this apparatus is given in the next section. This apparatus will not be discussed in detail since it is in the early stages of development and was not used to any significant degree in the experiments discussed in this work.

For each of the experimental apparatus used to introduce the organic vapor described above, an Agilent 4155C was used to record the electrical output of the OTFT. The devices themselves were fabricated using the techniques outlined in Section 2.3 and have channel lengths which range from 300 μm down to 60 nm. Both top and bottom contact devices were used in these studies.

3.3 TYPICAL ELECTRICAL RESPONSES OF OTFTS TO CHEMICAL ANALYTES FROM THE MICROSCALE TO THE NANOSCALE

Typical responses of microscale top contact pentacene and copper phthalocyanine (CuPc) OTFTs to several organic vapors are shown in Figure 31 [10].

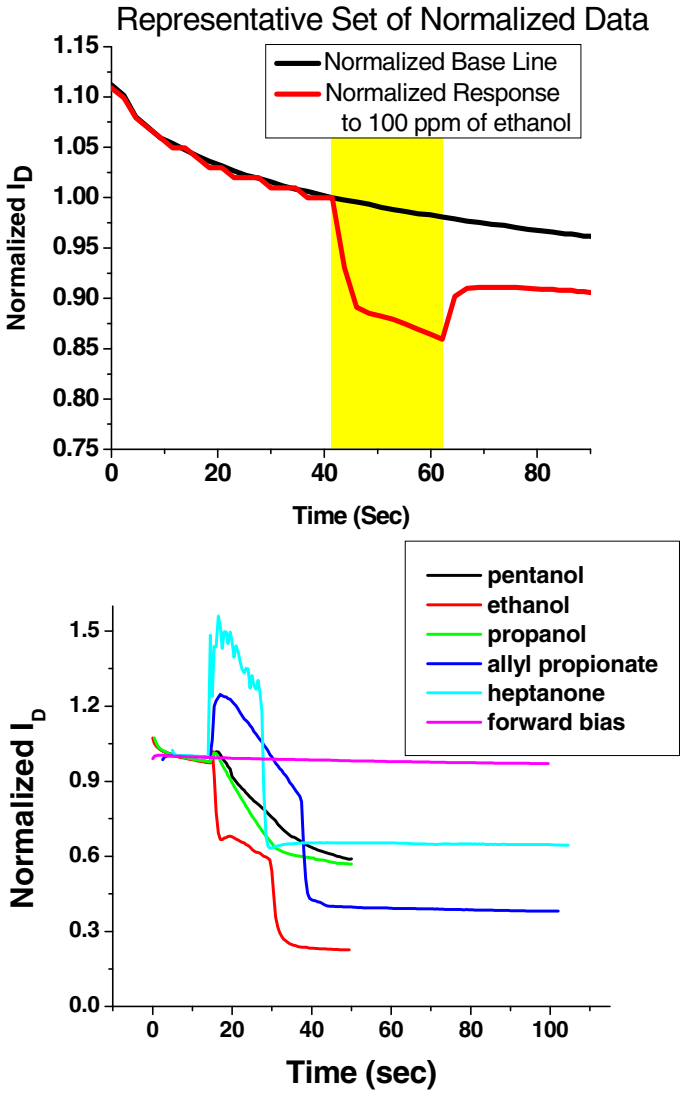

Figure 31. The top graph shows the response of a top contact pentacene OTFT to 100 ppm of ethanol [10]. The bottom graph shows the responses of top contact CuPc OTFTs to an array of highly concentrated (saturated) organic vapors [11]. The source to drain currents have been normalized at a point prior to analyte introduction for easier response comparison. The yellow portion of the top graph shows the period of time

that the ethanol vapor was presented to the sensor. In the bottom graph, the exposures of single analytes to separate CuPc OTFTs have been experimentally timed so that all exposures initially occur at roughly the same time.

The response of the pentacene OTFT to ethanol (the only example of a sensing response measured using experimental apparatus number 3) shows a decrease of the source to drain current upon exposure to ethanol vapor and then a slight recovery of the current when the exposure has ended. Not all organic vapor/organic semiconductor combinations produce the same response, as can be seen from the bottom graph in Figure 31 for CuPc OTFTs (this CuPc data was measured using experimental apparatus number 1). Crone *et al* demonstrated that the responses of a large number of semiconductors to various organic vapors can result in a response pattern, or chemical fingerprint as shown in Figure 32, similar to the one recorded for olfactory receptor neurons shown in Figure 1 (Chapter 1) [3].

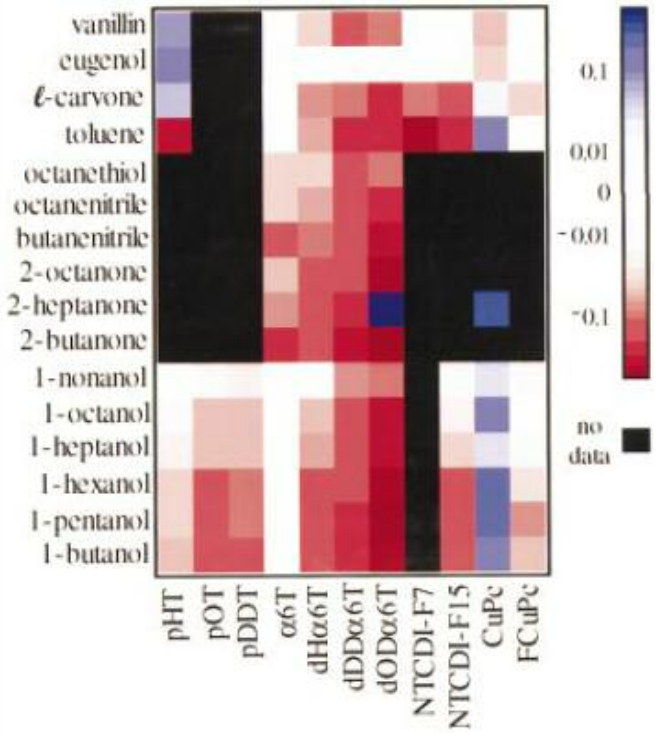

Figure 32. The chemical responses of various organic vapors to an array of organic semiconductors. Positive changes in source to drain current of

the semiconductor when exposed to the analyte are shown in blue and negative changes are shown in red. White indicates negligible responses and black represents that no data for that combination is available. For most of these combinations, the responses are reversible [3]. "Reprinted with permission from B. Crone, A. Dodabalapur, A. Gelperin, L. Torsi, H. E. Katz, A. J. Lovinger, Z. Bao, "Electronic sensing of vapors with organic transistors." *Applied Physics Letters* vol. 78, no. 15 (April 9, 2001) pp. 2229-2231 and the American Institute of Physics."

These responses are reversible over time. Source to drain current recovery time can be significantly shortened by means of applying a reverse bias to the gate of the OTFT [3]. Reverse biasing the gate is realized by flipping the gate voltage from negative to positive in the case of transistors made from p-type materials such as pentacene, or positive to negative for n-type materials, while maintaining a nonzero source to drain voltage (the reason for this will be explained later) [3]. By using this recovery technique, Crone *et al* also proved that these responses are highly reproducible, as shown in Figure 33 [3].

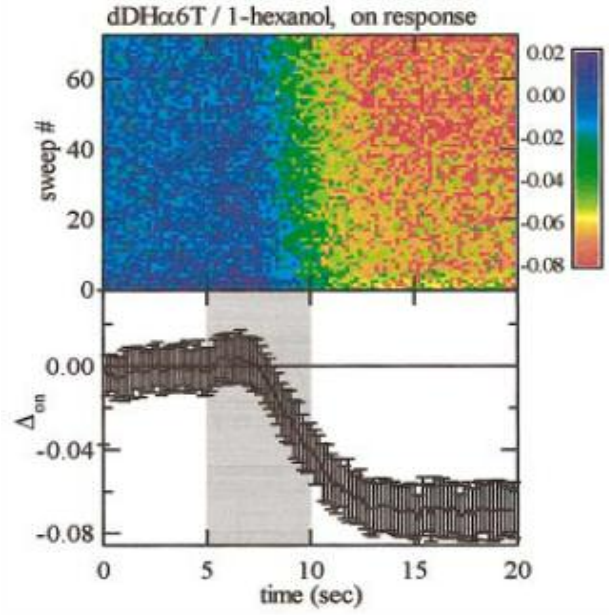

Figure 33. A demonstration of the highly reproducible responses which can be achieved for an OTFT, in this case di-dodecyl-alpha-sexithiophene (dH 6T), to an organic vapor, 1-hexanol. The gray area represents the duration of vapor exposure. The test was repeated greater than 70 times

[3]. "Reprinted with permission from B. Crone, A. Dodabalapur, A. Gelperin, L. Torsi, H. E. Katz, A. J. Lovinger, Z. Bao, "Electronic sensing of vapors with organic transistors." *Applied Physics Letters* vol. 78, no. 15 (April 9, 2001) pp. 2229-2231 and the American Institute of Physics."

An interesting phenomenon occurs, however, when the channel length of these devices is scaled down below a few hundred nanometers, as illustrated in Figure 34 (measure with experimental apparatus number 1) [12].

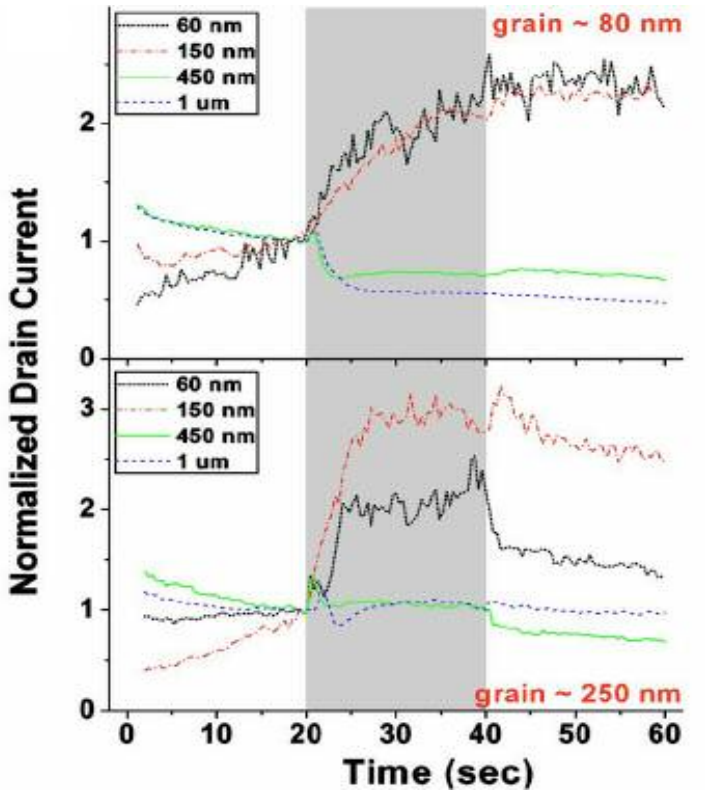

Figure 34. Chemical sensing responses of pentacene OTFTs to a saturated vapor of 1-pentanol for several channel lengths ranging from 1 μm down to 60 nm. A clear crossover can be observed whereby the response changes from a decrease to an increase upon exposure to the 1-pentanol. These responses are normalized at a point prior to analyte introduction for purposes of comparison. "Reprinted with permission from Liang Wang, Daniel Fine, Ananth Dodabalapur, "Nanoscale chemical sensor based on organic thin-film transistors" *Applied Physics Letters* vol. 85, no. 26 (December 27, 2004) pp. 6386-6388 and the American Institute of Physics."

The pentacene OTFTs' responses to 1-pentanol change from a decrease upon analyte exposure to an increase. As noted in section 2.7 in Chapter 2, this also happens to correspond to the length scale around which the OTFTs begin to become injection limited (see Figure 30).

This same type of response, an increase in source to drain current upon exposure to 1-pentanol, was observed when a metal with a lower work function than the ionization energy of pentacene is used as the contact material, shown in Figure 35 (also measured with experimental apparatus number 1) [13]. The contacts for this bottom contact device are made from nickel. The lower work function of nickel creates a barrier to injection of holes at the source, as is evident by the low source to drain currents achieved for the device pictured in Figure 35 when analyte is not present.

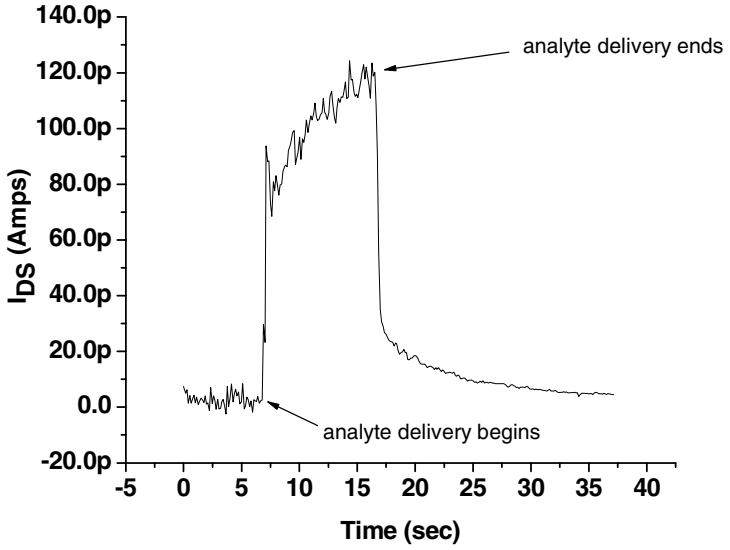

Figure 35. The response of a bottom contact pentacene transistor to 1-pentanol when nickel, a low work function metal, is used as the contact material. Since the work function is significantly lower than the ionization energy of the pentacene, nickel is a poor injector of holes into the active region of this transistor [13].

Thus it appears that as the devices become injection limited, their response to organic vapors changes from a decrease to an increase. In some cases, as illustrated in the bottom graph of Figure 31, this same phenomenon can occur with some semiconductor/analyte pairs when the strength of the dipole of the polar functional group increases, as it does when switching from an alcohol group to a carbonyl group (as an example, the dipole moment of methanol is 1.69 D (debye) [14] whereas the dipole moment of formaldehyde is 2.33 D [15]).

3.4 ORIGINS OF THE CHEMICAL SENSING RESPONSES OF OTFTS

What then creates the decrease or increase in current upon analyte exposure and what physical characteristics of the transistor affect how it interacts with these analytes? To begin to answer this it is first necessary to understand whether the material is actually chemically reacting with the analyte or interacting with the analyte in another non chemical way, such as an electrostatic interaction. There are examples of analytes which do chemically dope the semiconductor, such as electrophilic gases like NO_2, which remove electrons from CuPc and dope the material with holes [2]. The fact that the responses of many of the microscale organic semiconductor devices exposed to many of the organic vapors are reversible and reproducible reductions in current (not increases) would likely exclude any type of chemical reaction, including doping, as the predominant current modulation mechanism for most of these combinations. This would hold at low device dimensions as well since it would not seem likely that a switch in the response characteristics from negative to positive would now be caused by doping when neither the contacts nor the semiconductor have been changed [12]. One could the argue that the increased electric fields at these device dimensions might now allow for chemical doping

or another type of chemical reaction to occur. This argument would not, however, explain the increase in current magnitude seen by replacing the gold contacts with nickel (see Figure 35) [13], nor would it explain the increased current due to changing the strength of the dipole moment of the organic molecules (e.g., by switching from an alcohol functional group to a carbonyl functional group). Finally, Torsi *et al* demonstrated that when the semiconductor di-dodecyl-alpha-sexithiophene (dH 6T) was exposed to 1-pentanol, no swelling or thickness changes were recorded as measured by an ellipsometer [16], also helping to rule out a chemical change. This is believed to be similar for CuPc and pentacene [17]. Thus, it seems most likely that the interaction between the organic semiconductor and the organic vapor is not a product of a chemical reaction.

It is now beneficial to determine where physically on the device the current modulation occurs. The study performed by Torsi *et al* also showed that there is very little penetration of the organic analytes into the highly ordered crystalline grains evident by the fact that no appreciable swelling was measured [16], most likely due to the tight crystalline packing of the molecules in the grains [17] (in the case of conducting polymers, swelling is a known result of exposing them to organic vapors [16]). This would indicate that there is very likely little interaction, chemical or otherwise, between the molecules in the ordered grains and the organic vapors. In the same study, dH 6T was deposited on a quartz crystal microbalance and a change in the mass of the semiconductor was measured when exposed to varying concentrations of 1-pentanol (no contacts were deposited in this study) [16]. This demonstrated that although the 1-pentanol did not penetrate into the film, it nonetheless added to its mass. This means that the analyte adsorbed to the surface of the organic layer [16]. A decrease or increase in source to drain current must then be attributed to something which occurs outside of the

crystalline grain. Another study by Someya *et al* exploring the interaction between the semiconductor , -dihexylquarterthiophene and 1-pentanol demonstrated that the magnitude of the sensing response was directly related to the number of grain boundaries in the channel when the interaction resulted in a decrease in I_{DS} [18]. Remembering from Section 2.5 that almost all of the charge within the channel of an organic semiconductor lies close to the semiconductor/dielectric interface, it must be the case that the analytes percolate down to this dielectric interface through the grain boundaries. This cannot apply to increases in current magnitude since it has been established that doping is not a predominant mode of current modulation.

What then happens when the change in current magnitude transitions to an increase? Someya *et al* further demonstrated that when the number of grain boundaries in the device was very small, there was very little appreciable change to the channel current [18]. Analyzing the results from the nanoscale transistor sensor study (Wang *et al* [12]), the , -dihexylquarterthiophene experiments (Someya *et al* [18]), the results from Figure 35 and the bottom graph of Figure 31, and finally to the contact limitations of nanoscale transistors discussed in Section 2.7, it becomes clear that in the case of many of these analyte/semiconductor combinations, the increases in magnitude of the source to drain current must be due to changes in the nature of how charge is injected into the channel and not by any type of doping effects. The fact that this magnitude increase was not seen in the Someya *et al* experiments would indicate that the devices used were not injection limited.

A structural explanation of where the current modulation occurs therefore becomes clear. The decrease in current must be due to a phenomenon which occurs in the grain boundary and an increase in current must be the result of a phenomenon which occurs at the contact. What then is the nature of these phenomena? In Section 2.6, there

was a discussion of how important the local polar environment was to how well carriers can move through organic semiconductors. Changes in the local crystal structure near carriers localized on a single molecule, and thus changes to the polarizability of the lattice, could drastically change the local distribution of energy states. This problem was further exacerbated in the grain boundaries due to a large amount of disorder. When we consider most of the analyte organic molecules used in this study, most of them have one thing in common, they all have dipoles (hexane does not but, as mentioned earlier, it did not produce any appreciable response). The predominant mechanism which leads to a decrease in the magnitude of the current is increased trapping of carriers in the grain boundaries due to a modulation of the local electronic environment caused by the presence of the polar organic vapors (an increase in the polarizability of the semiconductor in the grain boundaries). An increased number of traps in the grain boundary would lead to an increase in the activation energy for hopping through the grain boundaries (*see* Section 2.6) which was demonstrated by Sharma *et al* using top contact pentacene transistors exposed to ethanol [19]. The measured activation energy changed from 77meV to 92meV when the analyte concentration was changed from pure nitrogen to 100 ppm of ethanol as measured in experimental apparatus number 2 [19]. Further evidence for this trapping effect will be demonstrated in the next Section along with a device architecture which uses this phenomenon to great advantage to achieve a much lower detection limit than these more conventional OTFTs.

Increases in the magnitude of the current are caused by the same polar nature of the analytes that causes trapping. Several studies utilizing ultra-violet photoemission spectroscopy (UPS) [20, 21] and inverse photoemission spectroscopy (IPES) [21] indicated that at the interface between the metal contact and the semiconductor a dipole forms. This dipole is the result of a work function/ionization energy mismatch which can

be further increased by a shift in the vacuum level of the organic material [20, 21]. The physical realization of this dipole is that for some carriers near the contact it is more energetically favorable to be drawn back to the contact as opposed to progressing towards the drain (as suggested by Bürgi *et al* [22]; *see* Section 2.7). This small population of charge can induce an image charge in the contact and create a reverse electric field which hinders further injection. This is also commonly referred to as an interface dipole. This also creates a problem when trying to accumulate charge in the channel near the contacts where the concentration of gate-field induced charge can be significantly less than the rest of the channel [22]. Contact effects are further complicated by the fact that band splitting occurs at the semiconductor/contact interface (also covered in Section 2.7 [21, 23]) creating a decreased forbidden gap between the HOMO and LUMO levels. When carriers are injected into the semiconductor, a large portion of them are likely to be trapped in the increased number of tail states in the forbidden gap close enough to the interface to enhance the aforementioned image charge in the metal and thus the reverse electric field [21, 23]. This trapping is further increased by disorder due to poor crystal growth at the metal/semiconductor interface. The polarity of the analytes can work to shield carriers in the semiconductor from the dipole which results from the reverse electric field due to the image charge. The larger the dipole in the analyte the greater the shielding effect. When pentacene devices are scaled down, at some point the size of the gap approaches the size of the grain and very poor morphology at the contact results. This creates a large amount of disorder and therefore a significant amount of trapping at the contact. This would indicate that the effective injection barrier in nanoscale pentacene devices (an increase of the reverse electric field) is more likely due to traps. This is opposed to the nickel contacts where there is a very bad energy level alignment

with the nickel work function being less than the pentacene ionization. In this case, the primary contribution to an effective injection barrier is energy level mismatch.

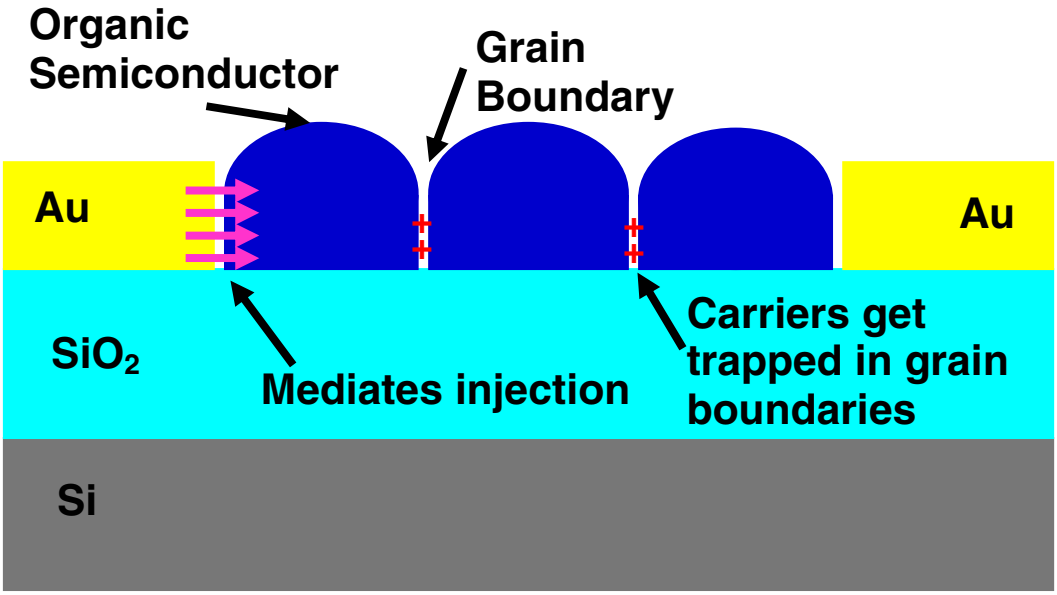

Illustration 1. A graphic summary of the origins of the sensing response. The response arises because of trapping in the grain boundaries and/or the mediation of carrier injection at the contacts.

In the case of some semiconductors, such as CuPc, it seems that there is a delicate balance between having its source to drain current dominated by the channel or the contacts. The final sensing behavior will have a strong dependence on the strength of the dipole, the strength of the interaction between the analyte molecule and the semiconductor, and the number of grain boundaries present.

One problem with being able to detect these analytes, and a main reason experimental apparatus number 2 was used (since it could be used under vacuum), is that water is also polar. In a high humidity environment water can mask the effects of some of the weaker analyte dipoles which were tested. It is one of the reasons almost all of the devices used in these experiments demonstrate a current fall off over time even without the presence of an analyte when tested under atmospheric conditions, as with

experimental apparatus number 1. Humidity also introduces some small amount of experimental variability, especially when measuring the responses of an analyte with a smaller dipole like ethanol. Water vapor also happens to be one of the predominant problems with consistent operation of organic transistors in general, especially for those applications where exact performance must be maintained. This problem should also be alleviated using experimental apparatus number 3 because it should be possible to completely purge the Teflon chamber with nitrogen before performing the experiment.

3.5 THE HYBRID SILICON/ORGANIC TRANSISTOR SENSOR

As mentioned earlier, organic transistors in the more standard top or bottom contact configuration have been shown to achieve detection limits of 10 ppm.

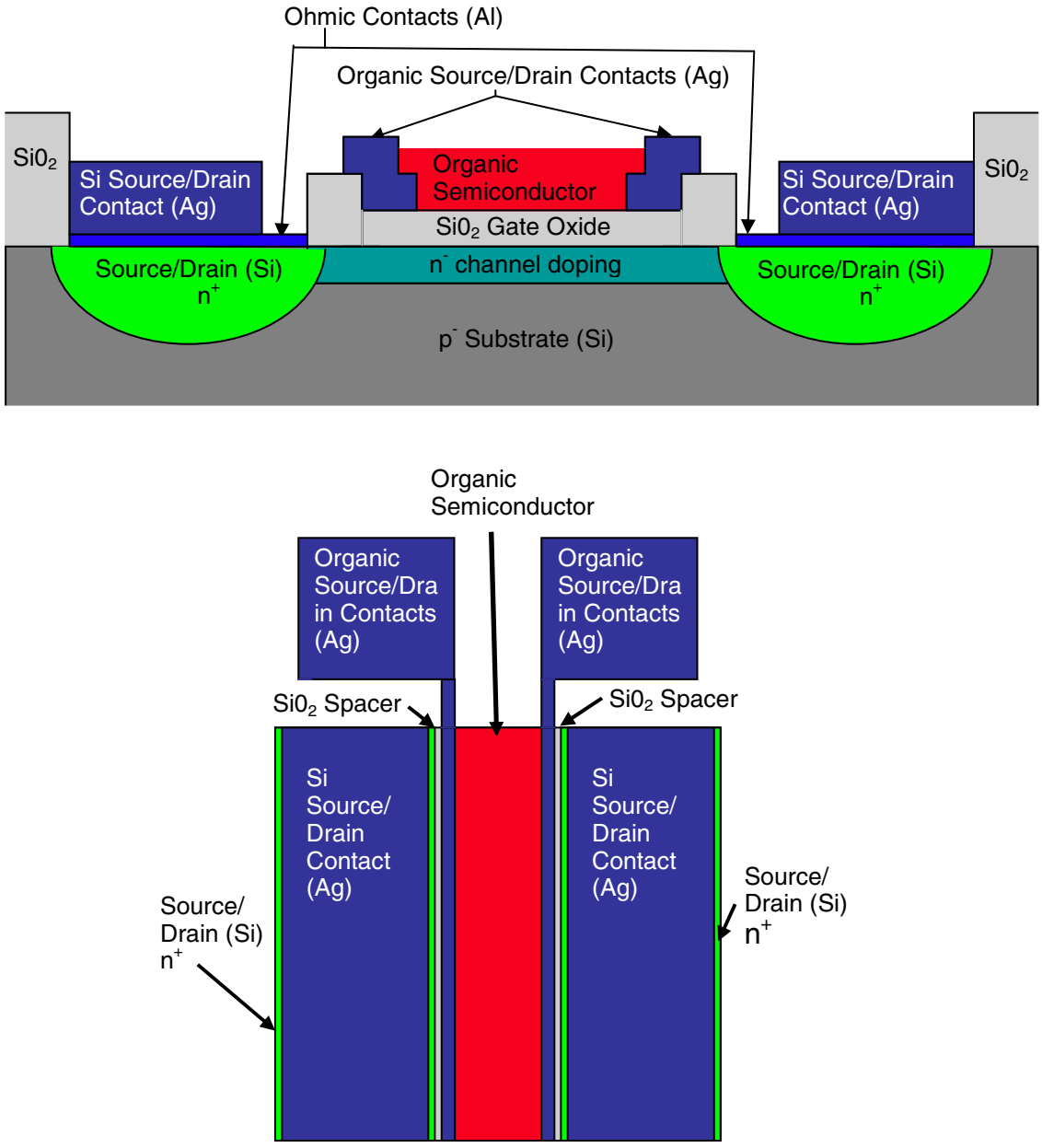

Figure 36. The side and top view of the hybrid organic/silicon transistor sensor

In an effort to lower that detection limit further, a new configuration was developed. This configuration blended the chemical sensitivity of an organic device with the

reliability and high transconductance of a silicon device into a new hybrid silicon/organic device shown in Figure 36 [24]. As can be seen from the top diagram of Figure 36, the device is created by first building a silicon transistor with a gate dielectric but no polysilicon or metal gate, just like a chemical field-effect transistor (CHEMFET). This was an n-type silicon transistor since it was designed to work with pentacene, a p-type organic semiconductor. Then a bottom contact organic transistor is built on top. The channels of the two transistors are cross coupled, the charge accumulated in the organic device acting as a gate for the inversion charge in the silicon device and visa versa. The silicon device has a channel implant which attempts to place the middle of its subthreshold slope at zero volts (*see* Figure 37) in order to get the maximum change in the silicon transistor source to drain current for a minimum change in the organic current characteristics (essentially the silicon gate voltage).

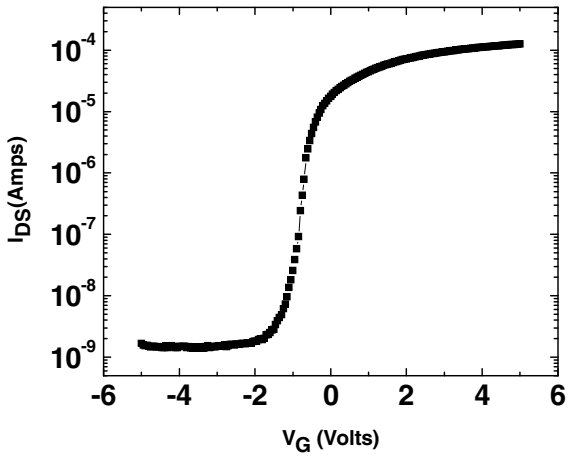

Figure 37. An example of the subthreshold characteristics of a silicon transistor used in the hybrid device [26].

In the subthreshold regime, the source to drain current follows the proportionality in equation X [25].

$$I_{DS} \propto e^{(V_{GS}-V_T)} \qquad \text{X}$$

Thus a large change in I_{DS} can be achieved in the silicon channel from a small change in charge in the organic transistor's channel. If the subthreshold regime is not pinned at zero gate voltage, a substrate bias can be applied to shift the threshold voltage.

This device could then be operated in four primary modes. The first mode was to use the unbiased organic semiconductor as the sensitizing layer for the gate of the silicon device just like a CHEMFET. The second was to use the silicon device only as a gate for the organic transistor by keeping its source and drain biased to the same potential. In this mode the organic device performed the same as the other OTFTs explored earlier in this Chapter. The third mode of operation was to bias both the silicon and organic field-effect transistors simultaneously such that they were both on at the same time. This was performed by applying a differential potential to the source and drain of both transistors, but with a DC offset on the organic device which was positive with respect to the silicon device (for instance the source potential might be 15 volts and the drain potential might be 10 volts for the organic) and a DC offset on the silicon device which was negative with respect to the organic device (the source potential might be -10 volts and the drain potential might be -5 volts).

The final mode of operation, and the most interesting, is called the chemical memory mode. Prior to turning both devices on at the same time, the off current through the silicon device was measure while no bias was applied to the organic device. Then the devices were operated in the both on mode in the presence of an organic vapor. Upon turning off the organic device, the source to drain off current was measured again in the silicon device without biasing the organic device (leaving the gate of the silicon device to float).

The change in response of a hybrid silicon/pentacene device in CHEMFET mode when exposed to ethanol turned out to be a small percentage increase, around 2.5%, for a representative device. The total response change for the more standard OTFT mode was a decrease of about 57% for the same device (this accounts for a much lower absolute current change than the silicon current change in CHEMFET mode due to the organic transistor's on current being much lower than that of the silicon on current). The chemical memory mode, however, produced a post-exposure off current in the silicon transistor which was around 45 to 65 times higher than the pre-exposure off current when measured in air also on the same device (devices tested in air, as mentioned earlier have a very steep fall off). When measured in nitrogen, the post-exposure off current was about 95 to 97 times higher than the pre-exposure off current. These were by far the best results recorded for any of the modes tested, including the both on mode. The both on mode is not listed here because it did not produce as consistent an output as the chemical memory mode due to the fact that the coupling of the gates while both devices are on can produce results which can shift in a relatively short time frame. Both on mode also does not operate the silicon device in subthreshold and so does not produce as great of a percentage change as the chemical memory mode. The responses quoted n this paragraph measured for the CHEMFET, OTFT and chemical memory mode as measured in air were recorded using experimental apparatus number 1 and a stock gas of 5 ppm of ethanol (not saturated filter paper). The devices measured in nitrogen were measured using experimental apparatus number 2 [26].

Why then would the chemical memory mode produce better results than any of the other modes? The reason, as described in Section 3.4 has to do with trapped charge. When operating in CHEMFET mode, the silicon device is forced to measure the adsorbed dipoles on the organic semiconductor as a result of having no carriers present in the

organic transistor channel. Although the organic analytes interact better with the semiconductor than they would with no material on the gate, these dipoles cannot make a significant change to the amount of charge on the gate of the silicon device since any positive charge is automatically accompanied by negative charge. The dipoles may align at the gate interface which would contribute to the 2.5% change seen in the CHEMFET mode of the device. But ultimately they would cause very little change to the inversion charge in the silicon field-effect transistor (FET). In the OTFT mode, the trapped charge can be detected only as a change in mobility and must rely on only the OTFT to produce the sensing result. No amplification can be achieved from this mode. The chemical memory mode, however, directly measures the charge trapped in the OTFT after exposure to an analyte. By turning both devices on during the exposure, there is charge present in the channel to be trapped. This trapped charge leaves over a very long time scale if the organic device is not reverse biased. Thus, the large transconductance of the silicon device when operated in its subthreshold mode produces large shifts in the threshold voltage and thus more substantial changes in the off current of the silicon transistor. This is also superior to the both on mode in which the response can shift due to the shifting charge distributions as more carriers get trapped, and which does not benefit from the large current changes that can occur when the silicon FET is operated in the subthreshold regime. The lowest repeatable detection limit achieved using this hybrid device, when operated in the chemical memory mode (using experimental apparatus number 2), is 100 ppb as shown in Figure 38.

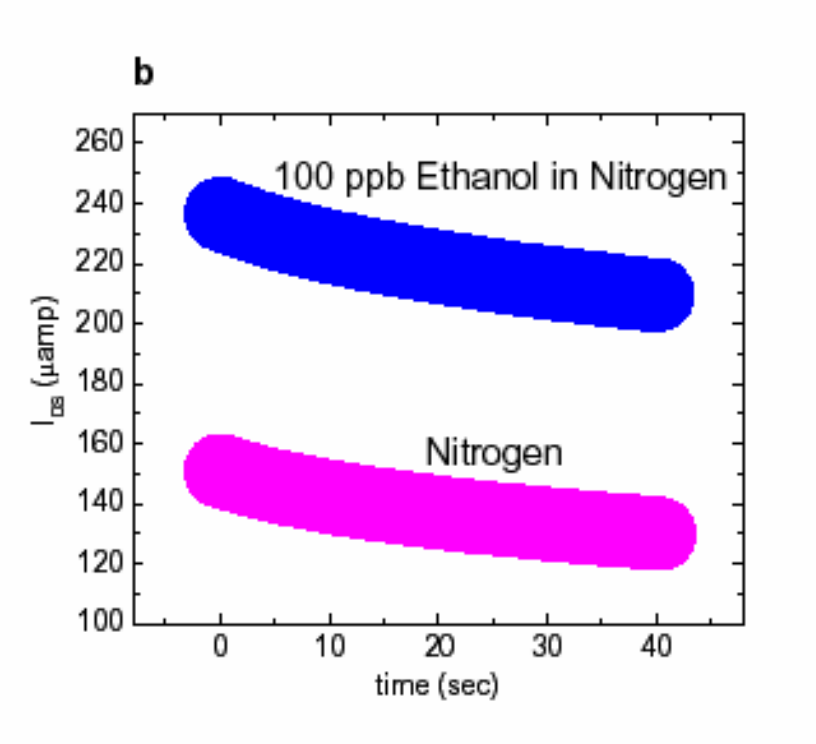

Figure 38. A graph showing the difference between the off currents of the silicon transistor before (magenta) and after (blue) the hybrid silicon/pentacene sensing device is exposed to 100 ppb of ethanol. This is referred to as the chemical memory mode. Each band represents multiple measurements and thus demonstrates the devices reproducibility [26].

3.6 THE USE OF SMALL MOLECULE RECEPTORS

Combining organic transistor sensors with a silicon device, which acts as an amplifier and trapped charge detector, is one way to improve the sensitivity of the OTFT sensors. This does not, however, improve the OTFTs selectivity. In an attempt to increase the sensitivity and selectivity of the simpler bottom and top contact geometry OTFT transistor sensors and to augment the sensitivity of the hybrid silicon/organic transistor sensor with increased selectivity, a second response enhancing technique was pursued. As mentioned earlier, Torsi *et al* demonstrated the importance of the analyte's alkyl chain length in terms of its interaction with the organic transistor [5]. The longer

the carbon chain length, the greater the interaction of that analyte molecule with the semiconductor and the higher the mass uptake. The same group also showed that increased mass uptake occurred when the side chain of the polythiophene derivative was made to be polar (by putting an ester in the side chain) [5] (*see* Figure 39).

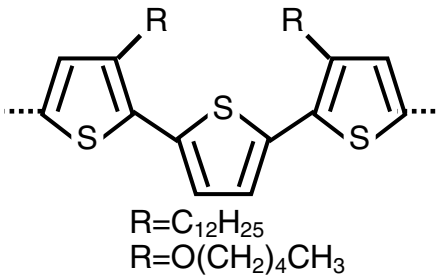

Figure 39. The polar (3,3”-dipentoxy-2,2”:5’,2”-terthiophene) and nonpolar (3.3”-didodecyl-2,2”:5’,2”-terthiophene) polythiophene derivatives used in the Torsi *et al* study demonstrating the increased mass uptake of the organic alcohols ethanol and 1-hexanol when the side chain is switch from nonpolar to polar [5].

This enhancement of the mass uptake was even more pronounced than the increase produced by longer analyte carbon chains [5]. This particular study did not show a significant change in electrical response with 1-hexanol given the switch in side chain even though there was a significant increase in mass uptake. One reason for this could have been the result of an adjustment to the mobility corresponding with the switch in side chain [5]. Ethanol, however, showed no electrical response with the nonpolar side chain but did show a response with the polar side chain. This was most likely due to a poor interaction of the short ethanol alkyl chain to the nonpolar side chain and a much better interaction of the polar ethanol to the polar side chain. This response could be adjusted with the use of polar versus nonpolar side chain moieties [5].

Given the demonstration by Torsi *et al*, was it possible to do the same thing with a small organic molecule semiconductor like pentacene or CuPc without the necessity of chemically editing the molecule and without significantly lowering the device's mobility? Could this further be used to enhance not only the sensitivity but also the selectivity of the semiconductor? The answer to both questions was yes. By using small receptor molecules, a few of which are shown in Figure 40, deposited by drop casting from a solution of chloroform after the fabrication of a top contact OTFT, it was possible to adjust the response of the semiconductor (for most of the experiments performed using this technique the semiconductor was CuPc) to several of the organic vapors listed in Figure 34. This now enabled the OTFT to select definitively between several chemical functional groups with a much more pronounced response.

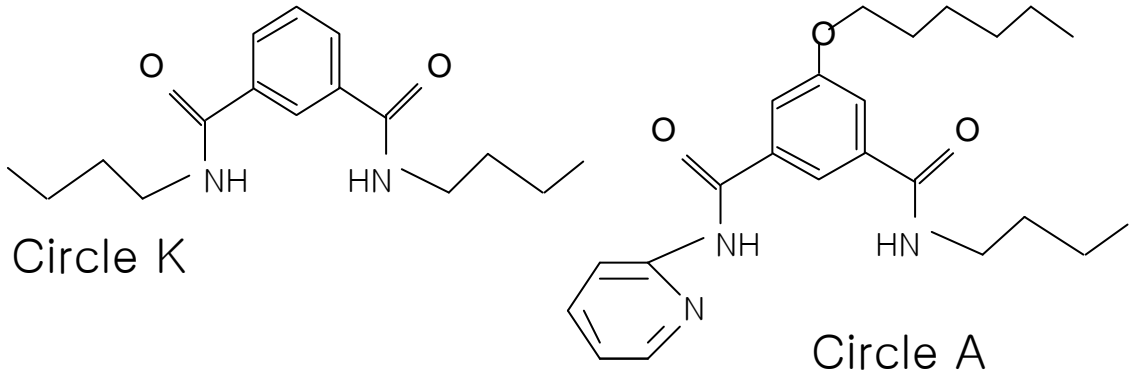

Figure 40. Two representatives of the small molecule receptors used to adjust the sensing responses of small organic molecule semiconductors to various organic analytes. The basic interaction between these receptors and the organic molecules is hydrogen bonding. The receptors shown here were provided by David F. Cauble and Professor Michael J. Krische at the University of Texas at Austin, Department of Chemistry.

Figure 41 shows the response of CuPc OTFTs modified with the receptors shown in Figure 40 to several organic analytes, measured with experimental apparatus number 1. As can be seen from these graphs, the responses of the receptor modified organic

transistors (modified with the two receptors shown in Figure 40) to the alcohols do not change significantly from those of the unmodified OTFTs in the bottom graph of Figure 31, although the devices now seem to react to all the alcohols roughly the same, irrespective of chain length (the brief increase at the beginning of the responses to alcohols may be due to the displacement of water vapor, a more polar molecule than most of these alcohols). The responses to heptanone and allyl propionate change dramatically.

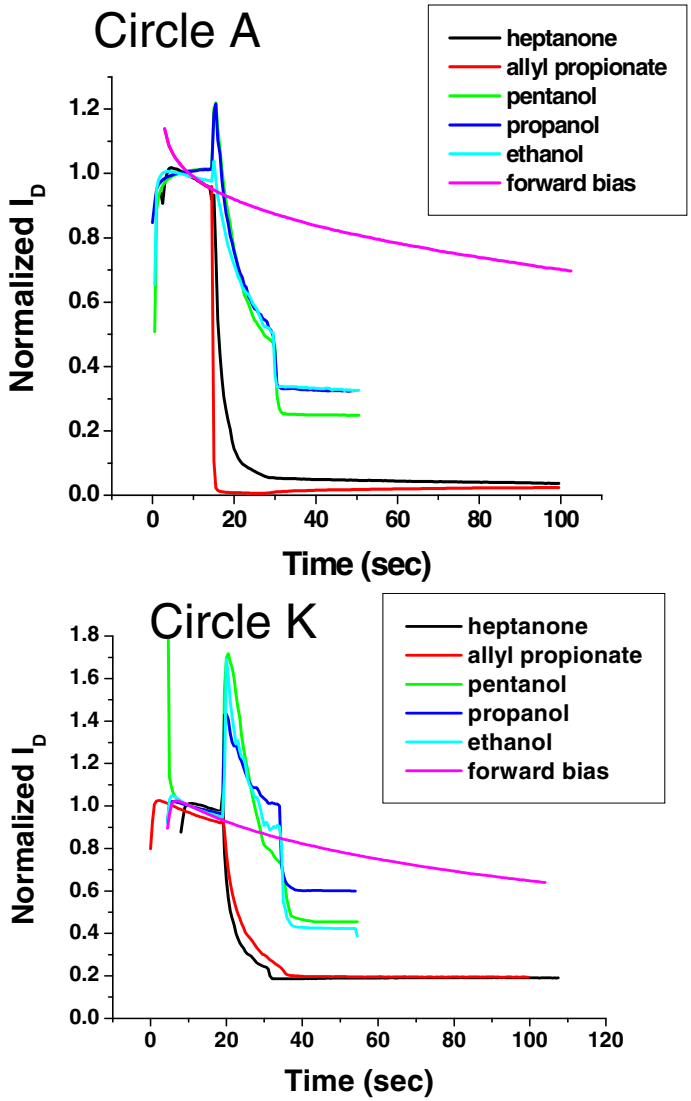

Figure 41. Responses of top contact CuPc OTFTs modified with the two receptors shown in Figure 40. The responses of the receptor modified

OTFTs to the organic alcohols are not significantly different from the responses of neat CuPc OTFTs shown in the bottom graph of Figure 31 and no longer seem to differ with alkyl chain length. The responses of the receptor modified CuPc OTFTs to allyl propionate and heptanone are dramatically different from the neat CuPc OTFTs from Figure 31, the most dramatic change being seen from Circle A. These results were measured using experimental apparatus number 1.

In fact, for the devices which use the receptor from Figure 40 referred to as Circle A (the name is derived from this receptor being designed to interact with carboxylic acids as opposed to Circle K which is targeted for ketones), the receptor causes the device to nearly turn off upon exposure to heptanone or allyl propionate, an almost 100% reduction of the source to drain current. Circle K led to an 80% reduction. This is in stark contrast to an increase in source to drain current seen in the neat CuPc OTFTs (*see* the bottom graph of Figure 31) for heptanone and allyl propionate. Based on these results, it now becomes apparent that these modified OTFTs are showing responses that are now almost totally dependent on the polar functional group in the analyte instead of the length of its alkyl chain. Furthermore, whereas in the neat CuPc devices where there seemed to be a delicate balance between whether the analyte dipole enhanced injection more than it caused trapping in the channel, in these modified devices trapping was dramatically favored over injection enhancement in the case of the strongest dipoles, the carbonyl groups.

What is causing this dramatic change in response? CuPc and pentacene are hydrophobic materials, meaning that they do not have as strong a reaction to dipoles as to nonpolar molecules. One reason that neat CuPc may show injection enhancement and not trapping at the grain boundaries in the presence of strong dipoles like heptanone is that this analyte has a difficult time percolating to the dielectric/semiconductor interface in the hydrophobic CuPc. Another reason, which would explain the relatively low

amount of trapping for all the analytes seen in CuPc sensing responses, may be that these are high vapor pressure analytes and therefore the individual molecules interact with the semiconductor for a short amount of time. The receptors shown in Figure 40 were designed to form hydrogen bonds with the analytes. When the very electronegative atoms nitrogen, oxygen, or fluorine, are covalently bound to a hydrogen atom, they draw a large amount of the electron density off of the hydrogen forming a very strong dipole [27]. Since hydrogen is a small atom with most of its electron density drawn off by its more electronegative covalently bound neighbor (hydrogen only has one electron in its valence shell to begin with), it can get very close to the lone pair of electrons of the nitrogen, oxygen, or fluorine of the neighboring molecule and form a strong electrostatic interaction [27]. These bonds can also be slightly covalent in nature since electrons can be shared between both of the electron withdrawing neighbors (O, N, and F) and the hydrogen in between them [27]. These bonds are not quite as strong as a full covalent bond but are much stronger than other inter-atomic forces like van der Walls forces. It is the network of these hydrogen bonds which causes the boiling point of water to be much higher than would be predicted by its molecular mass [27]. The receptors (*see* Figure 40) have alkane side chains which make them soluble in organic solvents and can help them to interact more favorably with the CuPc and allow them to permeate into the grain boundary. The amine (nitrogen containing) groups designed into these molecules could then form hydrogen bonds with the oxygen containing analytes and significantly increase their interaction with (including the time that the analyte is held in the grain boundary), and their percolation depth into, the grain boundaries of the CuPc (*see* Figure 42). Circle K has the ability to form two hydrogen bonds as it is equipped with two amine groups containing an H-N moiety. Circle A has two H-N moieties and a nitrogen containing aromatic ring. All of these moieties can contribute to hydrogen bonding with the analyte

(it appears that Circle A, with its three amine moieties is slightly better than Circle K with its two amine moieties). The hydrogen bonding of the polar analytes would then contribute to improving analyte induced charge trapping.

Is it possible that another analyte/semiconductor interaction is occurring, such as a dipole-dipole interaction (a weaker type of interaction than hydrogen bonding)? The reason to suspected hydrogen bonding instead of an alternative interaction, such as a dipole-dipole interaction, as the predominant analyte receptor interaction is based on the difference between the alcohol response and the carbonyl response in the two receptors with differing hydrogen bonding capabilities.

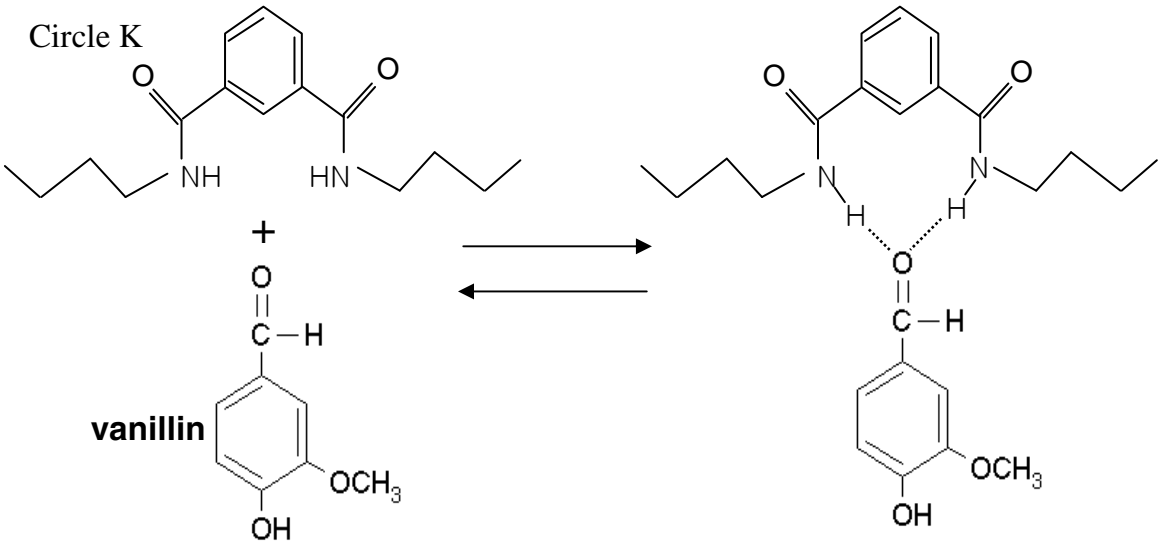

Figure 42 The formation of hydrogen bonds between Circle K and the organic analyte vanillin.

Circle K has two amine moieties with nitrogen bound to hydrogen which constitute hydrogen bond donors. Since the alcohols also have hydrogen atoms bound to their oxygen atoms, this interaction should not be as strong because both hydrogen bonding groups on the receptor and the alcohol are hydrogen bond donors. This is exactly the case that can be seen in the bottom graph in Figure 41; Circle K does not interact strongly

with the alcohols. The carbonyl groups have no hydrogen atoms bound to the oxygen atom which now constitutes a hydrogen bond acceptor. Thus the carbonyl interaction with Circle K is much stronger with the receptor providing hydrogen bond donors and the carbonyl group supplying a hydrogen bond acceptor. In the case of Circle A, nitrogen incorporated in the aromatic ring is a hydrogen bond acceptor as it has no hydrogen atom. The alcohols therefore have a greater interaction with Circle A than with Circle K since they can now form hydrogen bonds with the aromatic amine group, which can also be seen in Figure 41. The organic alcohols still do not have as great an interaction with Circle A as do the carbonyl groups with their capability of forming two hydrogen bonds. For these reasons hydrogen bonding is considered to be the most likely type of interaction. One would expect less significant variation between the sensing responses of the two receptor modified OTFT sensors to the various polar functionalities of the analytes assuming another type of interaction.

A third receptor, whose molecular structure is not pictured here but whose sensing responses are shown in Figure 43, has demonstrated the ability to exhibit some distinction between the sizes of the analytes and where the functional groups are located on the molecules (e.g., an O-H group located at the end, as opposed to the middle, of the analyte carbon chain as can be seen with the difference in response between 1-pentanol and 2-propanl). It is a molecular cage also referred to as a cavitand, an example of which is given in [28]. This cavitand was able to distinguish ethanol from most of the other analytes (in terms of the response rate and magnitude). The results in Figure 43 were also measured using experimental apparatus number 1.

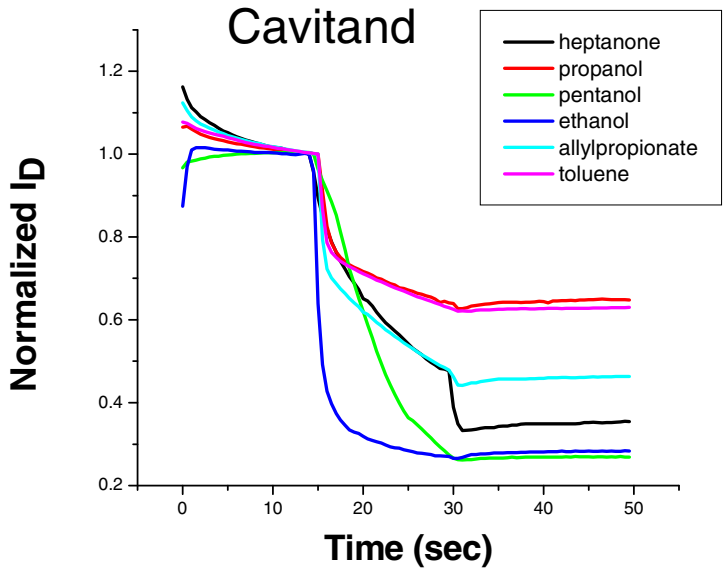

Figure 43 The responses of CuPc OTFTs to a receptor modified with a molecular cage referred to as a cavitand. This modified device apparently can make distinctions between the size of the analyte as well as the position of the functional group (based on rate of change of the response and the extent of the response change) as it appears to be most sensitive to the smallest analyte, ethanol, closely followed by 1-pentanol which has its functional group at the end of the alkane chain.

Devices modified with small molecule receptors showed the same ability to be refreshed as unmodified OTFT sensors. The current, however, did not fully recover to the original level, probably due to the strong receptor/analyte interaction. They also had lower mobilities than the neat OTFTs, due to the presence of the relatively unconductive receptors in the grain boundaries. A better understanding of the relationship between sensing response and mobility adjustment to receptor quantity, which has not been performed to date, will alleviate these issues to a large extent. Furthermore, the added flexibility the receptors offer in tuning the responses of organic semiconductors to various analytes allows for the selection of the semiconductors which possess the highest mobility. Finally, if used in conjunction with the hybrid silicon/organic device, to first order, the mobility of the organic is not as important when using the chemical memory

mode. The only requirement is the need to have enough charge in the channel to trap. Modifying the organic component of the hybrid silicon/organic sensing device with receptors may lead to better sensitivity then the hybrid device already achieves, by increasing the trapping probability and hold time through receptor enhanced analyte/semiconductor interaction, with the added quality of making the hybrid devices much more selective. Using the hybrid device will also lead to an understanding of whether these small molecule receptors improve the response characteristics by increasing the amount of trapped charge or, by some other mechanism, causing a larger modulation of the semiconductor mobility while not significantly altering the trapped charge density.

In order to understand these modified devices more completely, they must be used in a system like experimental apparatus number 3 (the apparatus which uses the small sensing chamber fed by mass flow controllers) which is currently in development. This will yield a better feel for the lower detection limits of receptor modified OTFT sensors as well as help to determine more quantitatively the exact interaction occurring in the device between the analyte and the receptor.

Small molecule receptors seem to be a very promising direction to pursue when attempting to further enhance the selectivity and sensitivity of the analyte/semiconductor interaction. These enhancements would reduce the need for full fingerprint pattern recognition and could do so without greatly increasing device fabrication complexity. These receptors could also be used in conjunction with other response enhancement techniques, such as the hybrid silicon/organic device configuration, to achieve even greater improvements of the sensor characteristics.

3.7 REFERENCES

1. A. Oprea, U. Weimar, E. Simon, M. Fleischer, H. P. Frerichs, Ch. Wilbertz, M. Lehmann, "Copper phthalocyanine suspended gate field effect transistors for NO_2 detection." *Sensors and Actuators B* vol. 118 (2006) pp. 249-254

2. Marcel Bouvet, "Phthalocyanine-based field-effect transistors as gas sensors" *Analytical and Bioanalytical Chemistry* vol. 384 (2006) pp. 366-373

3. B. Crone, A. Dodabalapur, A. Gelperin, L. Torsi, H. E. Katz, A. J. Lovinger, "Electronic sensing of vapors with organic transistors." *Applied Physics Letters* vol. 78, no. 15 (April 9, 2001) pp. 2229-2231

4. Molecular formulas are listed at the Sigma-Aldrich online chemical catalog http://www.sigmaaldrich.com/Area_of_Interest/The_Americas/United_States.html

5. L. Torsi, A. Tafuri, N. Cioffi, M. C. Gallazzi, A. Sassella, L. Sabbatini, P. G. Zambonin, "Regioregular polythiophene field-effect transistors employed as chemical sensors" *Sensors and Actuators B* vol. 93 (2003) pp. 257-262

6. M. C. Tanese, L. Torsi, N. Cioffi, L. A. Zotti, D. Colangiuli, G. M. Farinola, F. Babudri, F. Naso, M. M. Giangregorio, L. Sabbatini, P. G. Zambonin, "Poly(phenyleneethynylene) polymers bearing glucose substituents as promising active layers in enantioselective chemiresistors" *Sensors and Actuators B* vol. 100 (2004) pp. 17-21

7. L. Torsi, A. Dodabalapur, N. Cioffi, L. Sabbatini, P. G. Zambonin, "NTCDA organic thin-film-transistor as humidity sensor: weaknesses and strengths" *Sensors and Actuators B* vol. 77 (2001) pp. 7-11

8. Zheng-Tao Zhu, Jeffrey T. Mason, Rüdiger Dieckmann, George G. Malliaras, "Humidity sensors based on pentacene thin-film transistors" *Applied Physics Letters* vol. 81, no. 24 (December 9, 2002) pp. 4643-4645

9. Deepak Sharma, "Combining silicon and organic/polymer semiconductors in a new class of sensor devices" *Masters Thesis* (December 2005) p 22

10. Cynthia Burham, Daniel Fine, Ananth Dodabalapur, unpublished

11. Daniel Fine, Liang Wang, Debarshi Basu, Ananth Dodabalapur, unpublished

12. Liang Wang, Daniel Fine, Ananth Dodabalapur, "Nanoscale chemical sensor based on organic thin-film transistors" *Applied Physics Letters* vol. 85, no. 26 (December 27, 2004) pp. 6386-6388

13. Deepak Sharma, Ananth Dodabalapur, unpublished

14. Maryadele J. O'Neil, Ann Smith, Patricia E. Heckelman, John R. Obenchain, Jo Ann R. Gallipeau, Mary Ann D'Arecca, Susan Budavari, The Merck Index, (Merck & Co., Inc., 1996) p. 5985

15. William H. Brown, Christopher S. Foote, Organic Chemistry, 2nd Edition, (Saunders College Publishing, 1998) p. 25

16. L. Torsi, A. J. Lovinger, B. Crone, T. Someya, A. Dodabalapur, H. E. Katz, A. Gelperin, "Correlation between Oligothiophene Thin Film Transistor Morphology and Vapor Responses" *Journal of Physical Chemistry B* vol. 106, (2002) pp. 12563-12568

17. Luisa Torsi, Ananth Dodabalapur, “Organic thin-film transistors as plastic analytical sensors” *Analytical Chemistry* vol. 77, no. 19 (October 1, 2005) pp. 380A-387A

18. Takao Someya, Howard E. Katz, Alan Gelperin, Andrew J. Lovinger, Ananth Dodabalapur, “Vapor sensing with , -dihexylquarterthiophene field-effect transistors: The role of grain boundaries” *Applied Physics Letters* vol. 81, no. 16 (October 14, 2002) pp. 3079-3081

19. Deepak Sharma, Ananth Dodabalapur, (unpublished)

20. Hisao Ishii, Kazuhiko Seki, “Energy Level Alignment at Organic/Metal Interfaces Studied by UV Photoemission: Breakdown of Traditional Assumption of a Common Vacuum Level at the Interface” *IEEE Transactions on Electron Devices* vol. 44, no. 8 (August 1997) pp. 1295-1301

21. F. Amy, C. Chan, A. Kahn, “Polarization at the gold/pentacene interface” *Organic Electronics* vol. 6 (2005) pp. 85-91

22. L. Bürgi, T. J. Richards, R. H. Friend, H. Sirringhaus, “Close look at charge carrier injection in polymer field-effect transistors” *Journal of Applied Physics* vol. 94, no. 9 (November 1, 2003) pp. 6129-6137

23. Martin Pope, Charles E. Swenberg, Electronic Processes in Organic Crystals and Polymers, (Oxford University Press, 1999) pp. 202-369

24. Deepak Sharma, Liang Wang, Cynthia Burham, Daniel Fine, Ananth Dodabalapur, “Organic and Hybrid Organic/Inorganic, Transistors for Chemical and Bio Sensing” *Electron Devices Meeting, 2005, IEDM Technical Digest, IEEE International* ISBN # 0-7803-9268-x (December 5-7, 2005)

25. Ben G. Streetman, Sanjay Banerjee, Solid State Electronic Devices, 5th Edition, (Prentice-Hall of India, Inc., 2004) p. 302

26. Deepak Sharma, Daniel Fine, Ananth Dodabalapur, (unpublished)

27. David W. Oxtoby, H. P. Gillis, Norman H. Nachtrieb, Principles of Modern Chemistry, 4th Edition, (Saunders College Publishing, 1999) pp. 147-148

28. Laura Pirondini, Francesca Bertolini, Barbara Cantadori, Franco Ugozzoli, Chiara Massera, Enrico Dalcanale, "Design and self-assembly of wide and robust coordination cages" *Proceedings of the National Academy of Sciences* vol. 99 no. 8 (April 16, 2002) pp. 4911-4915

CHAPTER 4 THE PLANAR NANOSCALE ARCHITECURE FOR ORGANIC THIN-FILM FIELD-EFFECT TRANSISTORS

So far all the nanoscale transistors demonstrated in this work have been fabricated on degeneratively doped silicon wafers (silicon wafers that are doped until their properties approach that of a metal are referred to as being "degeneratively doped"). These wafers not only act as the substrate on which the devices are fabricated, but as the gate electrode as well. Although this reduces fabrication complexity, it creates a number of problems. The most obvious problem is that every device is now fabricated on the same gate and so there is no ability to control the gate bias of the nanoscale OTFTs individually. The large area gate also increases the switching capacitance of the devices. Gate leakage is significantly increased since a large number of pin holes (oxide defects which allow current to shunt from the semiconductor on top of the gate dielectric to the silicon substrate below the gate dielectric) are now accessible due to the whole substrate acting as the gate and the fact that the semiconductor cannot be patterned to nanoscale dimensions during deposition. Finally, the large area gate adds to the spreading currents as well as the small transistor width to length ratios used for most of the nanoscale transistors (to avoid electrode shorts during fabrication) and the contact limitations which most of these nanoscale OTFTs suffered from. It was therefore necessary to fabricate guarding electrodes simultaneously with the source and drain electrodes. These guarding electrodes, biased at the same potential as the drain, collected the spreading currents which resulted from the large amount of accumulation that occurred outside the nanoscale channel area as a result of such a large gate electrode. They also enabled the exploration of the true nanoscale transistor behavior.

The device architecture outlined in this Chapter is an attempt to reduce or eliminate many of these problems. The devices were still fabricated on a silicon wafer (with a layer of 100nm of silicon dioxide on top to prevent shorting between the electrodes through the substrate), but instead of using the substrate as the gate electrode, an aluminum electrode was deposited in close proximity to the gold source and drain electrodes. Aluminum oxide (usually Al_2O_3), known to grow spontaneously in atmospheric conditions to a thickness of around 1-3 nm [1, 2] and possess a relative dielectric constant in the range from 7 to 8 (about twice as high as silicon dioxide) [3], was used as the gate dielectric. The schematic structure is shown in Figure 44.

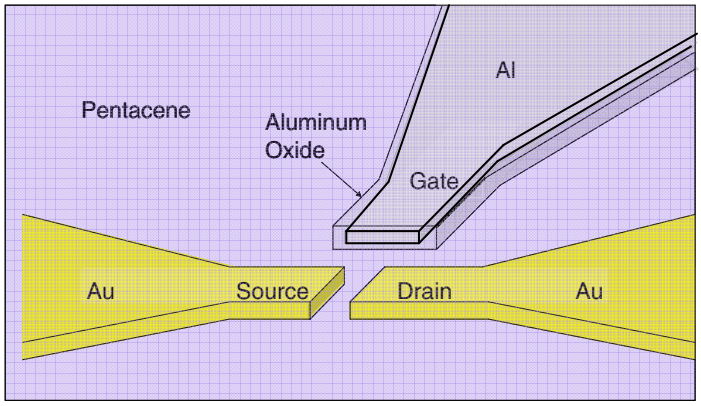

Figure 44. A schematic representation of the planar nanoscale device showing the aluminum gate electrode in close proximity to the gold source and drain electrodes on the surface of the silicon/silicon dioxide substrate. The gate dielectric is comprised of the natural oxide which forms on aluminum in atmospheric conditions.

This device geometry is suited to a wide range of deposited semiconducting materials including organic and polymer semiconductors as well as recently reported inorganic semiconductors with high mobility that can be cast from solution [4].

It is the goal of this Chapter to discuss the fabrication procedure for realizing this device geometry followed by a discussion of the device's electrical characteristics. The

chapter will conclude by detailing the possible use of this nanoscale device in future sensing applications. The primary source for most of the following material is reference [5].

4.1 Fabrication of the Planar Nanoscale Transistor Architecture

The JEOL JBX-6000FS/E Electron Beam Lithography system allows for the alignment of new patterns to previously processed patterns with a misalignment error as low as 30 to 40 nm. The first step in fabricating these devices was to pattern alignment marks which the electron beam lithography system could use to align the gold/titanium source and drain electrodes to the aluminum gate. These marks consisted of four crosses etched 1 μm deep into the surface of the silicon wafer at equal distances from the center in the four cardinal directions, as shown in Figure 45.

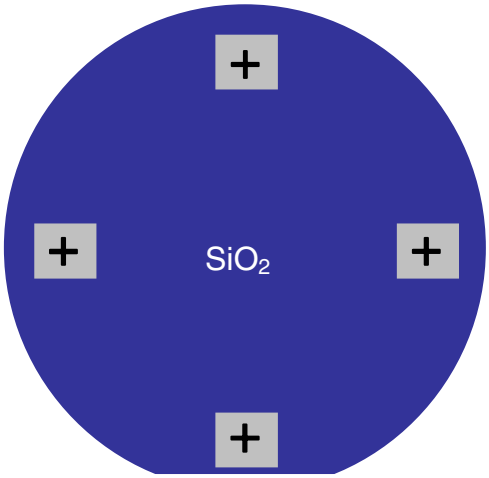

Figure 45. Position of the alignment marks used by the electron beam lithography system to align the gold/titanium source and drain electrodes to the aluminum gate electrode. The marks were etched to a depth of 1 μm. Windows through the silicon dioxide were etched around the alignment marks to prevent electron beam charging of the dielectric which might cause a distortion of the mark and lead to poor alignment.

It was then necessary to etch windows through the silicon dioxide around the marks to prevent charging of the substrate during mark detection which could distort the marks and lead to misalignment. A lithography pattern for the aluminum gate electrode was then defined using the same electron beam lithography techniques outlined in Section 2.3. This included dose testing and designed pattern dimension variation to account for the small unavoidable misalignment inherent in the electron beam lithography system as well as any wafer curvature and dielectric charging issues. The alignment procedure was also executed to align the aluminum gates to the previously patterned alignment crosses. This was then followed by the deposition of 100nm of aluminum deposited by sputtering (sputtering uses accelerated argon ions to knock aluminum atoms off of a target of aluminum which then deposit on the silicon dioxide/silicon substrate) followed by the lift off procedure (also outlined in Section 2.3). Next the patterns for the source and drain electrodes were exposed also using the alignment procedure. Once the lithography was complete, 3 nm of titanium was deposited immediately followed by 50 nm of gold using an electron beam evaporation system succeeded by another lift off procedure. The source and drain electrodes were placed in close proximity to the aluminum gate (in a co-planar geometry) as opposed to on top of the aluminum gate for three reasons. The first is that having the source/drain electrodes on top of the gate electrode increases the chance of having them short together. The second is that the surface of the silicon dioxide is smoother than the surface of the aluminum since aluminum forms very tiny grains when deposited at room temperature. Cooling the substrate to liquid nitrogen temperatures alleviates this problem by making the metallic film more amorphous [1], but this was not attempted here because the sputtering system is not equipped to cool the substrates. Finally, even if it were possible

to cool the substrates to get flatter gate surface areas, the gate electrode would still have to be fairly wide to accommodate the ends of the source and drain electrodes and to have a nice flat channel area. This would not eliminate the necessity of guarding electrodes (patterning the semiconductor at these dimensions is not feasible). By patterning the gate near the source and drain electrodes, as shown in Figure 44, there is a much smaller risk of shorting the electrodes together. The semiconductor can still be deposited on the very flat silicon dioxide, and side guards are not necessary because the gate can be designed to span a distance on the order of the channel length (the channel width is now defined as the thickness of the deposited pentacene as long as it is thinner than the deposited electrodes). The gate still has to overlap the source and drain electrodes to some extent, in order to compensate for the aforementioned misalignment problem, but to a much lesser degree. The device geometry also insures that most of the current is confined to the channel region due to a large electric field at the closely spaced, narrow tips of the gate, source, and drain electrodes that falls off quickly as the distance between the electrodes rapidly increases outside the channel. Upon completion of the source/drain and gate electrode patterning, the semiconductor was deposited, in this case 35 nm of pentacene, using vacuum thermal evaporation on top of the electrodes.

The source and drain electrodes of some of the nanoscale planar transistors were treated with nitrobenzenethiol prior to semiconductor deposition. Nitrobenzenethiol is a sulfur containing molecule which readily forms self-assembled monolayers on gold and has been shown to improve the injection qualities of organic transistors [6].

Figures 46(a) and 46(b) are scanning electron microscopy (SEM) images representing two different electrode patterns used in fabricating these devices. Figure 46(a) represents the first design used for fabrication which shows a source to drain

spacing (the channel length) around 100 nm and a gate electrode to channel spacing which is larger than the channel length. Figure 46(b) represents a second design where the channel length is on the order of the gate to channel spacing, about 50 nm. As has been shown in previous work, the channel length can be reduced to around 10 nm [7]. The granular morphology in Figure 46(a) is due to the pentacene [8].

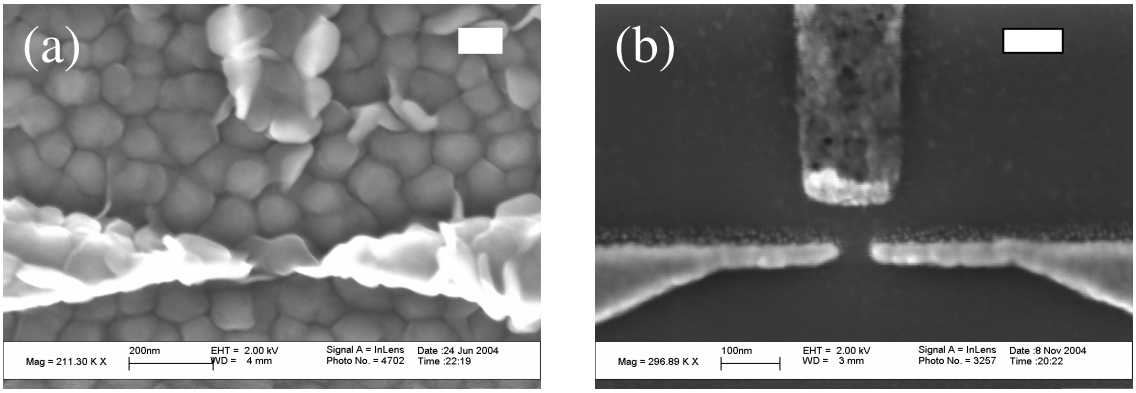

Figure 46. Scanning electron micrographs showing two different representative transistors with a viewing angle perpendicular to the substrate surface. The vertical electrode is the aluminum gate and the two horizontal electrodes are the titanium/gold source and drain electrodes. Micrograph (b) shows a device prior to pentacene deposition whereas (a) shows a device after pentacene has been deposited and after the device has been electrically characterized. The white scale bars for both (a) and (b) are 100nm. "Reprinted with permission from Daniel Fine, Liang Wang, Deepak Sharma, Ananth Dodabalapur, "Planar nanoscale architecture for organic thin-film field-effect transistors" Applied Physics Letters vol. 89, article # 203118 (2006) pp. 1-3 and the American Institute of Physics."

4.2 MEASUREMENT OF THE PLANAR NANOSCALE OTFT'S ELECTRICAL CHARACTERISTICS

The electrical characteristics of the transistors were evaluated with an Agilent 4155C semiconductor parameter analyzer. Figures 47 and 48 show the current-voltage characteristics for two representative devices similar to those represented in Figures 46(a) and 46(b). These differing characteristics demonstrate that these transistors have

current/voltage dependences which vary with exact device geometry (source/drain spacing and channel to gate spacing), semiconductor film morphology, and injection properties, all factors which become more significant as OTFTs shrink in size.

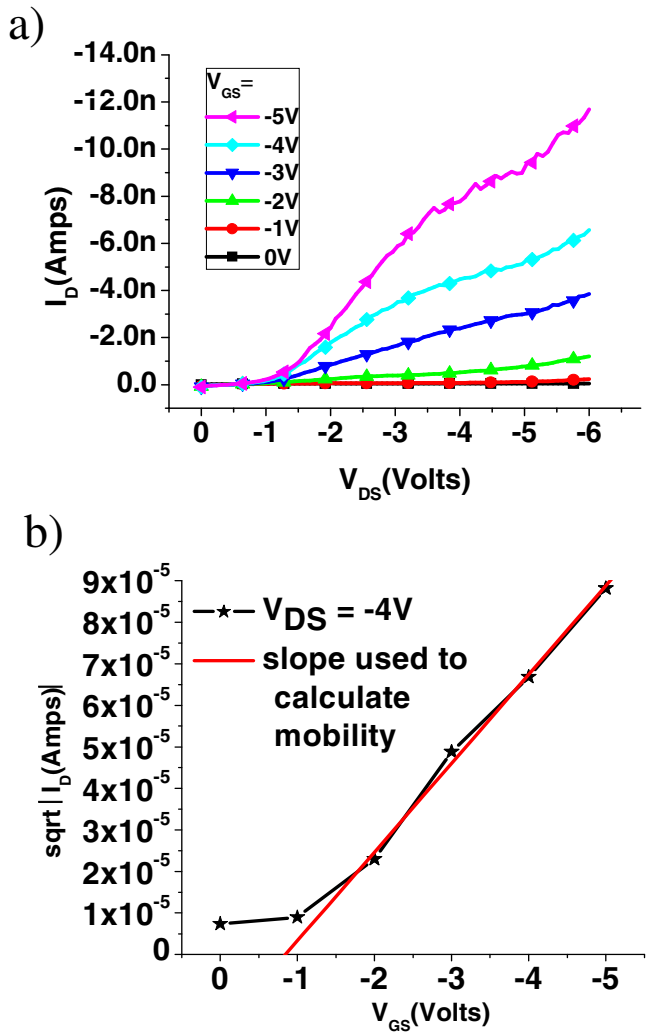

Figure 47. (a) Drain current vs. source/drain voltage characteristics of a transistor with a geometry similar to Figure 46(b), which behaves as a p-channel accumulation mode field-effect transistor but shows evidence of severe contact limited injection at very low V_{DS} and space-charge limited current at high V_{DS}. (b) •I_{DS} vs. V_{GS} for the same device shown in Figure 47(a) at V_{DS} = -4V. The solid line lacking symbols is the linear fit used to calculate the mobility. "Reprinted with permission from Daniel Fine, Liang Wang, Deepak Sharma, Ananth Dodabalapur, "Planar nanoscale architecture for organic thin-film field-effect transistors" Applied Physics

Letters vol. 89, article # 203118 (2006) pp. 1-3 and the American Institute of Physics."

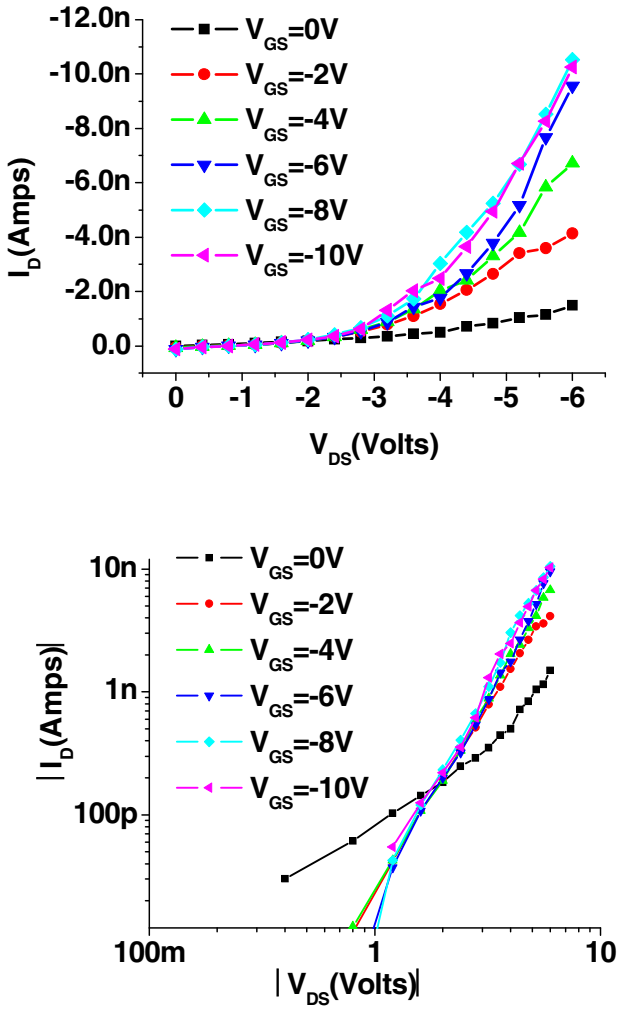

Figure 48. (a) Drain current vs. source/drain voltage characteristics of a second transistor with a geometry similar to Figure 46(a) showing space-charge-limited current which is gate modulated due to adjustments to the injection barrier by the gate and/or a gate induced filling of traps at the semiconductor/contact interface. (d) The $\log(I_D)$ vs. $\log(V_{DS})$ plot for the device from (a) showing the power law dependence of current to voltage. "Reprinted with permission from Daniel Fine, Liang Wang, Deepak Sharma, Ananth Dodabalapur, "Planar nanoscale architecture for organic thin-film field-effect transistors" Applied Physics Letters vol. 89, article # 203118 (2006) pp. 1-3 and the American Institute of Physics."

The device whose characteristics are presented in Figures 47(a) and 47(b) had source and drain electrodes treated with nitrobenzenethiol. The gate leakage current in all the devices was negligible. The mobility of the device whose characteristics are described in Figure 47(a), and whose design is depicted in the SEM image of Figure 46(b), was 3.68*10-4 cm^2/V-s (as measured from the linear part of the •IDS vs. VGS plot at VDS = -4V shown in Figure 47(b)). This is two orders of magnitude lower than previously reported values for nanometer sized pentacene field-effect transistors [7].

4.3 A DISCUSSION OF THE FEATURES OF THE ELECTRICAL CHARACTERISTICS OF THE PLANAR NANOSCALE OTFT

The DC characteristics shown in Figure 47(a) are comprised of three distinct regimes with increasing V_{DS}. The first is the relatively high magnitude of source/drain voltage (slightly higher than 1V) required to obtain any appreciable amount of current followed by a short region where current increases exponentially with source/drain voltage. This is typical of current which is severely injection limited at low magnitudes of V_{DS} [9, 10, 11]. Previous attempts to describe this injection limited regime have mainly followed the diffusion-limited thermionic emission model for injection from a Schottky barrier into a low mobility semiconductor [9]. More recently, modifications to that model have been suggested due to a measured injection barrier, using scanning probe potentiometry, which does not match the expected injection barrier which would result from a simple calculation of the metal work function/ionization energy mismatch [10]. As outlined in detail in Section 2.7, these changes to the theory are explained as thermally assisted tunneling through the Schottky injection barrier [7], or thermally assisted tunneling through or thermally assisted injection into the highly disordered

region around the contacts in these nanoscale devices [10]. If the disordered region is relatively small, tunneling through the disordered region into the channel could occur (tunneling is exponentially dependent on source to drain voltage). On the other hand, injection into the disordered region actually becomes easier due to a Gaussian or exponential distribution of tail states in the semiconductor, as well as HOMO and LUMO level splitting near the contacts, also outlined in Section 2.7, which reduces the HOMO/LUMO separation [12]. If this disordered region is relatively wide, transport is adversely affected due to significantly increased trapping. These models both generally depict super-linear current which varies exponentially with the contact injection barrier height (which can be enhanced through he formation of interface dipoles, also discussed in Section 2.7) which has been shown to be a function of both gate voltage and source to drain voltage. Both models are also heavily dependent on the morphology near the contact [9, 10].

The second distinct regime of this device's characteristics is that expected from a short-channel organic field-effect transistor (OFET), comprising a linear region and saturation region where changes in current arise from gate modulation of the accumulated charge in the channel. The saturation region of this device has a nonzero slope most likely due to source/drain voltage assisted tunneling. As mentioned above, at the high electric fields achieved with these nanoscale devices, the source/drain voltage can increase band bending at the semiconductor/metal interface and thereby enable thermally assisted Fowler-Nordheim tunneling through the injection barrier by reducing the barrier width [7]. The $\bullet \mathbf{I}_D$ vs. V_{GS} in Figure 2(b) measured at V_{DS} = -4V clearly shows a quadratic dependence of source/drain current to gate voltage as is expected for an OFET in saturation [13]. Finally, the super-linear region at high V_{DS} is due to space-charge-limited current (SCLC). This is the current through the bulk of the semiconductor without gate

control, parallel to the channel current, and follows a power law, where I_D is proportional to $(V_{DS})^n$ [11, 14]. The SCLC has a power index which arises from traps in the semiconductor and thus can reach values which are higher (n>2) than the square-law dependence in the trap-free case. This is usually referred to as SCLC at the trap filling limit [14, 15].

Thus, this device can be considered to have a total source to drain resistance consisting of three components, a contact resistance in series with a parallel combination of a channel resistance and a bulk resistance, as demonstrated in Figure 49. Since the source contact is injecting the charge, it faces the largest effects of the barrier at the contact and is thus much larger than the drain resistance. At larger device dimensions, the channel resistance is typically much higher than the contact resistance and the electric fields are typically not high enough to create significant SCLC. Thus the channel resistance dominates the overall characteristics. At the smaller dimensions presented here, however, all three components must be taken into account to obtain an accurate picture of device operation.

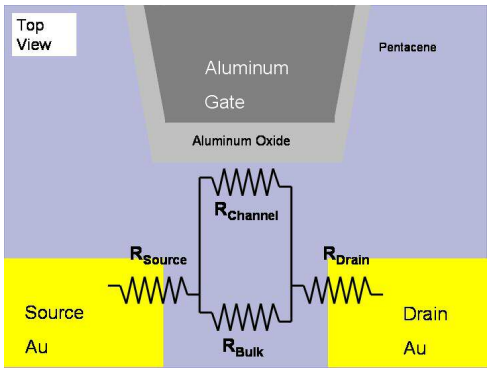

Figure 49. The resistance network diagram illustrating the main resistances involved with current flow through the device. R_{source} and R_{Drain} are the contact resistances at the source and the drain, respectively (R_{source} » R_{Drain}). $R_{Channel}$ is gate modulated and R_{Bulk} is governed by space-charge-limited current (SCLC). "Reprinted with permission from Daniel Fine, Liang Wang, Deepak Sharma, Ananth Dodabalapur, "Planar nanoscale

architecture for organic thin-film field-effect transistors" Applied Physics Letters vol. 89, article # 203118 (2006) pp. 1-3 and the American Institute of Physics."

The characteristics of the device depicted in Figure 48, whose design is depicted in the SEM image in Figure 46(a), show no classical linear or saturation region but are super-linear over their entire range. Figure 48(b), a log-log plot of I_{DS} vs. V_{DS}, demonstrates that shortly after a high enough V_{DS} is attained, this device's characteristics follow a power law with a power index greater than 2 for nonzero gate voltages. It therefore depicts SCLC in the trap filling limit. The contact quality of this device is not as good as the device with the nitrobenzenethiol treatment (as is evident from the higher necessary drain voltage to achieve significant conduction). The fact that there is gate modulation can be attributed to a lowering of the injection barrier with gate voltage and/or gate induced filling of some of the traps in the disordered semiconductor region near the contact [9, 10]. These effects increase the amount of voltage dropped over the bulk as opposed to the contact [10, 11]. The difference in the nature of the gate control of the drain current in this device compared to the device depicted in Figure 47 is probably due to geometry considerations. As can be seen from the SEM image in Figure 46(a), the channel length is much smaller than the gate to channel spacing. A high ratio of the gate to channel spacing to the channel length would mean that the accumulated charge would be farther away from the channel, and therefore the resistance to get from the source to the gate or the gate to the drain would be higher than the resistance to get directly from the source to the drain. This would mean that conduction through the bulk would dominate once the contact limitations had been overcome. This device demonstrates the effect device geometry variability can have on the output. It also demonstrates that injection barrier modulation can cause a change in the conductance of the device. The

fact that the drain current saturates with gate voltage in this device indicates that at some point the injection barrier becomes low enough to be ignored.

4.4 A POSSIBLE ROLE OF THE PLANAR NANOSCALE OTFT AS A SENSOR

This planar nanoscale architecture has the potential to allow for a great deal of flexibility in its use as a chemical and biological sensor. In addition to chemical analyte detection modes based on interactions between the chemical species of interest and the OTFT's channel and contacts, discussed in Chapter 3, it can now also be used as a very sensitive organic CHEMFET. The small amount of gate charge variation which should be able to be detected by this device is evident from the geometry. In sensing experiments utilizing capacitive coupling to the gate where small quantities of excess charges are generated, the tapered geometry of the aluminum gate electrode and the resultant electrostatics at its apex will maximize the influence of the excess charge on the drain current, since electric fields are highest around surfaces with high degrees of curvature (the tip of the gate electrode has a high degree of curvature due to its very small size). Since charges will not conduct through the aluminum gate electrode due to the insulating gate dielectric, only the charges near the apex of the gate electrode will participate in conduction. Furthermore, fringing currents in this configuration should be quite small as compared to a vertically stacked device, where by necessity the gate capacitively couples a large amount of active area outside the defined channel [16]. This extraneously coupled charge, by the vertically stacked gate, in essence leads to a device with a much larger effective length and width than the nanoscale dimensions would indicate, since larger portions of the electrodes can be used to inject carriers (one way to reduce this is to use guarding electrodes [7]). Finally, as long as the semiconductor is deposited thinner than the gate electrode (which is the case for this device), or the device

utilizes single macromolecules or self-assembled semiconductors as the active regions, there will be a lower amount of charge accumulation and thus very little conduction on the top surface of the gate. Although the semiconductor may cover the side walls of the aluminum oxide on the gate, that semiconductor should be fairly disordered, and thereby less conductive, when compared to the semiconductor in the channel. The semiconductor can be patterned down to 1 or 2 μm with photoresist if charge accumulation along the sides or top of the gate becomes a concern. This may not be necessary as the dielectric constant of organic semiconductors is small, which when coupled with the favorable geometry considerations, means parasitic coupling will be low. These unique features of the planar architecture all potentially enhance its sensitivity as a sensor. Figure 50 summarizes these potential sensing capabilities.

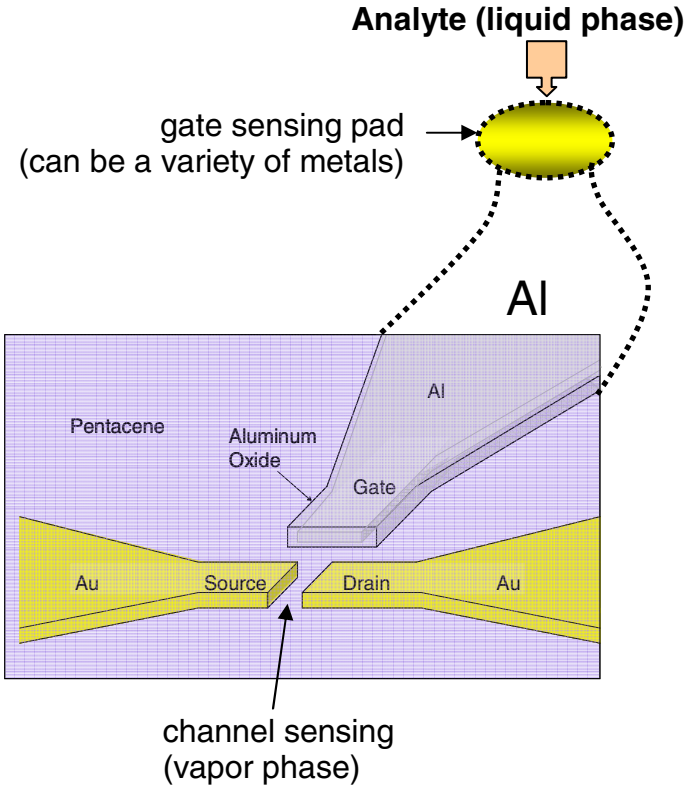

Figure 50. A schematic representation of the potential flexibility afforded by the planar nanoscale OTFT architecture when used as a sensor. In

addition to allowing analytes to interact with the charges in the channel and at the contacts, the high coupling capacitance between the gate and the channel (as a result of its nanoscale geometry) should allow for very sensitive detection when using the device as an organic CHEMFET.

4.5 REFERENCES

1. Adrian Bachtold, Peter Hadley, Takeshi Nakanishi, and Cees Dekker, "Logic Circuits with Carbon Nanotube Transistors" *Science* vol. 294, (November 9, 2001) pp. 1371-1320

2. Xavier Batlle, Bart Jan Hattink, and Amílcar Labarta, "Quantitative x-ray photoelectron spectroscopy study of Al/AlOx bilayers" *Journal of Applied Physics* vol. 91, (June 15, 2002) pp. 10163-10168

3. ELNA CO., LTD. "Introduction to Aluminum Electrolytic Capacitors: How Capacitors Work" (ELNA CO., LTD., 2001-2007)
http://www.elna.co.jp/en/ct/c31_inde.htm

4. David Mitzi, "Solution-processed inorganic semiconductors" *Journal of Materials Chemistry* vol. 14, no. 15 (2004) pp. 2355-2365

5. Daniel Fine, Liang Wang, Deepak Sharma, Ananth Dodabalapur, "Planar nanoscale architecture for organic thin-film field-effect transistors" Applied Physics Letters vol. 89, article # 203118 (2006) pp. 1-3

6. David J. Gundlach, LiLi Jia, Thomas N. Jackson, "Pentacene TFT With Improved Linear Region Characteristics Using Chemically Modified Source and Drain Electrodes" *IEEE Electron Device Letters* vol. 22, no. 12 (December 2001) pp. 571-573

7. Liang Wang, Daniel Fine, Taeho Jung, Debarshi Basu, Heinz von Seggern, and Ananth Dodabalapur, "Pentacene field-effect transistors with sub-10-nm channel lengths" *Applied Physics Letters* vol. 85, no. 10 (September 6, 2004) pp. 1772-1774

8. D. Knipp, R. A. Street, A. Völkel, J. Ho, "Pentacene thin film transistors on inorganic dielectrics: Morphology, structural properties, and electronic transport" *Journal of Applied Physics* vol. 93, no. 1 (January 1, 2003) pp. 347-355

9. Anna B. Chwang, C. Daniel Frisbie, "Field Effect Transport Measurements on Single Grains of Sexithiophene: Role of the Contacts" *Journal of Physical Chemistry B* vol. 140 (2000) pp. 12202-12209

10. L. Bürgi, T. J. Richards, R. H. Friend, H. Friend, "Close look at charge carrier injection in polymer field-effect transistors" *Journal of Applied Physics* vol. 94, no. 9 (November 1, 2003) pp. 6129-6137

11. Yulong Shen, Ahmad R. Hosseini, Man Hoi Wong, George G. Malliaras, "How to Make Ohmic Contacts to Organic Semiconductors" *ChemPhysChem* vol. 5, (2004) pp. 16-25

12. F. Amy, C. Chan, A. Kahn, "Polarization at the gold/pentacene interface" *Organic Electronics* vol. 6 (2005) pp. 85-91

13. B. G. Streetman, Solid State Electronic Devices, 4th Edition, (prentice-Hall, Inc., 1995)

14. Peter Mark, Wolfgang Helfrich, "Space-Charge-Limited Currents in Organic Crystals" *Journal of Applied Physics* vol. 33, no. 1 (January, 1962) pp. 205-215

15. P. W. M. Blom, M. J. M. De Jong, J. J. M. Vleggaar, "Electron and hole transport in poly(*p*-phenylene vinylene) devices" *Applied Physics Letters* vol. 68, no. 23 (June 3, 1996) pp. 3308-3310

16. Josephine B, Lee, Paul C. Chang, Alexander Liddle, and Vivek Subramanian, “10-nm Channel Length Pentacene Transistors” *IEEE Transactions on Electron Devices*, vol. 52, no. 8 (August 2005) pp. 1874-1879

CHAPTER 5 ION CHANNELS IMMOBILIZED IN TETHERED LIPID MEMBRANES TO REALIZE SENSITIVE AND SELECTIVE BIOSENSORS AND THEIR POSSIBLE INTEGRATION WITH SOLID-STATE DEVICES

As was briefly discussed in Chapter 1, biological organisms and systems contain a myriad of highly specialized, highly evolved recognition constructs and mechanisms for identifying important chemical and biological agents. One such construct is the antibody. Another, more complex entity, is the ion channel. Ion channels are transmembrane proteins which fulfill a number of extremely important cellular tasks. Ion channels, in conjunction with ion pumps, are crucial in maintaining the proper ionic gradients across the cell membrane [1]. These gradients are then used to fuel many important transmembrane exchange mechanisms [1]. The maintenance of these ion gradients also helps to insure that the cells do not collapse or burst because of increases in osmotic pressure [1]. Ion channels also serve as the key elements in the transfer of action potentials (neuron electrical signals), the main mechanism by which the brain communicates with other bodily systems in higher organisms [1]. It is the rapid depolarization and repolarization of cells through the voltage gated potassium and sodium ion channels that enables the rapid transfer of electrical action potentials along neurons [1]. These are just a few examples of the importance of these membrane proteins.

It is the ability of these ion channels to control ion flow across the membrane stochastically which makes them so attractive, coupled with their ability to be voltage and ligand gated. If a proper membrane support could be constructed which allowed the incorporation of these proteins to be arrayed in a manner where their biological function could be maintained, and if it were possible to isolate or engineer these channels to allow

for the expression of a variety of chemically and biologically important receptors, and if an appropriate solid state circuit solution can be devised to amplify and process signals from single ion channels, these devices should enable the highly selective, sensitive, portable, and relatively low cost detection of analytes through the direct monitoring of the ion channel's current flow characteristics. No extraneous mechanism, such as fluorescence, would then be needed to turn the output of the sensing event into an electrical signal. The ability of ion channels to detect small concentrations of various analytes has already been demonstrated by several groups by using methodologies which utilize both single channel and ensembles of channels [2, 3, 4, 5]. To date, however, there are no reports of single channel current recordings through a single or small number of discreet devices in a framework which enables portable, in situ analyte detection.

This Chapter will begin by briefly looking at the lipid bilayer in which the ion channel is immobilized and the membrane tether used to attach the bilayer to the solid support. This will be followed by an investigation into the types of ion channels which have thus far been explored for incorporation into these sensors. A prevalent current methodology for recording single ion channel activity will then be explained showing how the bilayer is formed and how the currents are electrically measured. In order for these systems to function, the bilayers must be formed on very flat surfaces. The next Section will look into how to fabricate ultra flat gold surfaces in a repeatable fashion which lends itself to high throughput processing. These ultra flat gold electrodes can allow for the bilayers to form high impedance layers without the formation of defects in the lipid membrane caused by surface variation. These defects short the sensing pad to the bath and prevent the recording of single ion channel currents. This discussion will be followed by a demonstration of tethered bilayer systems in operation as measured on these ultra flat electrodes. Finally, this Chapter will conclude with an evaluation of a

device, the bipolar junction transistor (BJT), which has been selected as a promising candidate for amplifying these small single ion channel currents. In further circuit configurations, initial amplification will be necessary for the initially small signal to be processed (for instance calculating open and closed frequencies of the channels or determining whether there is more than one channel conductance state) and recorded. Amplification through a discreet device or a circuit composed of a small number of solid state devices will also demonstrate that portable, sensitive, selective and relatively low cost biosensing using single ion channel recordings is indeed a real possibility.

5.1 THE TETHERED LIPID BILAYER

One of the largest impediments to the use of immobilized ion channels as portable biosensors is the need for a very stable lipid membrane into which the ion channel is embedded. Initial experiments using solid-supported lipid membranes suspended on thin films of water on ultra flat substrates suffered from a few drawbacks. First, the fact that the lipid bilayer is only adsorbed to the surface on the thin film of water made it easier for the film to detach or otherwise lose structural integrity [6]. Second, the natural state of the lipid-to-surface coupling resulted in a fairly small separation of the lipid bilayer to the substrate. This then prevented the functional incorporation of some ion channels which possess particularly large sub-membrane protrusions [6]. Another technique for producing lipid bilayers is the use of the black lipid membrane (BLM) [7]. This is a membrane which is suspended in a pore or aperture which separates two buffer solution containing baths into which some kind of ion exchanging electrode is placed (usually silver/silver chloride) [7]. This has also been implemented in a microarray configuration [8]. The black lipid membranes (BLM) tend to rupture in a single catastrophic event due to mechanical distortion [9]. To increase the bilayer lifetime, nanopatterned alumina can be placed in the aperture which decouples the BLM over each pore from adjacent pores

[9]. Thus, the resistance falls as more pores rupture but it does not occur all in one event [9]. This BLM system, even with the nanopores, can still be potentially unstable, as the primary sensing element, the nanopatterned alumina, could be delicate. Furthermore, this apparatus adds significantly to device fabrication complexity.

The bilayer formation and stabilization methodology utilized in these studies (and by several other groups [10, 11]) was to use molecular tethers to attach the bilayer to a solid substrate support, in this case an ultra flat gold electrode [2, 12, 13]. This methodology should combine good stability, which is derived from the anchor points of the membrane covalently bound to the electrode, with the ability to produce large arrays of electrodes, which can be produced with lower fabrication complexity (the reason for this will be seen later). The phospholipids used in these studies, 1,2-diphytanoyl-*sn*-glycero-3-phosphocholine and 1,2-diphytanoyl-*sn*-glycero-3-phosphoethanolamine (depicted in Figure 51 and provided by Avanti Polar Lipids, Inc.), are derivatives of lipids found in the membranes of archaebacteria [12]. The membranes of these organisms, which are prokaryotes (no nuclear envelope) that make up a third domain, kingdom or "aboriginal line of descent," in addition to eubacteria (which are also a type of prokaryote) and eukaryotes (organisms containing nuclear envelopes), were selected to be used in this study due to their greater robustness forged by their extreme environments [14, 15]. Archaebacteria are found in such places as deep sea volcanic vents, hot springs, acidic bogs, and many other equally inhospitable locales [15].

The tethers, 2,3-di-*O*-phytanyl-*sn*-glycerol-1-tetraethylene glycol-$_{D,L}$- -lipoic acid ester lipid (DPTL), are single molecules, shown in Figure 52, comprised of three primary components, the hydrophobic ether linked isoprenoid tails (isoprenoid refers to a molecular moiety which is similar to isoprene), the polar tether group (a polyethylene glycol unit), and the surface binding residue (a sulfur containing unit) [16] (the tethers

were provided by Professor Dr. Wolfgang Knoll's group at the Max Planck Institute for Polymer Research in Mainz, Germany). Notice the hydrophobic tails composed of phytanyl chains are the same as the hydrophobic tails in the phospholipds shown in Figure 51. Reference [16] also details the procedure for synthesizing these tethers.

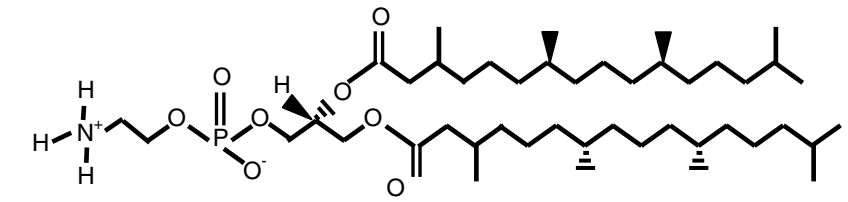

1,2-diphytanoyl-*sn*-glycero-3-phosphoethanolamine (DPhPE)

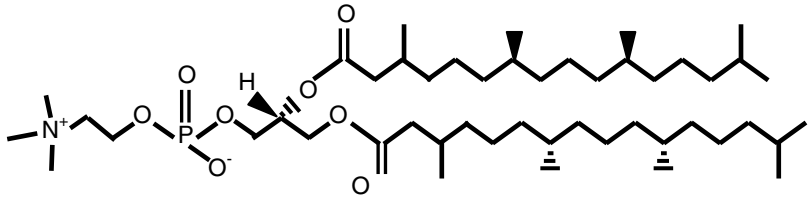

1,2-diphytanoyl-*sn*-glycero-3-phosphocholine (DPhPC)

Figure 51. The lipids used to form the bilayer in a molar ratio of 7:3 [12]

2,3-di-*O*-phytanyl-*sn*-glycerol-1-tetraethylene glycol-$_{D,L}$-α-lipoic acid ester lipid (DPTL)

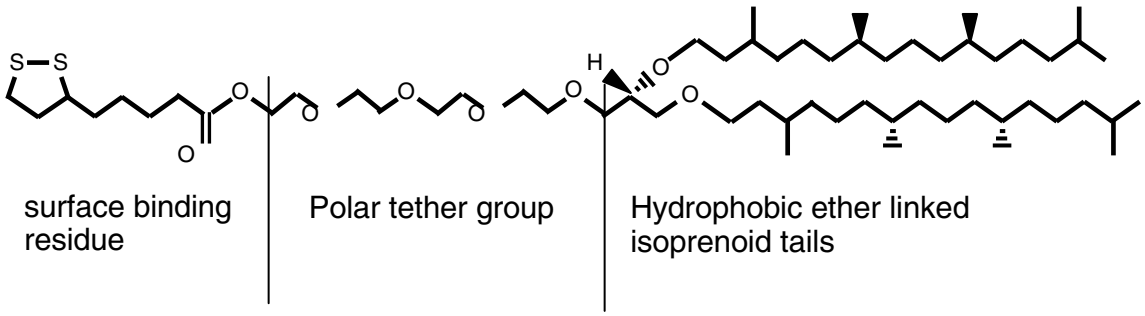

Figure 52. The molecule used to tether the lipid bilayer to the surface of the gold electrode [16].

The thiolated tethers are allowed to self assemble first on the ultra flat gold electrode [12]. The bilayer is formed through spontaneous vesicle fusion, as shown in Figure 53 [17]. The ion channels are also incorporated into the lipid bilayer by inclusion into the vesicle prior to fusion. Figure 54 shows a representation of the arrangement of the DPTL molecules when they form the lipid bilayers [16]. The surface roughness of the gold must be significantly lower than the length of the ethylene glycol spacer to insure dense monolayer and bilayer formation (producing ultra flat gold electrodes will be discussed in a later Section) [16].

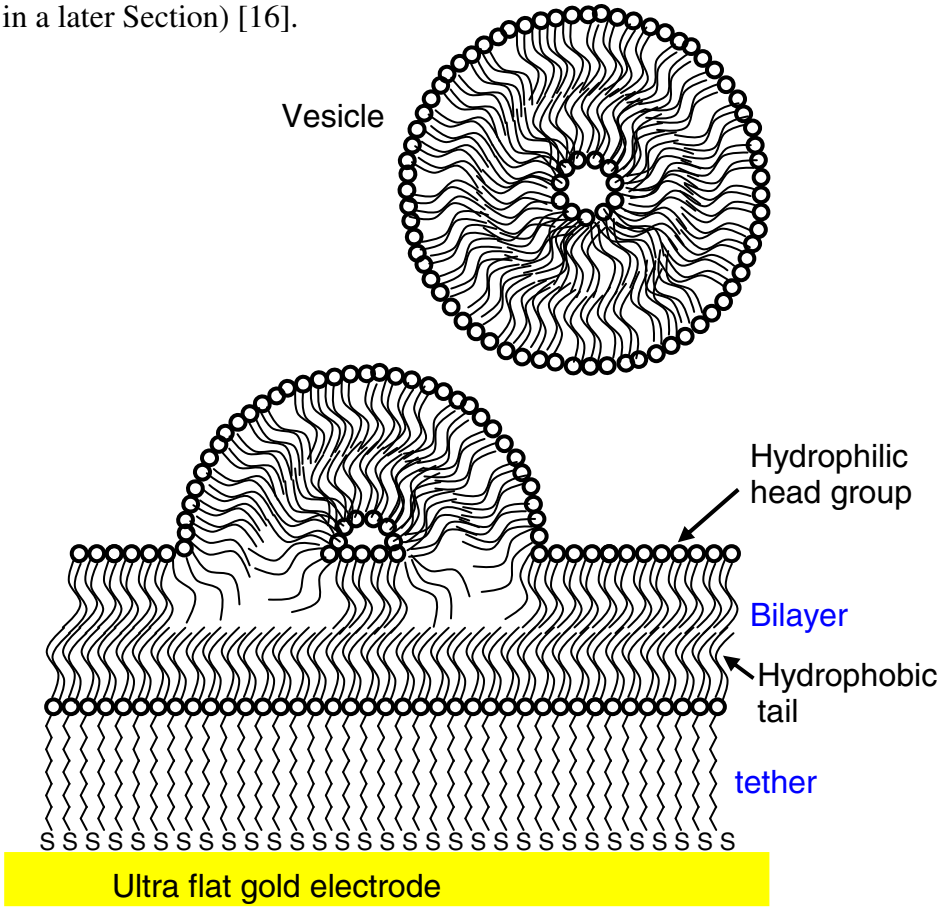

Figure 53. The process of bilayer formation through vesicle fusion. Ion channels can be incorporated into the final bilayer by including them in the initial vesicles [17].

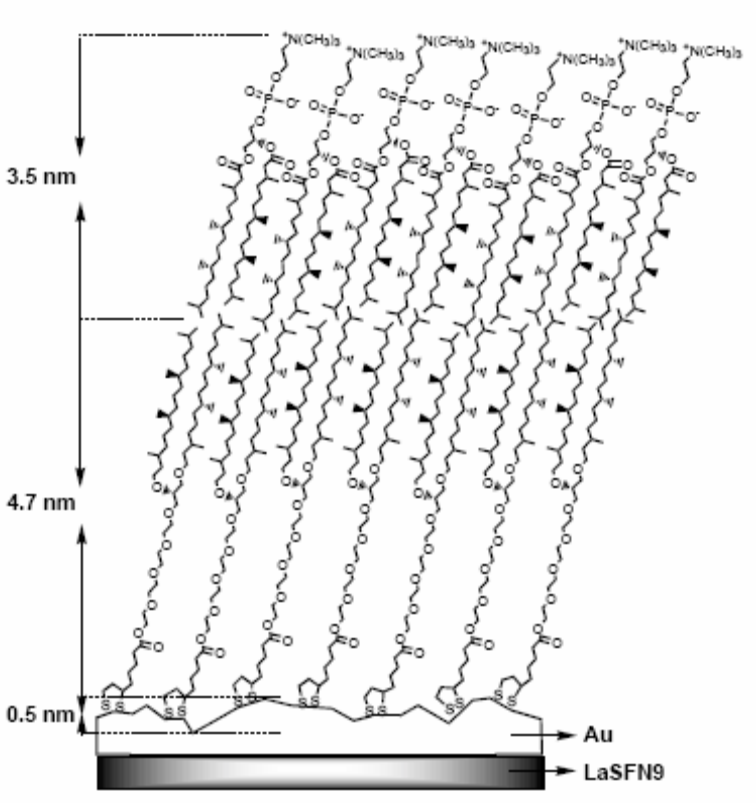

Figure 54. A schematic representation of the arrangement of the DTPL molecules in the tethered bilayer lipid membrane. The surface roughness of the gold electrode must be kept much lower then the dimensions of the molecules in order to insure stable, dense monolayer and bilayer formation. "Reprinted with permission from Stefan M. Schiller, Renate Naumann, Katherine Lovejoy, Horst Kunz, Wolfgang Knoll, "Archaea Analogue Thiolipids for Tethered Bilayer Lipid Membranes on Ultrasmooth Gold Surfaces" *Angewandte Chemie-International Edition* vol. 42, no. 2 (2003) pp. 208-211. Copyright © 2007 WILEY-VCH Verlag GmbH & Co. KGaA, Weinheim.

The tethers provide two very important services to the lipid bilayers. The first is that they maintain a larger fixed distance between the bottom of the membrane and the top of the electrode than supported lipid bilayers can achieve. This allows for both better decoupling of the lipid bilayer from the hydrophobic electrode and a larger submembrane

space [16]. Both these features enable a wider variety of channel proteins to be incorporated into the membrane [16]. The second important service these tethers provide is enhanced stability of the membrane while maintaining the membrane's fluidity and high ion resistance, important attributes for successful protein incorporation and measurement [6]. Experiments using photo-bleaching of fluorescently labeled lipids in a system which used polymer tethers showed that the diffusion coefficient of the lipids, and thus their fluidity, was mildly affected by the tethers (the diffusion coefficient was reduced by a factor of roughly three to four) [6]. Compared to a phase transition of the lipid to a gel state, which can have a diffusion coefficient 3 to 4 orders of magnitude lower than those recorded for both the untethered and tethered membranes, the hit to fluidity in the tethered membrane was minor [6]. Natural and synthetic membranes also need to have extremely high resistances to ionic current flow to maintain the proper intra and extracellular ion concentrations, or in the laboratory, to have a low enough background current to be able to measure the small ion channel currents [16]. Comparing the tethered bilayer lipid membrane (tBLM) systems to that of supported bilayer lipid membrane systems (a model system with good representative electrical properties), the resistance of the tBLM was between 2 and 12 M cm^2 which compares favorably to 10 M cm^2 or higher for the supported lipid bilayer membranes (sBLM) [16]. The capacitance of the tBLM system also measures up well to the sBLM system at 0.45-0.8 μFcm^{-2} and 0.5 μFcm^{-2}, respectively [16].

5.2 THE INVESTIGATED ION CHANNELS

Ion channels, when opened, provide a pathway for hydrophilic ions to cross the hydrophobic interior of the lipid bilayer membrane. They can do this using a variety of mechanisms, two examples of which are providing a water filled channel through the

membrane (such as gramicidin A described below) [12], or providing charged residues inside the ion pores that can take the place of the associated water molecules normally surrounding the ion while it is in solution [1]. The studies conducted for this work utilized four different types of ion channels. The ion channels were selected based on how well they were characterized in the literature and how easily they could be incorporated into the tethered lipid bilayer membrane (tBLM).

One of the ion channels used was a channel called M2 , a synthetic ion channel based on the channel-lining domain of the nicotinic acetylcholine receptor (nAChR) isolated from *Torpedo californica* [2]. The M2 primary structure is an -helix with no kinks [18], with five of these helices (a pentamer) combining to produce one transmembrane ion channel (*see* Figure 55) [18]. The M2 is selective to both potassium and sodium and is voltage gated (the nAChR receptor as a whole can also be ligand gated) [2]. The helical pentamers change orientation when a voltage is applied. The conductance of this channel is about 45 pS [2].

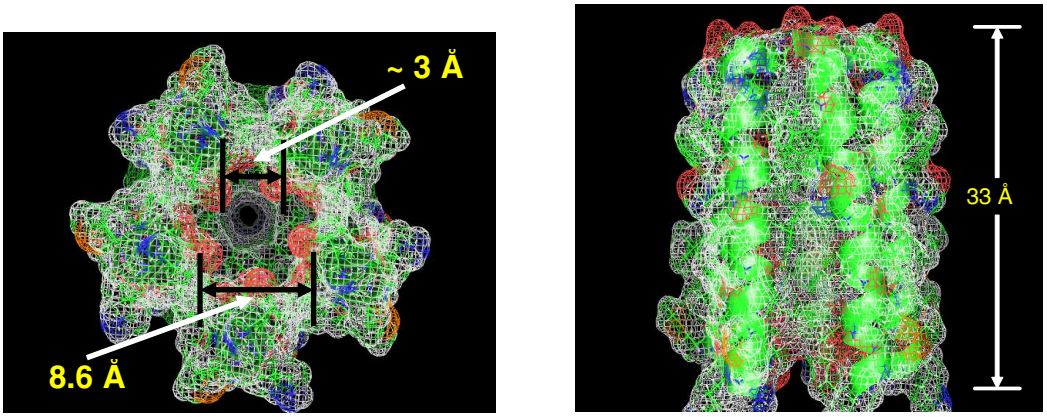

Figure 55. The structure of the ion channel formed by the combination of five M2 channel-lining domains (a pentamer) of the nicotinic acetylcholine receptor (nAChR) (as resolved by NMR). The left figure is a view through the channel showing the pore size, and the right figure is a side view of the channel showing three of the five M2 units and their -helical structure. "Reprinted with permission from S. J. Opella, F. M.

Marassi, J. J. Gesell, A. P. Valente, Y. Kim, M. Oblatt-Montal, M. Montal, "Structures of the M2 channel-lining segments from nicotinic acetylcholine and NMDA receptors by NMR spectroscopy" *Nature Structural Biology* vol. 6, no. 4 (April 1999) pp. 374-379 and copyright 1999 Nature America Inc."

A second ion channel utilized for some of these experiments was a highly conductive (> 200 pS) calcium (Ca^{2+})-activated potassium channel referred to as the BK, Maxi-K, or *Slo* channel [2]. This channel is a tetramer and can be voltage gated as well as activated by Ca^{+} [20] (*see* Figure 56).

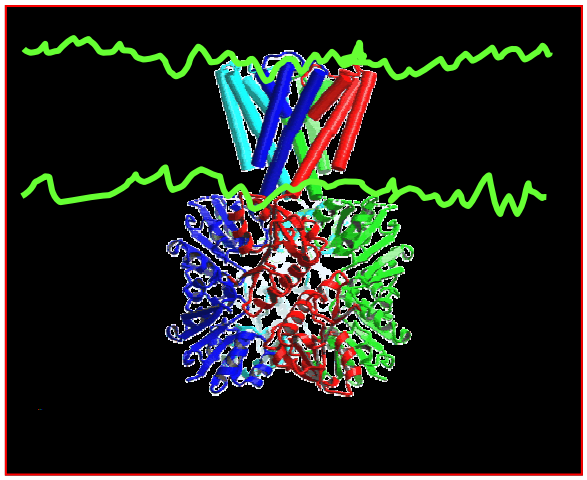

Figure 56. The Maxi-K calcium-activated potassium channel. The four colors represent the four identical component pieces of this tetramer channel (MacKinnon *et al.* [19, 20]). The green lines represent the bounds of the lipid bilayer membrane. This channel can be both voltage and Ca^{2+} gated [20].

A third ion channel used for these studies and one already proven to be able to be incorporated into biosensors [3] is called gramicidin A [12]. This channel consists of two segments which each span one half of the lipid bilayer. In a distinct demonstration of the need for bilayer fluidity, each half of the gramicidin A channel is randomly moving in its respective bilayer half until the two halves meet. The complex of the two sub units is

then maintained for some period of time by intermolecular hydrogen bonds [12]. The gramicidin A pathway is then a water filled transmembrane channel through which small monovalent ions can pass (such as potassium) [12]. Figure 57 shows a schematic representation of gramicidin A in a tethered lipid bilayer membrane [12]. The actual molecular structure of gramicidin A is delineated in reference [21]. This channel has a conductance of 67 pS [12].

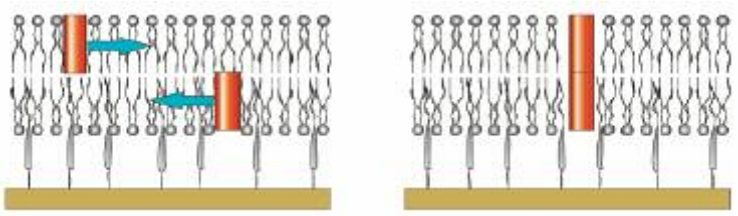

Figure 57. A schematic representation of the operation of gramicidin A incorporated in a tethered lipid bilayer membrane. The left figure represents a closed state and the right figure represents an open state. "Reprinted with permission from Martin Andersson, Henk M. Keizer, Chenyu Zhu, Daniel Fine, Ananth Dodabalapur, Randolph S. Duran, "Detection of Single Ion Channel Activity on a Chip Using Tethered Bilayer Membranes" *Langmuir* vol. 23 (2007) pp. 2924-2927 and copyright 2007 American Chemical Society."

The final ion channel used is a mechanosensitive large conductance channel from the MscL family of ion channels [22] (*see* Figure 58). This channel is gated through mechanical stress applied to the lipid bilayer membrane by an external electric field and has a conductivity which has been shown to be between 2.5 and 3 nS [13, 23]. This channel is thought to be primarily responsible for regulation of osmotic pressure [22]. The channel itself is a homopentamer with each unit containing two transmembrane -helices and one -helix which extends into the cytoplasm [22].

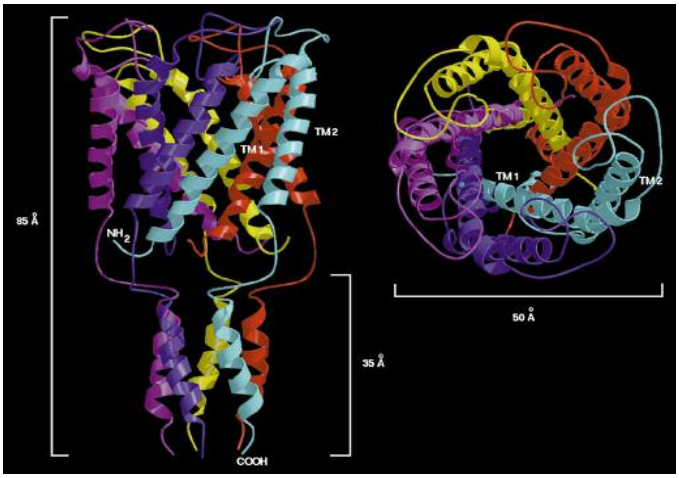

Figure 58. The molecular structure of a mechanosensitive large conductance channel (~3 nS) from the MscL family of ion channels. This channel is a homopentamer with two transmembrane -helices and one -helix which extends into the cytoplasm. It is gated when mechanical stress is applied to the membrane. "Reprinted with permission from Geoffrey Chang, Robert H. Spencer, Allen T. Lee, Margaret T. Barclay, Douglas C. Rees, "Structure of the MscL Homolog form *Mycobacterium tuberculosis*: A gated Mechanosensitive Ion Channel" *Science* vol. 282 (December 18, 1998) pp. 2220-2226 and copyright 1998 The American Association for the Advancement of Science (AAAS)."

5.3 MEASUREMENT OF ION CHANNEL ACTIVITY USING THE VOLTAGE CLAMPED TIP DIP TECHNIQUE

For over 20 years, one of the preferred methodologies used to investigate ion channel conduction characteristics has utilized a lipid bilayer on the surface of a micro pulled pipette and has been referred to as tip dip [24]. This technique utilizes a micropipette created by pulling a glass capillary tube with a microforge until the tip opening is only 1.5 μm in diameter [12]. A buffer solution is prepared and put into both the micropipette and a small reservoir 1cm deep and 1 cm in diameter along with a silver/silver chloride (Ag/AgCl) electrode (one electrode fed into the pipette and one in

the bath) [12]. A drop of lipid containing solution is then dispensed on top of this reservoir where the lipids will self assemble into a monolayer with their hydrophilic head groups in contact with the water and their hydrophobic tails sticking up into the air [12]. The pipette tip is then carefully lowered into the reservoir using a micromanipulator. On the first lowering of the pipette, the tip is allowed to penetrate into the reservoir below the lipid monolayer at the surface for some time and removed completely from the bath [24]. Since the pipette surface is hydrophilic and the opening is small (1.5 μm), lipids will be withdrawn from the solution coating the tip with the hydrophilic head groups in contact with the glass [24]. If the pipette outlet is small enough, a monolayer of lipids will also form over the opening [24]. The tip is then very carefully lowered back towards the reservoir but this time not with the intention of puncturing the monolayer on the surface. Instead, the objective is to lightly push the tip in a small distance on the surface, just enough to put the lipid monolayer on the opening of the pipette in firm contact with the lipid monolayer on the surface of the bath without puncturing it [24]. While lowering the tip (on both occasions), the current is measured between the tip and the reservoir using the Ag/AgCl electrode (in the form of pulses to see the transient response) [24]. During the first tip lowering phase, the current was zero when the tip was not in contact with the bath and large when the tip had punctured the surface and was deep in the reservoir [24]. When the tip is lowered the second time, and the two monolayers come into contact, a much smaller current is observed [24]. This is because, as mentioned earlier, if the lipid bilayer membrane has formed correctly, an extremely high resistance to ion flow will result (in excess of several gigaohms) given the dimensions of the pipette tip [12, 16]. The ion channels are then incorporated into the bilayers by introduction into the pipette [24]. Figure 59 shows schematically how this process takes place.

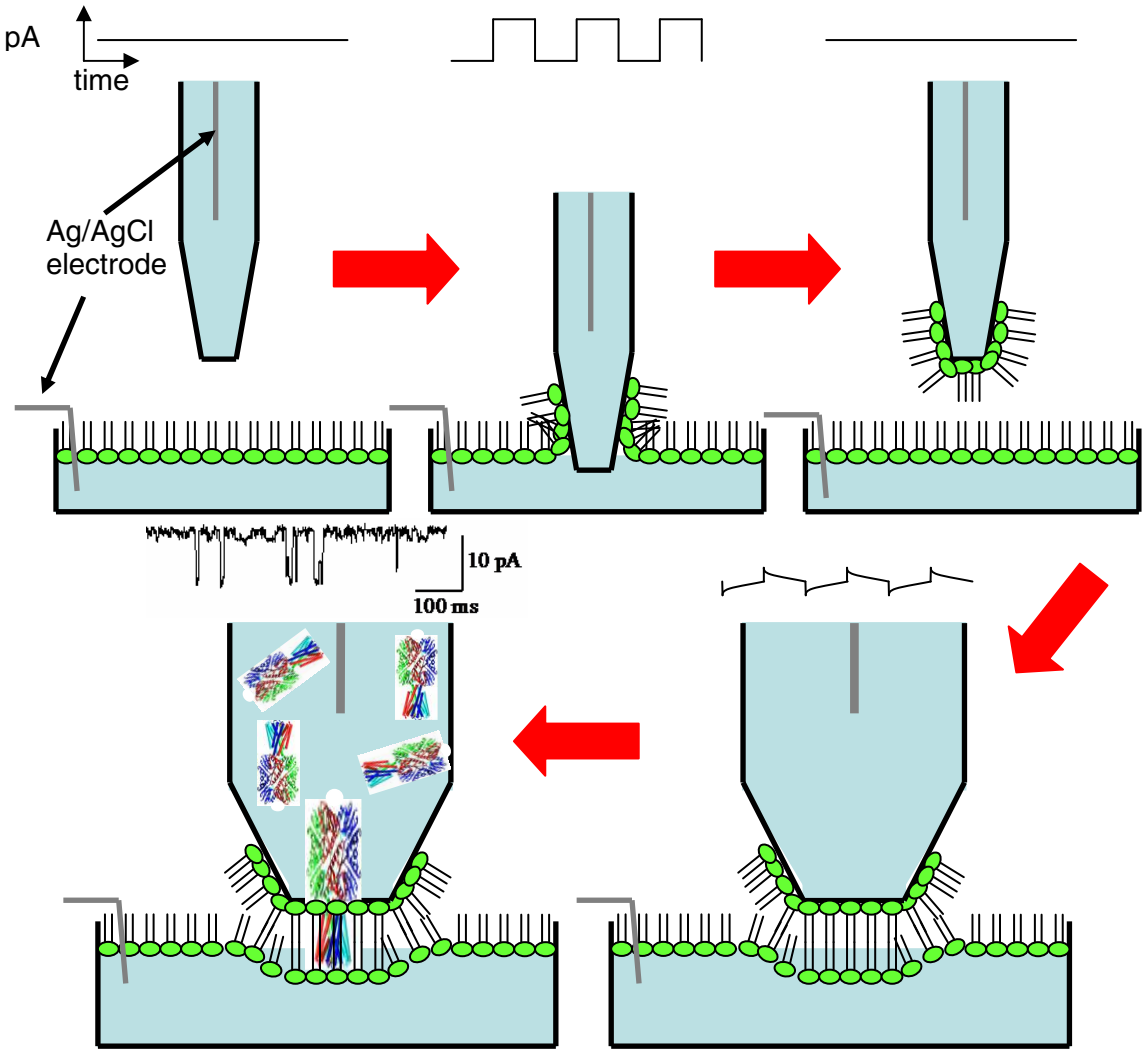

Figure 59. A schematic representation of how the tip dip process works starting from the figure on the top left and following the red arrows. The electrical signals corresponding to each step are shown above that step. The first four steps use pulsed current and the last step uses clamped voltage. The last two steps are blown up for easier viewing [12, 24].

Current measurement in the tip dip technique was performed using an Axopatch 200B (Molecular Devices Corporation) patch-clamp amplifier [12]. Single ion channel currents are measured by designating a desired voltage drop across the membrane and

providing enough ionic current to maintain that voltage. This is called voltage clamping [25, 26]. This function is performed through the use of one or more operational amplifiers configured with negative feed back loops. An operational amplifier has two signal inputs, an inverting and noninverting terminal, and one signal output (it also has power inputs but they are not important for understanding its operation). The Ag/AgCl electrode in the pipette is connected to the inverting input of the amplifier. In a resistive feed back configuration, the output terminal of the amplifier is also shorted to the inverting input terminal through a resistor [25, 26]. The noninverting terminal is keep at the desired transmembrane potential and is referred to as the command voltage [25, 26]. When a differential voltage is applied to the inverting terminal by the Ag/AgCl electrode, the voltage at the output terminal of the amplifier rises and creates a current through the feedback loop [25, 26]. This current restores the voltage at the inverting terminal of the amplifier to the same level as the command voltage [25, 26]. This amplifying circuit is in the head stage of the Axopatch 200B Patch Clamp Amplifier (the unit which is directly connected to the glass pipette and Ag/AgCl electrode) in order to amplify the signal very close to its source [26]. The resistive feed back amplifier configuration is shown in Figure 60a). The relationship between the incoming current and the output voltage is determined by Ohm's law and is defined as $V_o = I_{inj}R_f$, where R_f is the feedback resistance [25, 26]. The problem with the resistive feedback amplifier is that in order to get a voltage at the output which is sufficiently high enough to read with a display component like an oscilloscope, the resistor needs to be very large, i.e., in the gigaohm range or higher [26]. Currently manufactured gigaohm resistors suffer from a number of drawbacks which include very high noise, much higher than would be expected just from thermal noise considerations, low bandwidth (the RC time delay is quite high when considering a resistance greater than a gigaohm and a typical shunting capacitance of

under a picoamp), and nonuniform conduction due to distributed stray capacitance which can create a complex frequency response [26]. Thus, resistive feedback is largely reserved for whole cell measurements, not single ion channel recordings [25, 26].

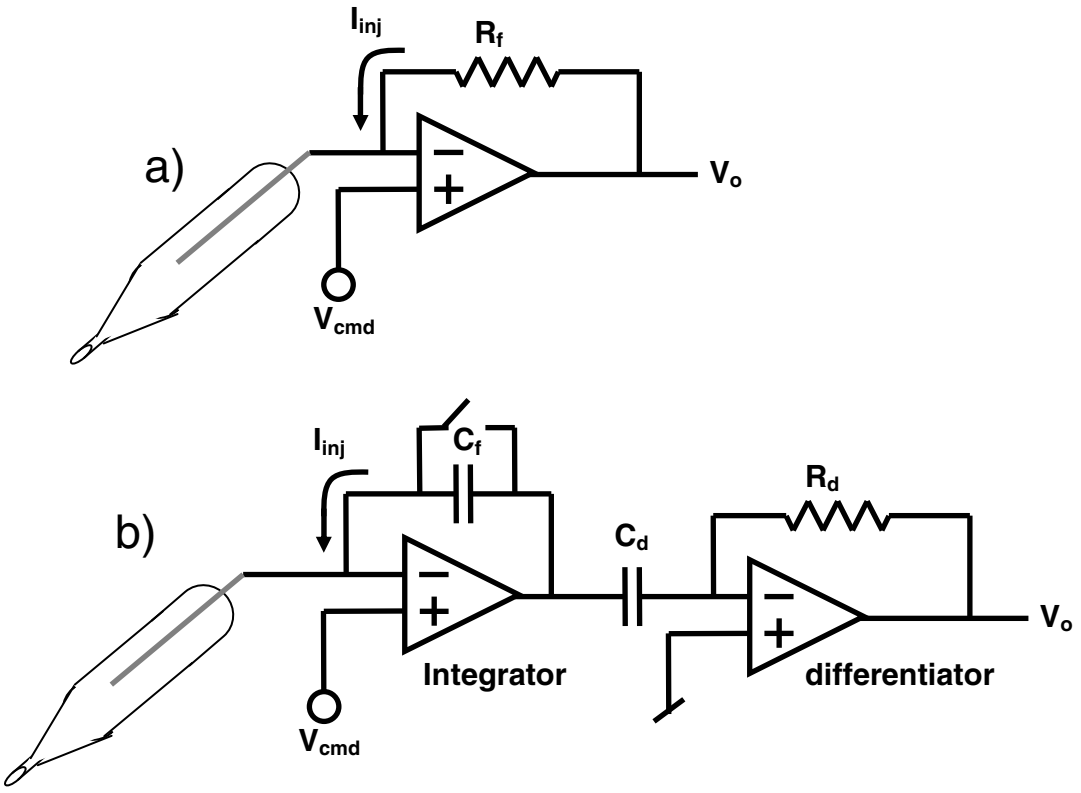

Figure 60. The basic components of resistive a) and capacitive b) feedback amplifiers in the head stage of the Axopatch 200B Patch Clamp Amplifier. The resistive feedback amplifier in a) is used primarily for whole cell recording whereas the capacitive feedback amplifier in b) is used for single channel recording. The capacitive feedback amplifier requires two operational amplifier stages. One stage integrates the injection current to get that stage's output voltage. The following stage differentiates the output voltage from the previous stage to get its injection current, which is then sourced through the differentiators resistor to get the final output voltage (which is then usually passed through several filters) [25, 26].

The Axopatch 200B also contains a capacitive feedback amplifier, shown in Figure 60b), from which single ion channel measurements are usually performed. Small capacitors do not typically suffer from the same noise problems that large resistors suffer from and have very nice linear responses over the voltage range of interest when measuring ion channels [26]. This type of amplification requires two operational amplifier stages. The first stage is called the integrating stage and uses a capacitor instead of a resistor in the feedback loop [25, 26]. Recalling that the voltage drop across a capacitor is proportional to the integral of the current and inversely proportion to the capacitance, the first stage integrates the injection current (feedback current) to get the output voltage of that stage [25, 26]. This stage feeds directly into another capacitor which differentiates the voltage to get an injection current (I = C (dV/dt)) for the next component, which is a resistive feedback amplifier that produces a final output voltage. This second stage which includes the second capacitor and the resistive feedback circuit component is called the differentiator [25, 26] (this circuit is shown in Figure 60b). The output voltage of the differentiator stage is still a linear function of the injection current into the input of the integrating stage, but the resistance is now a function of both capacitors and the feedback resistor [25.26].

$$V_o = I_{inj} R_d (C_d / C_f), \qquad \text{XI}$$

where I_{inj} and C_f are the injection current into and the feedback capacitance in the integrating stage, respectively, and C_d and R_d are the input capacitance and the feedback resistance in the differentiator stage. Thus, a large output voltage can be obtained without the necessity of having a gigaohm resistance if the capacitors are chosen appropriately [25, 26]. The only drawback to the capacitive feedback amplifier is the feedback capacitor in the integrator stage needs to be discharged periodically, since extended DC current will saturate it. When measuring small currents corresponding to

single ion channels, this is not a big problem. For whole cell measurements it may saturate too quickly. For this reason, the Axopatch 200B allows for the selection of either type of amplifier which are both included in its head stage. The signals are passed through several filters after leaving the head stage including a 1kHz low pass filter.

Several ion channels were measured using this technique and are shown in Figure 61. The measurements depicted in Figure 61 were recorded by Professor Randolph S. Duran's analytical chemistry group in the Department of Chemistry at the University of Florida, Gainesville.

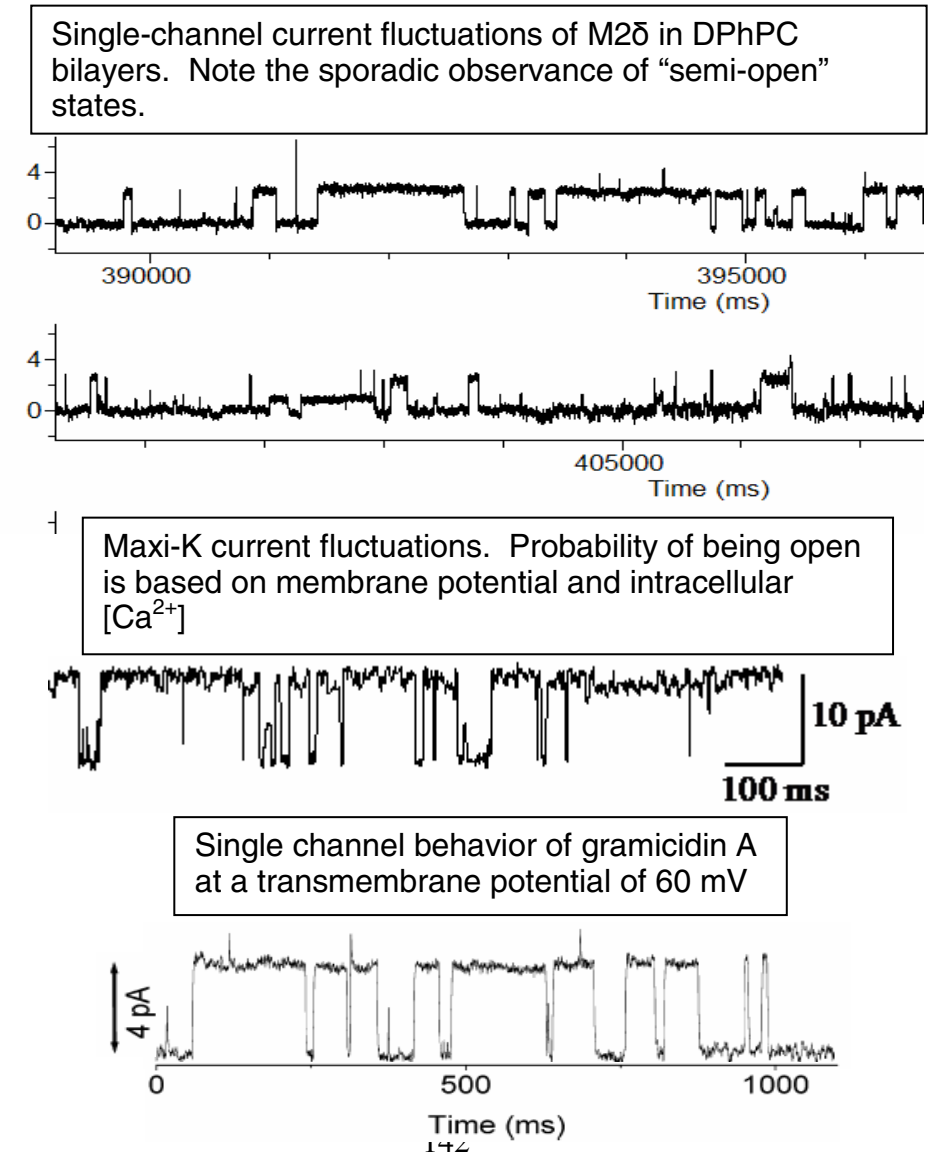

Figure 61. Single ion channel current fluctuations for M2 , Maxi-K, and gramicidin A recorded in Professor Randolph S. Duran's analytical chemistry group in the Department of Chemistry at the University of Florida, Gainesville. The gramicidin A data is "reprinted with permission from Martin Andersson, Henk M. Keizer, Chenyu Zhu, Daniel Fine, Ananth Dodabalapur, Randolph S. Duran, "Detection of Single Ion Channel Activity on a Chip Using Tethered Bilayer Membranes" *Langmuir* vol. 23 (2007) pp. 2924-2927 and copyright 2007 American Chemical Society."

5.4 CREATING ULTRA FLAT GOLD ELECTRODES

Up until now, all the ultra flat gold electrodes used in the tethered bilayer lipid membrane (tBLM) experiments were fabricated using a technique whereby gold is first evaporated on an ultra flat silicon wafer. This evaporated gold is then epoxied onto a high refractive-index glass using an optical epoxy [16]. The root-mean-square (rms) surface roughness of these pads is 0.5 nm over several μm^2 as measured by an atomic force microscope (AFM). This is one order of magnitude smaller than the length of the tethers [16]. This does indeed create electrodes which are very flat. It does not lend itself particularly well, however, to a mass production scheme for producing large arrays of electrodes. The use of an adhesive to transfer the gold from the silicon wafer to the glass slide is time consuming. Furthermore, it is difficult to pattern micron-scale electrodes on the surface of the slide due to the epoxy's low glass transition temperature. Finally, the large amount of unpatterned gold also increases the coupling capacitance which could wash out the small single ion channel currents. Thus, if tBLM systems are ever to be integrated with a solid state device, a new methodology had to be identified for producing the ultra flat gold electrodes which could be compatible with all the patterning techniques currently available for silicon and organic transistor fabrication. A material would also have to be developed which could cover the sides of the pads to eliminate the

possibility of leakage from the edges of the sensing electrodes and to protect the surface of the silicon, and, consequently, the solid state device, from the various solvents and buffers which are used when building tBLM systems and testing for single ion channel current.

It was pointed out early on, by several of our collaborators, that standard evaporated gold was not smooth enough for the purposes of building tBLMs on them. If it were not possible to evaporate the ultra flat gold then either another technique, such as electroplating, would have to be used (will not work on insulating substrate) or the template stripped gold technique would be needed with an attempt to pattern on top of the epoxy. Gold-palladium alloys are used in scanning electron microscopy (SEM) to cover the surfaces of samples and prevent charging [27]. These films are used specifically because the grains that form when the film is deposited are very small. The best mixture was 60% gold and 40% palladium (ratio by weight) [27]. Figure 62 shows AFM scans of a pure gold film and a 60%-40% gold-palladium film (film thickness is approximately 50 nm). The surface roughness of the gold palladium film is about half that of the pure gold film (0.46 nm rms as compared to 0.93 nm rms).

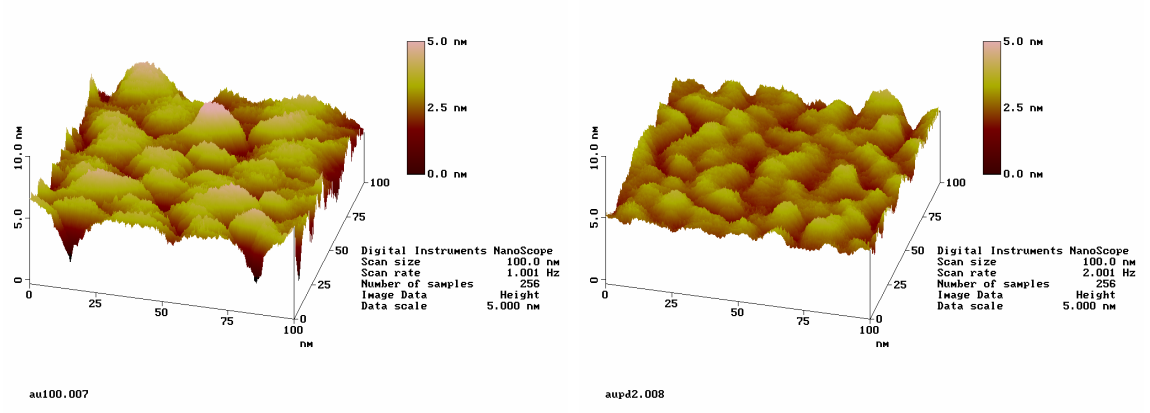

Figure 62. AFM scans of a pure gold film on the left and a 60%-40% gold-palladium alloy film on the right. The root-mean-square surface roughness of the gold film is 0.93 nm as opposed to that of the gold-

palladium alloy which is 0.46 nm rms. The film thicknesses are around 50 nm.

Given this reduction in grain size with the gold-palladium alloy, it was determined that the metal electrodes could meet the high smoothness requirements for tBLMs when deposited by electron beam evaporation. After the silicon/silicon dioxide substrate surface had undergone a piranha clean (sulfuric acid and hydrogen peroxide) to insure a high degree of cleanliness, the final sensing electrode metal stack was deposited. It consisted of 3 nm of titanium, required to allow gold or gold alloys to properly adhere to the silicon dioxide surface, followed by 50 nm of the 60%-40% gold-palladium alloy, followed by 20 nm of pure gold to insure that the alloy did not interfere with the proper formation of the self assembled monolayer of tethers on the surface of the electrode. The initial electrodes were deposited using a liftoff procedure as described in Section 2.3. Electrodes made in this fashion have worked quite successfully [2, 12, 13]. It has since been determined, however, that the metal film after liftoff is not as flat as can be possibly achieved. Figure 63a shows an AFM scan of an electrode fabricated using liftoff. The surface roughness is 0.849 nm rms. Although this is not as ideal as the template stripped gold, it has shown to be sufficient for achieving gigaohm seals [2, 12, 13]. Figure 63b shows an AFM scan of an electrode which has been etched instead of going through a liftoff procedure. Its rms surface roughness is only 0.625 nm, much closer to the template stripped gold. Both of these scans are 10 um square. Electrodes fabricated by using an etching procedure have not been tried in experiments yet but should allow for higher yields in terms of the number of electrodes capable of maintaining gigaohm seals.

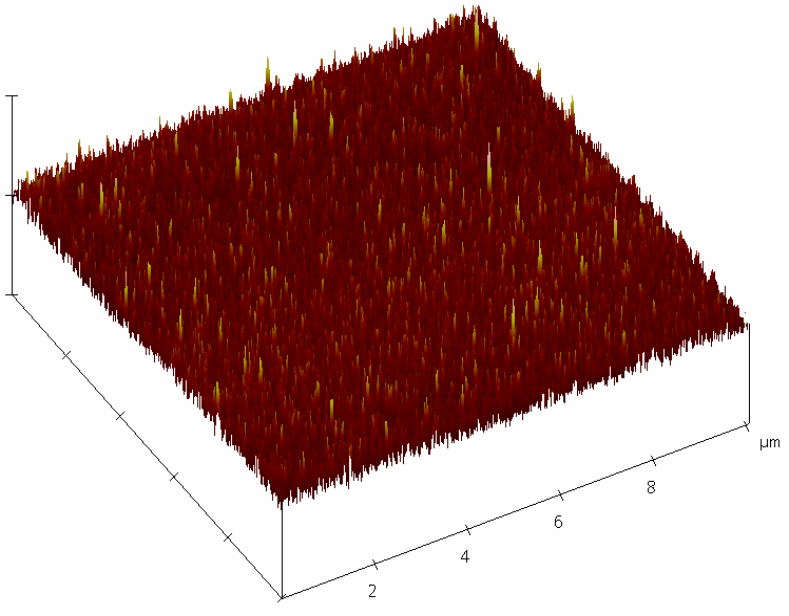

Figure 63a. An AFM scan of an electrode fabricated using liftoff. The rms surface roughness for this sensing pad was 0.849 nm.

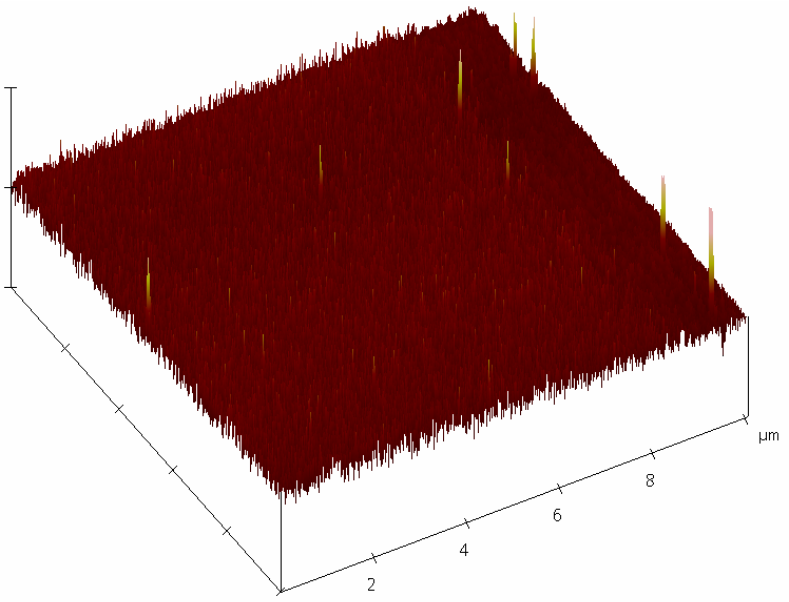

Figure 63b. An AFM scan of an electrode fabricated using an etch procedure. The rms surface roughness for this sensing pad was 0.625 nm.

One possible reason for this discrepancy could be that during the etch procedure, the titanium/gold-palladium/gold electrodes are deposited over the entire wafer. Photoresist is then spun and subsequently patterned on top of the gold. This means that during metal deposition, the metal is able to arrange itself over the largest possible area thereby increasing smoothness. In the liftoff procedure, the deposition is now confined to a much smaller area since the photoresist has been patterned prior to deposition. Now the deposition of the metal is occurring into the trenches which have been patterned into the photoresist. The metal may have a hard time arranging itself into small grains near the photoresist wall and could to some extent affect grains over the entire surface of the sensing pad (especially with the smaller electrodes). Another possibility is that the liftoff procedure is stressing the pad because the photoresist is not presenting a good enough edge profile. There may still be a thin layer of metal connecting the metal layers on top of the resist to the metal layers on the top of the substrate (recall for liftoff to work well, the edge profile should have a negative slope such that the top of the resist, not in contact with the substrate, should extend farther into the patterned area than the bottom of the resist). Thus, during sonication after the samples have been soaked in acetone, this thin connecting film is pulling on the edge of the sensing pad and stressing it. A final possible explanation is that liftoff can often require long sonication times to make sure all undesirable gold is removed. The large amount of energy released during this process could be partially annealing the sample. It has been shown by Schiller *et al.* [16] that annealing the gold electrodes causes the surface roughness to worsen. Etching takes very little sonication to remove the photoresist after patterning because the resist is not covered by any other material.

In order to cover the edges of the electrodes and protect the surface of the wafer, a polyimide material, PI-5878G, was acquired from HD Microsystems

(http://www.hdmicrosystems.com/). The polyimide material can be patterned with photoresist and etched in the photoresist developer. Thus, the patterning and etching step occur simultaneously. Windows into this layer were patterned to expose the surface of the sensing pads, but not the pad edges, as well as the remote probing pads to be able to electrically access the sensing pads. Once fully cured, at 360ºC for one hour (see the technical information on PI-5878G for processing instruction), the film is very chemically inert, capable of withstanding a large array of solvents.

Fabricating pads using this methodology allows for high throughput processing coupled with good reproducibility. The smaller pads also allow for a significant reduction in coupling capacitance. Different substrates are also being pursued which could further cut down on coupling capacitance such as single crystal quartz. These substrates are insulating through their entire width, as opposed to silicon/silicon dioxide wafers which are insulating only over the 200 nm or so of silicon dioxide dielectric and then become semiconducting in the silicon. These new wafers would of course require any solid state devices to be soldered on their surface as opposed to fabricated into the substrate.

5.5 Measuring Single Ion Channel Activity in a Tethered Bilayer System and Demonstration of Preliminary Sensing Data

The format for measuring single ion channel activity also utilizes the Axopatch 200B Patch Clamp Amplifier. Instead of using the glass pipette as the support for the bilayer lipid membrane, as is done when using the tip dip technique, the membrane is now tethered to the surface of the ultra flat gold electrode and the glass pipette and the Ag/AgCl electrode inside are used solely as the counter electrode. First, the electrode is cleaned to insure no residue is left on the surface of the electrode. Softer techniques than

the piranha clean are used, such as soaking in ethanol and UV ozone, so as not to damage or roughen the surface of the electrode. UV ozone is a technique whereby the sample is placed into a chamber containing ozone and is then irradiated with UV light. This irradiation creates free radicals which can react with any organic material on the surface of the electrode and remove it. This is similar to plasma cleaning but creates no ions which can bombard the surface and roughen it. Next, the electrodes are soaked overnight in a solution containing the tethers to enable the formation of a uniform, appropriately dense monolayer. When the samples are ready to receive the vesicles with the ion channels, a small piece of parafilm, with a dimension much larger than the sensing pad, is placed around the pad to contain the drop. This is allowed to sit without drying for up to several hours to achieve bilayer formation. Then, an appropriate buffer solution is introduced and the channels are ready to measure. Illustration 2 shows a depiction of the tBLM configuration. The glass pipette tip is lowered into the drop of buffer solution above the sensing pad, and single ion channels can now be recorded. The probing pad of the electrode is contacted with a Cascade electrical probe micromanipulator with a tungsten probe tip. These procedures are outlined in references [2, 12, 13]. Figures 64, 65, and 66 show single channel measurements of the four aforementioned ion channels immobilized in the tethered lipid bilayer membranes. These measurements were performed by Professor Randolph S. Duran's analytical chemistry group in the Department of Chemistry at the University of Florida, Gainesville. The tethers were provided by Professor Dr. Wolfgang Knoll's group at the Max Planck Institute for Polymer Research in Mainz, Germany. The electrodes were provided by our group at the University of Texas at Austin.

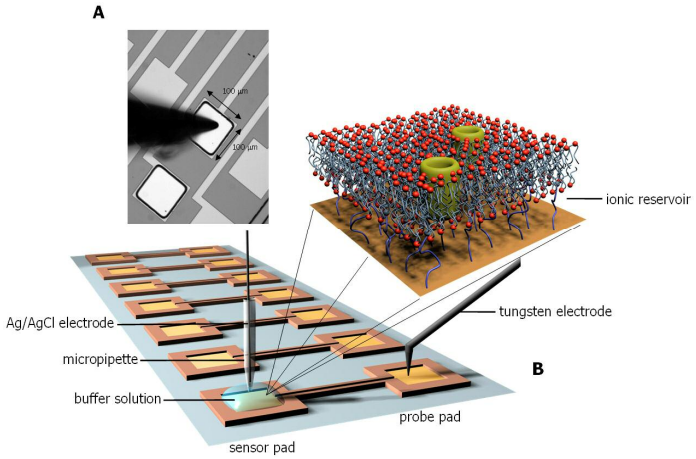

Illustration 2. A representation of the experimental set up for measuring ion channel activity using the tBLM approach. The electrodes are shown with the polyimide in place and the drop of buffer properly positioned over the sensing pad. One inset shows a representation of the tBLM with incorporated ion channels. The other inset shows an actual optical image of the probing pad with electric probe in place [2, 13].

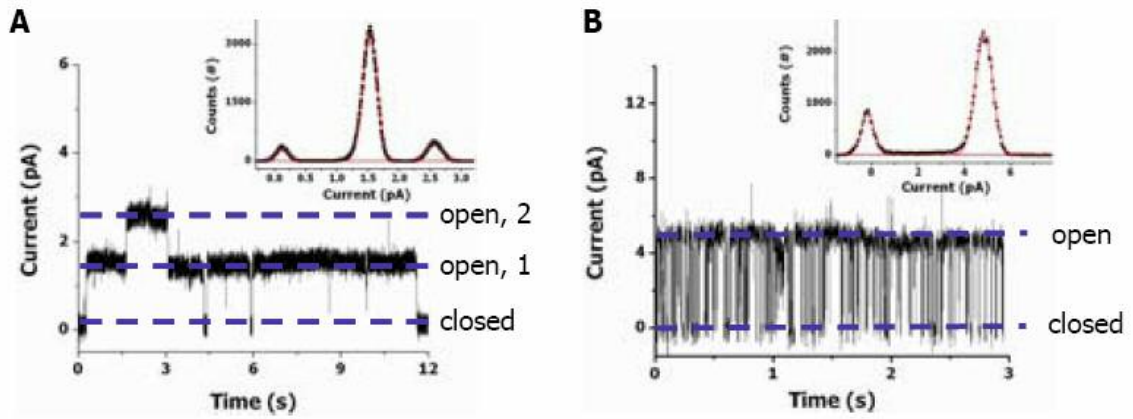

Figure 64. Measurements of the ion currents through single ion channels incorporated in tethered lipid bilayer membranes. Figure 64A depicts measurements of single M2 ion channel currents showing two conductance levels at 1.6 pA and 2.6 pA (three distinct levels) indicating a couple of operating channels. Figure 64B depicts measurements of single Maxi-K channel ion currents with only one conductance level at 5.5 pA (only two distinct levels). The insets in both figures are current histograms which follow a typical Gaussian distribution (the red fit line) with a peak at the aforementioned designated current levels. The

maintained transmembrane potential for both measurements was 100mV [2].

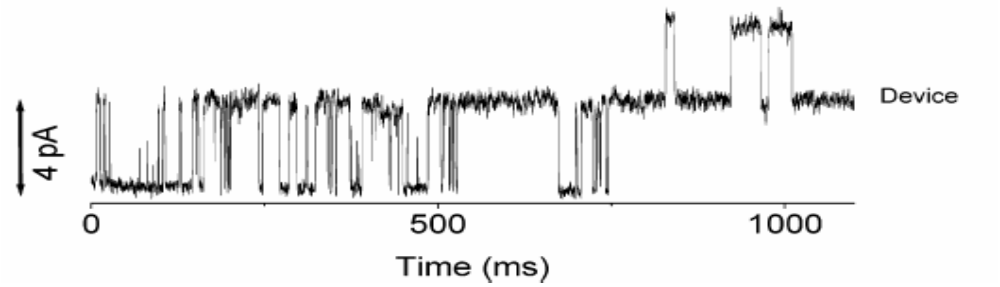

Figure 65. Measurements of single gramicidin A ion channel activity showing two conductance levels of 4 pA each (multiple operating channels). The transmembrane potential for this measurement was 60 mV. "Reprinted with permission from Martin Andersson, Henk M. Keizer, Chenyu Zhu, Daniel Fine, Ananth Dodabalapur, Randolph S. Duran, "Detection of Single Ion Channel Activity on a Chip Using Tethered Bilayer Membranes" *Langmuir* vol. 23 (2007) pp. 2924-2927 and copyright 2007 American Chemical Society."

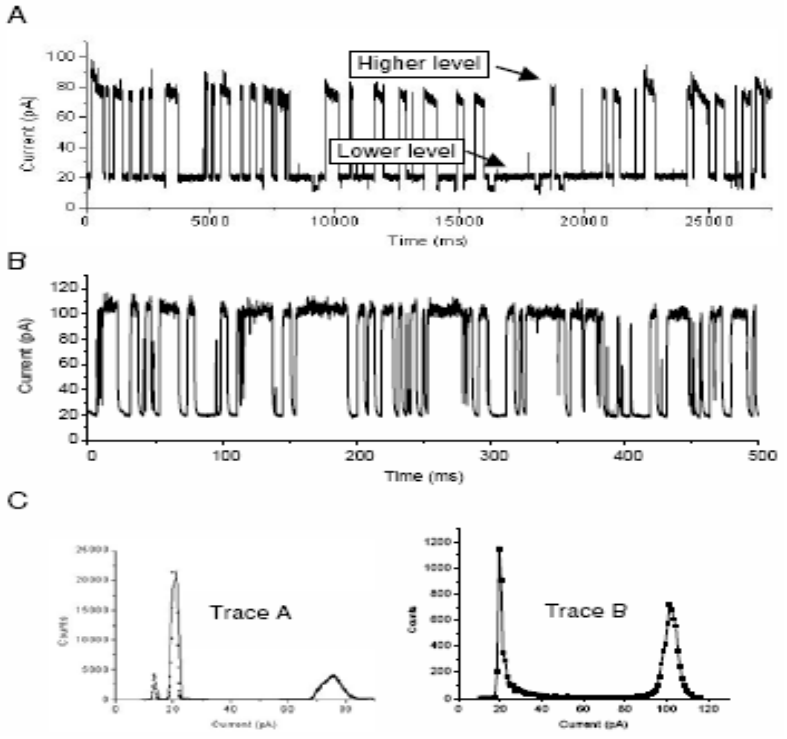

Figure 66. Two distinct measurements of the single channel activity of the mechanosensitive large conductance channel from the MscL family of ion

channels. The transmembrane potential for this experiment was maintained at 300 mV. The trace in Figure 66A shows two distinct conductance states for one ion channel, a low level conductance and a high level conductance. Figure 66B shows only one conductance level for a single ion channel. Figure 66C shows the current histograms for the traces in Figures 66A and 66B with the typical Gaussian distributions centered at the conductance levels seen in the traces. The histogram for Trace A shows three peaks, two of which correspond to the high and level conductance levels, whereas the histogram for Trace B shows only the one conductance level [13].

The conductance measured for each of the ion channels incorporated in the tethered bilayer lipid membranes were 15 pS for M2 , 37 pS for Maxi-K, 67 pS for gramicidin A, and 23 pS for the lower conductance level and 203 pS for the higher conductance level of the MscL. The conductance measured for M2 , Maxi-K and the MscL channels were all several times less than the previously stated values found in the literature. Maxi-K and MscL were an order of magnitude less. Gramicidin A was the only channel which performed close to what was found in the literature. There may be several reasons for this. The first is that the tethers occupy significant space beneath the membrane. This may make it harder for carriers to diffuse to the electrode surface and therefore increase the ionic resistance in the submembrane compartment [2]. The second reason may be due to the fact that gold is being used as the second electrode, not Ag/AgCl which at the voltages used in these studies is capable of carrier transfer at the electrode. Whenever a charged surface, such as a gold electrode, is present in an aqueous solution, an electric double layer can form [28]. Ions charged oppositely to the charge on the electrode accumulate near the surface, and like charges are driven away. This creates a depletion region near the surface which has a nonzero potential inside the solution (the bulk of the buffer solution is electrically neutral) [28]. Given the fact that no charge transfer is happening across the gold/buffer solution boundary, this effect could shield the

electrode from the ion channel current. This is similar to a charging capacitor where the amount of current which can be accumulated over time is reduced. This could be alleviated to some extent by reverse biasing of the membrane and allowing some ions to leach out through the very small membrane leakage current. Finally, this conductance reduction may occur due to the limited number of ions in the submembrane reservoir to begin with, such that the depletion region may extend for most of the electrode to bilayer distance. These effects that work to lower the conductance may be more pronounced the larger the ion channel's submembrane domain is, which might explain why gramicidin A is less affected. Efforts are currently underway to try to model this tBLM system using electronic circuit element models with such circuit simulators as T-Spice [29]. This will be extremely valuable in determining what effects may be causing this reduction in conductance, and what can be done to reduce the influence of these effects.

The two ion channels M2 and Maxi-K, immobilized in the tBLMs, were exposed to two analytes for which they have known affinities as a preliminary test of the biosensing capability of these tBLM systems [2]. The M2 ion channel was exposed to triethylphosphate (TEP), a possible model for various harmful organophosphate agents such as sarin and VX gas which are known to block nAChR [2]. A concentration of 6 μM of TEP was able to block M2 activity in 89% percent (8 out of 9) of the test trials [2]. This response was completely reversible after washing [2]. Maxi-K immobilized ion channels were exposed to tetraethylammonium (TEA), an organic cation known to block Maxi-K currents when introduced in the micromolar range [2]. When micromolar concentrations of TEA were exposed to the Maxi-K channels, the ion current reduced. The half activation concentration determined from these measurements was 64 μM at 100 mV, less than half of the previously reported value of 158 μM [2]. Therefore, these preliminary results are promising in terms of the ability of the ion channels to detect these

analytes and the fact that this tBLM system compares very favorably to similar ion channel experiments already performed by other groups [2].

5.6 Evaluation of the Bipolar Junction transistor (BJT) as a Candidate for use in Amplifying Ion Channel Signals

The bipolar junction transistor (BJT), first demonstrated in 1951 by Shockley, Sparks, and Teal [30], is a current coupled amplifier. BJTs have been shown to be effective for measuring the extracellular voltages of single cardiac rat myocytes [31]. The BJT has many advantages over metal oxide semiconductor field-effect transistors (MOSFETs). One advantage is that the BJT has a higher transconductance (the change in collector current versus the change in base-emitter voltage) than the MOSFET [32]. A second advantage is that it can operate at higher speeds, even as compared to a MOSFET with the same cutoff frequency (cutoff frequency is the operating frequency at which the transconductance becomes unity), since high current is advantageous for driving parasitic capacitance (the MOSFET is a device which minimizes gate current) [32]. The BJT does not suffer from the same problem of surface defects as the MOSFET [32]. The turn on voltage of a *p-n* junction, two of which comprise the BJT, is more controllable than the MOSFET threshold voltage [32]. Finally, the BJT also has a higher analog gain, defined by the transconductance multiplied by the output resistance [32]. High gain is a very important characteristic of these devices, as the single channel ion currents are quite small (inherent device noise is also another important consideration which will be discussed later). These factors make the bipolar junction transistor very promising in terms of identifying a device which can amplify the small single channel ion currents reliably.

When two semiconductor regions of opposite doping (p-type and n-type) are brought into contact, referred to as a *p-n* junction, the carriers from one region diffuse to the other region and recombine with an opposite carrier in that region [32, 33]. This leaves a large number of uncompensated charged dopant atoms near the junction in both regions. This creates an electric field with acts against the further diffusion of carriers across the junction. This is depicted in Figure 67 [32]. In equilibrium, the current due to diffusion exactly balances the current due to the junction electric field (the drift current). When the junction is forward biased, which indicates a positive voltage applied to the p-type region and a negative voltage applied to the n-type region, diffusion becomes stronger than drift, and large amounts of carriers flow across the junction. When the junction is reversed biased, drift wins over diffusion, and very few carriers traverse the junction. Under these conditions only carriers which are thermally generated in or near the junction, or carriers in a particular region with thermal energy sufficient enough to overcome the reverse electric field, will flow across the junction [32, 33]. The relation of current to voltage is exponential in the forward biased regime (higher voltage applied to the p-type region) and constant in the reverse biased regime (higher voltage applied to the n-type region) (see the right side of Figure 67) [32, 33]. This is the basis for understanding how a BJT operates.

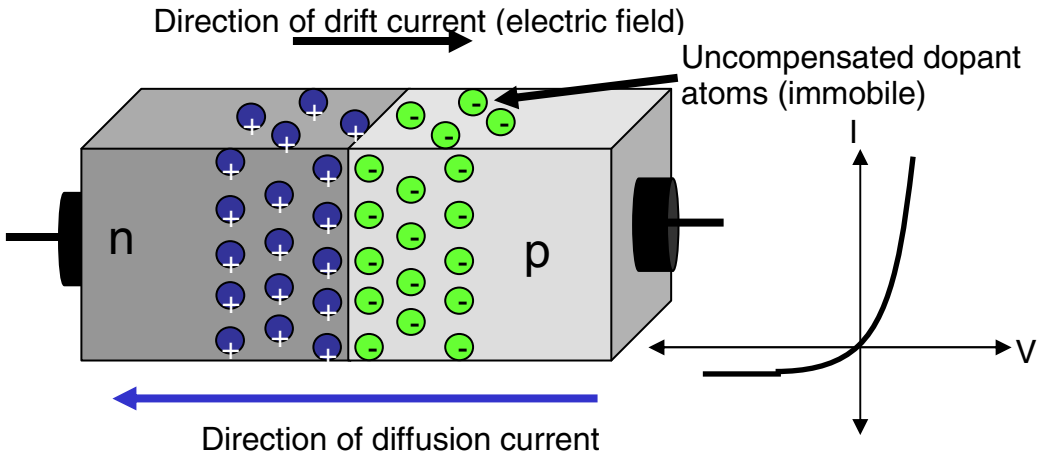

Figure 67. A graphic representation of the equilibrium state of a *p-n* junction. Carriers diffuse out of the *n* and *p* regions leaving immobile, uncompensated dopant atoms behind. This creates an electric field which acts against the diffusion current until no net displacement of mobile carriers occurs across the junction. The current flow arrows point in the direction of the flow of holes (by convention). The graph on the right is the current-voltage characteristics of the diode showing exponential current increase with a positive voltage drop across the junction (a higher voltage applied to the p-type region compared to the n-type region) and constant current when the voltage dropped across the junction is negative [32, 33].

The BJT consists of two *p-n* junctions back to back, either *p-n-p* (p-type, n-type, p-type) or *n-p-n*, which act as back to back diodes, shown in Figure 68 [32, 33]. The device circuit element schematic is shown in Figure 69 [33].

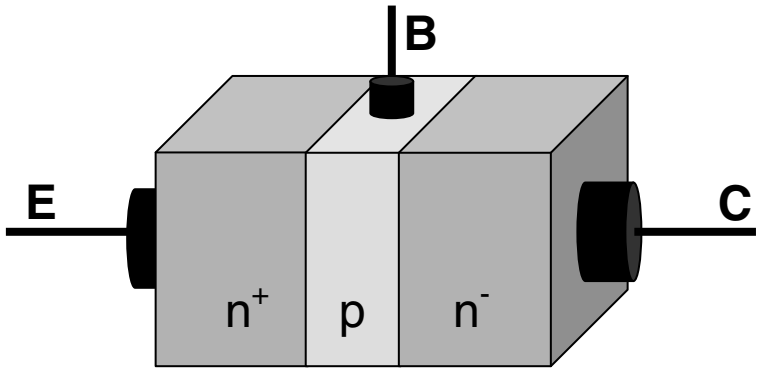

Figure 68. A conceptual picture of the three doped regions (two back to back *p-n* junctions) which comprise a BJT. The signs next to the dopant

types indicate their relative amounts. The emitter (E), the source of carriers to the base, is more heavily doped than the base (B) which is more heavily doped than the collector (C). This insures the largest possible current injection into the collector from the emitter and thus the highest possible gain [32].

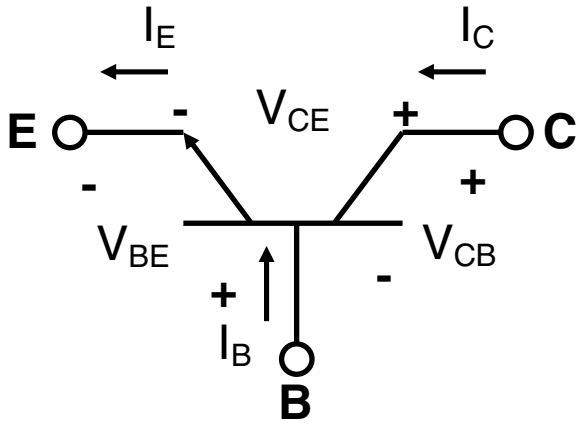

Figure 69. The circuit element schematic for the bipolar junction field effect transistor (BJT) biased in the forward active region of device operation (this is the region where the devices gain is the highest) showing the emitter (E), base (B) and collector (C) terminals. The arrow in the device schematic indicates the emitter and its direction indicates the current flow (direction of the flow of holes) [33].

In the common-emitter (emitter is grounded) device configuration in the forward active region of device operation (the configuration and region of operation with the highest gain), the emitter-base junction is forward biased while the base-collector junction is reverse biased [33]. This means that for an *n-p-n* transistor, the base is biased with a positive voltage as compared to the emitter, and the collector is biased with a positive voltage as compared to the base. In the absence of base current, the transistor's maximum current is the reverse leakage current through the collector-base junction (a reverse biased diode) [32, 33]. When the base is biased, the emitter-base junction becomes forward biased, and carriers can be injected from the emitter into the base. If

the base thickness is small enough, extra carriers from the emitter not required to balance the base current can traverse the base and reach the collector without recombining with opposite carriers in the base [32, 33]. These carriers will be swept across the correctly oriented electric field, which is present at the base-collector junction, and into the collector. The relationship between the amount of charge that needs to be injected into the base to achieve an amount of charge that leaves the emitter, traverses the base, and is collected in the collector, is the gain of the BJT (the gain, $=I_C/I_B$). Maximizing the gain characteristics requires that the three regions not be doped to the same concentration. The emitter is more heavily doped than the base which is more heavily doped than the collector. An imbalance between the base and emitter doping allows for a much larger amount of electrons to be injected into the base from the emitter for a given amount of base current than could be achieved if their doping levels were the same. A large imbalance in the base and collector dopant level means the depletion width (the area of uncovered immobile dopant atoms) will be large. This reduces the likelihood carriers can be back injected from the collector to the base. For detailed derivations of the collector, base and emitter currents, see reference [33].

There are two primary components which must be evaluated to ascertain whether the BJT is a good candidate for amplifying single ion channel signals, the gain of the device and the inherent device noise (even under the most ideal of shielding conditions the device itself generates some amount of noise). The gain of the device is defined as the ratio of the collector current to the base current [33]. Under the right conditions, an approximation of the gain can be calculated based on a few device parameters shown in equation XII.

$$\beta \approx \frac{D_B N_E L_E}{D_E N_B W} \qquad \text{XII}$$

where D_E and D_B are the minority carrier diffusion coefficients in the emitter and base, N_E and N_B are the doping levels in the emitter and base, L_E is minority carrier diffusion length in the emitter, and W is the base width [33]. L_E is quite short due to the extremely high doping level in the emitter. The base width is chosen to be less than the diffusion length of minority carriers in the base. Thus, to increase the gain as much as possible, the base width should be minimized (although not reduced to the extent to cause it to become fully depleted), and the difference between the emitter and base doping levels should be maximized [33]. The highest gain achieved from devices which would make good candidates for this purpose is =92.

Prior to device fabrication, simulations were performed using Medici, a two-dimensional device simulation program [34]. The simulated device consisted of an emitter, a base, a collector, and a collector contact. The collector contact was included in the simulation as well as the actual fabricated device so that current did not have to be carried for long distances through the low doped, high resistance collector region. Figure 70 shows the gummel plot of one of the simulations, which seemed to yield the best characteristics, along with a representation of the simulated device. A gummel plot is a plot of log(I) vs. V_{BE} where both the collector and base currents are displayed and gives an indication of the gain of the device [32].

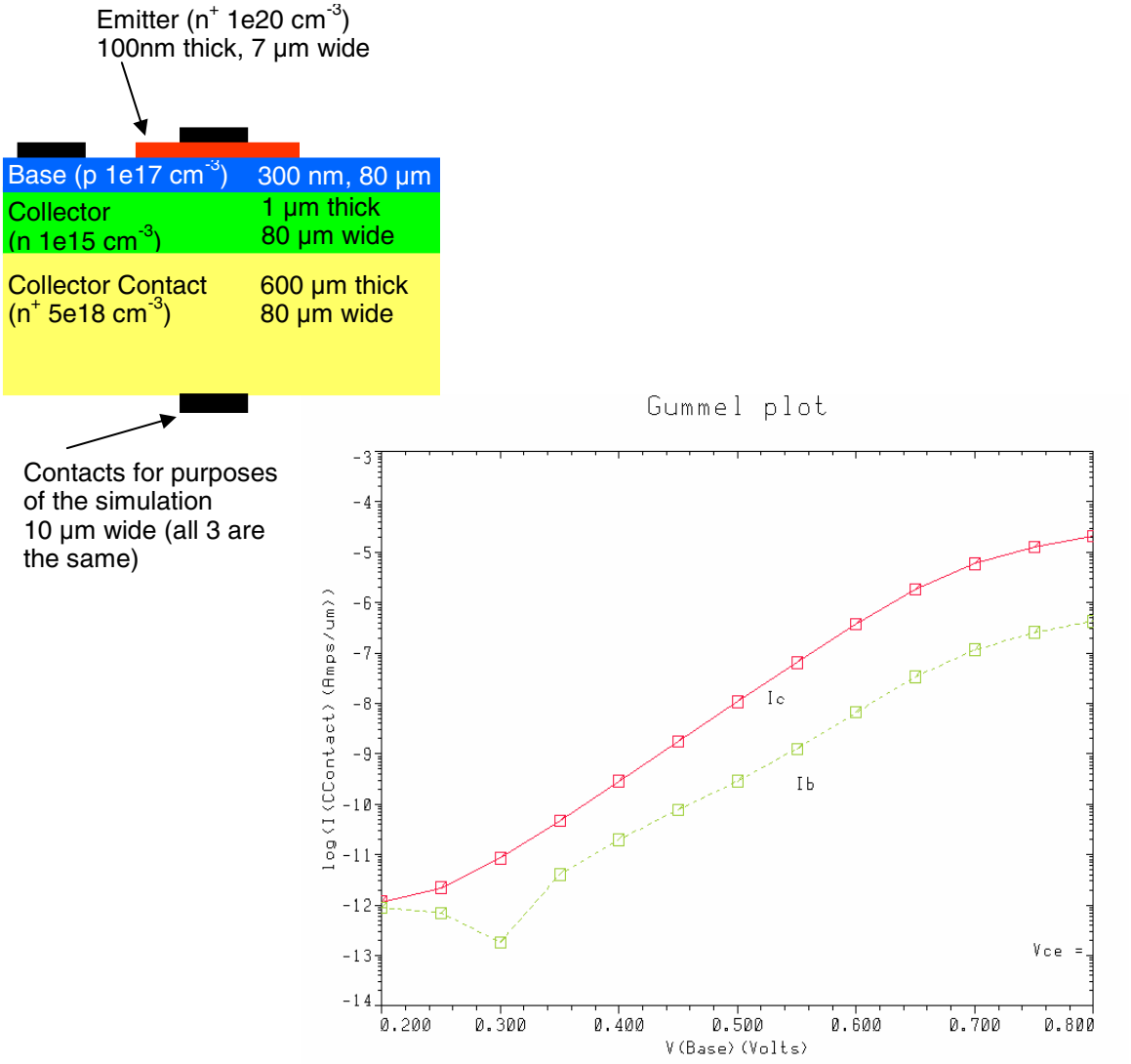

Figure 70. The gummel plot, log (I) vs. V_{BE} with both the collector and base currents plotted simultaneously, generated from the two-dimensional simulation program Medici [34]. This gives an indication of the potential gain of the device [32]. The figure in the upper left corner is a representation of the BJT, giving the doping concentrations, layer thicknesses, and dimensions of its various layers that was used in the simulation [34].

The emitter base and collector of the BJT were grown by use of epitaxy, a technique which allows for the creation of thin layers of single crystal silicon on top of silicon wafers (the term "grown" is used since the layers are perfectly crystalline and extend the crystalline structure of the underlying material). These layers can be doped during growth and accurately grown over a range of thicknesses [35]. The collector contact was formed by either a fourth grown epitaxial layer or by growing the other three layers on a heavily doped n-type wafer. The epitaxial layers for this study were grown by Lawrence Semiconductor Research Laboratory, Inc. After simulating the devices, a fabrication sequence, which will be outlined below, was used to produce working BJTs. After several rounds of fabrication the following layer thicknesses and doping concentration were determined. The collector contact consisted of either an entire wafer doped n-type to $5x10^{18}$ cm^{-3} or an epitaxial layer 1 μm thick doped n-type to a concentration of $5x10^{18}$ cm^{-3} grown on a lightly doped p-type silicon substrate. The reason for this was uncertainty as to the capability of the available etcher for deep etching (it is not designed for very deep etching). As it turned out, the etcher was able to perform the deep etch but not with consistent surface roughness characteristics post etching. It is desirable to have the substrate over which the sensing pad is formed be lightly doped to cut down on stray coupling capacitance when trying to record single ion channel behavior. The collector was grown next to a thickness of 1 μm and an n-type doping of 10^{15} cm^{-3}. This was followed by the base layer which was 600 nm thick and doped p-type to 10^{17} cm^{-3}. Finally, the emitter was grown to a thickness of 100 nm and doped n-type to 10^{20} cm^{-3}. The doping concentration of 10^{20} cm^{-3} was the highest possible doping which could be provided by Lawrence Semiconductor Research Laboratory, Inc. This was deemed to be too low. The epitaxial wafers were therefore sent out for an n-type (phosphorus) ion implant. The dose used was $5x10^{15}$ cm^{-2} and the acceleration voltage

was 20 keV. This is a relatively low energy for typical ion implants, but it was necessary to avoid implanting too deeply and shorting the emitter to the collector (this is also why the base width was doubled from that used in the simulation). The ion implants were activated using a rapid thermal annealer at 900ºC for 1 minute. It is with this extra ion implant that devices with gains around 90 were realized.

The BJTs are vertically defined devices, as can be ascertained from the use of sequentially grown epitaxial layers to form the emitter, base and collector. Using standard photolithography techniques (Az 5214 photoresist from Clariant and a Karl Suss UV mask aligner), a mesa was first defined by etching through all the epitaxial layers (using a Plasma-Therm reactive ion etcher (RIE)). This included all the wafer surface area not needed in the devices themselves. This was to remove all of the highly doped epitaxial layers from areas of the wafer where sensing pads were placed. Following the etching of the device mesas, each layer of the BJT was contacted by etching ever smaller mesas into the initial mesa (see Figure 71). Once this was completed, the devices were covered by 200 nm of low temperature oxide (LTO) followed by 200 nm of silicon nitride and finally 60 nm of low temperature oxide. These dielectrics are chemically deposited from airborne precursors not thermally grown like standard oxides. They therefore do not consume any of the silicon on the surface of the wafer. This was necessary for two reasons. The first is that thermal oxide growth takes place at very high temperature which could cause dopant diffusion and lead to mixing of the dopants in the epitaxial layers and ultimately destruction of these layers as individual elements. The second is that the emitter region is not very thick.

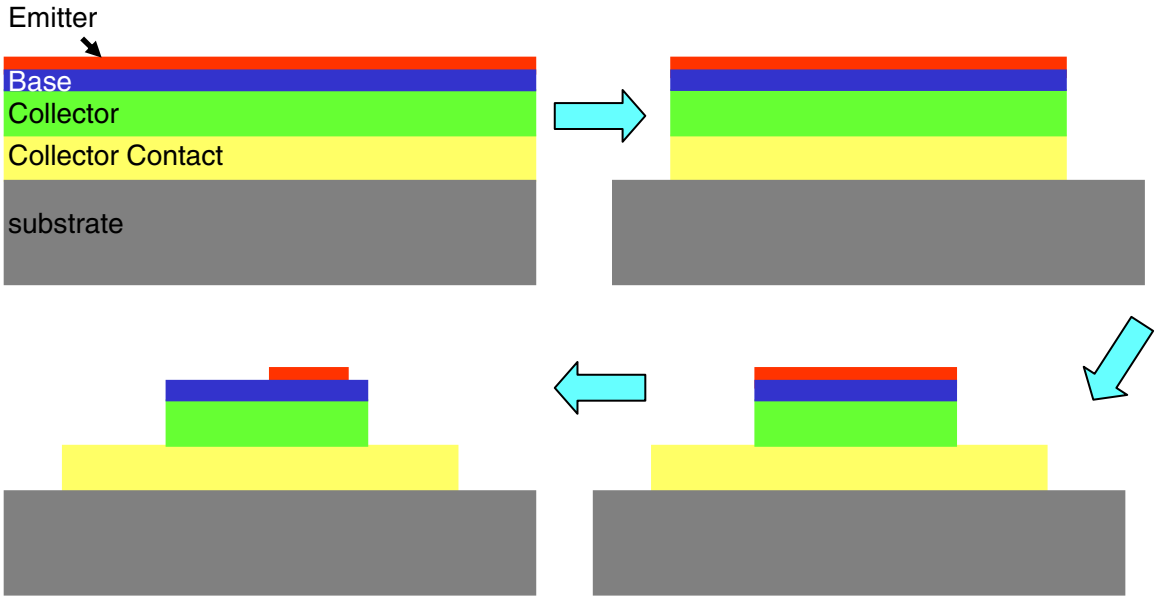

Figure 71. A representation of how the devices were etched into the epitaxial layers. The blue arrows indicate the process flow. First, the entire device was etched as one mesa to remove any highly doped areas from under the sensing pad. Following the initial etch, smaller mesas were etched through subsequent layers so that contact could first be made to the collector contact layer and second to the base.

Any consumption of oxide at the surface (turning into oxide) could remove the emitter layer. This dielectric stack was for purposes of surface passivation (so that metal lines don't short the regions of the BJT together) and not an integral component of device operation (such as a MOSFET gate dielectric). Following the dielectric deposition, vias were etched down to the collector contact, base, and emitter through which aluminum contacts were deposited. The first two layers of the dielectric, the thin LTO and the silicon nitride, and some of the third layer (the thick LTO) were etched using the Plasma-Therm RIE. The final amount of LTO was etched using a wet hydrofluoric (HF) acid etch. This was done for two reasons. The first is that the RIE is a dry etch (a plasma etcher) which is not nearly as selective between silicon and silicon dioxide as HF. The

second reason is that hydrofluoric acid (HF) passitvates the silicon surface with hydrogen for a short amount of time while the wafers are loaded into the aluminum sputtering tool [36]. This prevents native oxide from forming in the via causing severe injection problems. Silicon nitride is needed to mask this HF wet etch because silicon nitride's etch rate in HF is significantly lower than that of silicon dioxide, thus the alternating dielectric stack. Covering the top of the silicon nitride with a sacrificial thin layer of silicon dioxide should allow for a smoother and cleaner dielectric surface, since that oxide layer can shield the silicon nitride surface while being dry etched and then be removed when the via holes are wet etched. Wet etching is known to cause much less surface roughness than dry etching. Aluminum contacts and metal lines were then deposited after etching the via. The aluminum had to be quite thick, greater than 500 nm, to make sure it could reach the top of the mesa without being severed. The photoresist (Az 5214) and a wet etch of acetic acid, nitric acid, phosphoric acid and water was used to pattern the aluminum. The samples were then sintered at 400 ºC in forming gas (nitrogen with a small amount of hydrogen) for 15 minutes. Sintering converts some of the aluminum and silicon at the interface to a compound making the contact ohmic [35]. At this point the devices were ready to test. Figure 72 shows I_C vs. V_{CE} for a representative discreet device. This device had a gain of 40. When two devices are coupled such that the emitter of one device feeds the base of another, they are referred to as a Darlington Pair (*see* Figure 73) [37]. The gain of the circuit then becomes

$$\frac{I_{OUT}}{I_{IN}} = \beta_1 + \beta_2 + \beta_1\beta_2 \qquad \text{XIII [37]}$$

Thus, the gains can be quite large. Figure 74 shows I_{IN} vs. V_{OUT} for a Darlington Pair.

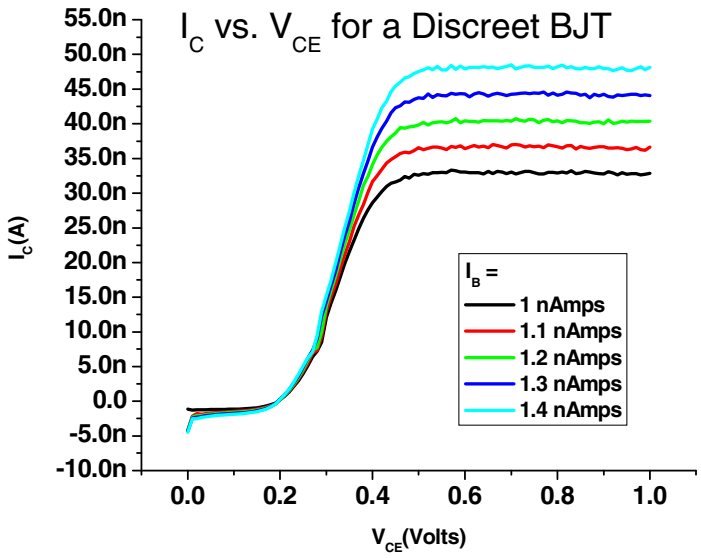

Figure 72. The current characteristics for a discreet BJT with a gain of 40. The initial base current is 1 nA because the device shows a little instability when the total collector current is low. The base current steps are 100 pA.

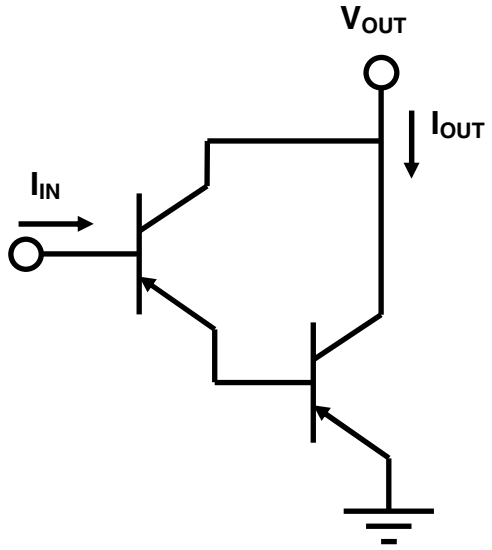

Figure 73. The circuit diagram for a Darlington Pair.

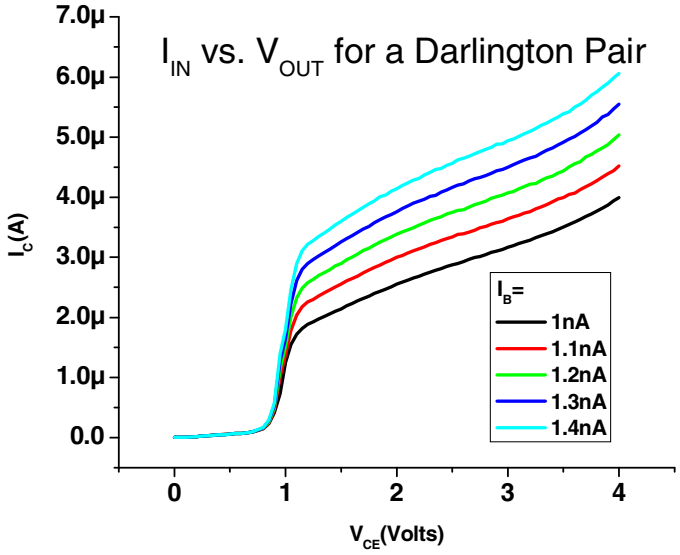

Figure 74. The current characteristics for a Darlington Pair (*see* Figure 73) with a gain of 4900. The initial base current (into the first device in the pair) is 1 nA because the circuit shows a little instability when the total of I_{OUT} is low. The base current steps are 100 pA.

The data in Figures 72 and 74 is very promising. It shows that very small changes in base current can be reliably amplified. Another experiment performed on a previous round of devices is shown in Figure 75. It consists of using the BJT to amplify the current flowing through a 10 G test resistor. As can be seen from Figure 75, a BJT with a gain around 10 can effectively amplify a current of 12.5 pA (125 mV across 10 G) at 1 kHz (remembering that the patch clamp amplifier uses a 1 kHz low pass filter). A 5 pA signal was tried as well, but it seems to be near the cut off of this device's capabilities. The signals recorded in Figure 75 generated with and without the BJT were preamplified by a Femto DLPCA-200 variable gain, low noise current amplifier. The reason for this is that at a gain of only 10, the BJT could not amplify the 12.5 pA current to a level which the oscilloscope could read, even passing the current through a 1 M resistor. Figure 75

still reflects the BJT's gain capability because the Femto gain characteristics were identical for both signals. A device with a higher gain may fare better at the lower current level of 5pA (not shown).

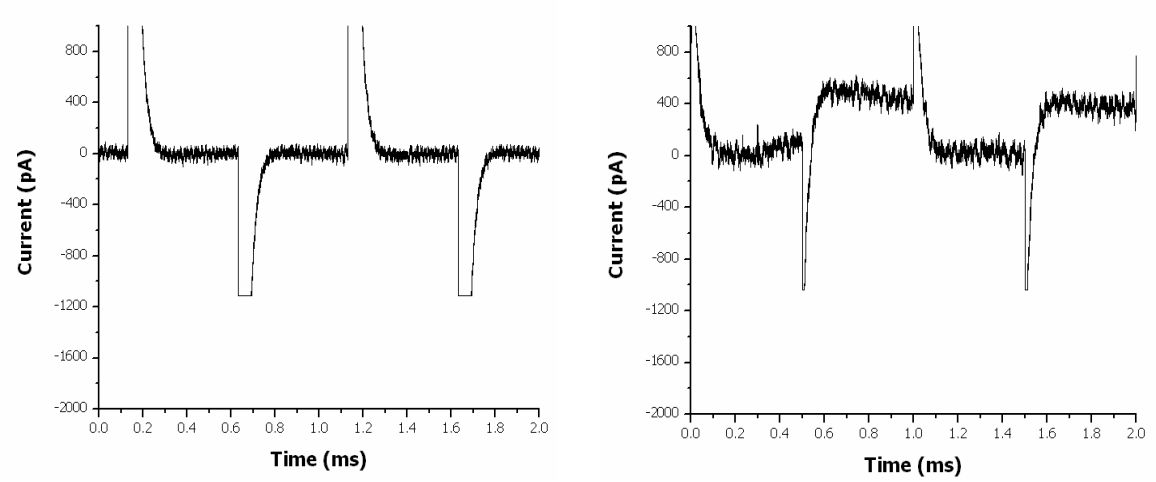

Figure 75. In order to test the viability of using BJTs to amplify single ion channel current, a 10 G test resistor was used. The voltage applied across the resistor was 125 mV for a current level of 12.5 pA applied at a frequency of 1 kHz. The graph on the left represents the 12.5 pA current fed directly into the oscilloscope (no BJT). No appreciable current is measured after the capacitive spike reaches equilibrium. When the signal is fed into the base of the BJT (graph on the right), definite gain is displayed. The gain of this device was about 10. Both signals are fed into a Femto DLPCA-200 variable gain, low noise current amplifier set to the same settings [39]. The gain of the amplifier is identical for both graphs and so the graph on the right accurately reflects the presence of gain from the BJT. The amplifier was necessary due to this BJTs low gain and the minimum detectable voltage of 1 mV on the oscilloscope. Improvements in device performance and the use of amplifier circuits like the Darlington Pair should remove this necessity.

Now that device operation has been verified, it is necessary to fabricate the sensing pads. The sensing pads are made using the same layers (titanium/gold-palladium alloy/gold) and placed in close proximity to the BJT. Silver is used in order to connect the aluminum lines to the sensing pad. Two silver depositions have to be performed.

One is to put a thin amount of silver on top of titanium to make sure it can adhere to the silicon dioxide surface. The second silver deposition is a thick layer to make sure that it can properly connect to the thick aluminum (the aluminum lines were quite thick due to the height of the device mesas). This is because aluminum and gold are known to form intermetallic complexes at elevated temperatures [38]. Since one of the steps for processing these devices after depositing the sensing pad is a polyimide cure at 350ºC (a temperature sufficiently high enough to cause intermetallic formation), it may be that putting the sensing pad directly on the aluminum or vise versa is not advisable [38]. After the metal layers are deposited, first the sensing pad and then the silver, polyimide is patterned on top of the sensing pads and the BJT. The emitter, base, and collector contact biasing pads are quite large. If the sensing pad as deposited on the LTO and nitride dielectric is not flat enough (LTO is much poorer quality than thermally grown oxide, which when with the plasma etching performed on the top of the wafer, may make these pads insufficiently smooth), the biasing pads are large enough to easily connect the BJTs to a sensing electrode fabricated separately as described in Section 5.4.

The other important component to evaluate is the inherent noise in the BJT. There are three main contributors to noise in a BJT, thermal noise, shot noise and flicker noise (also called 1/*f* noise) [40]. The origin of thermal noise is due to the random thermal motion of carriers [40]. All three components of the BJT, the emitter, base, and collector/collector contact, make a contribution to thermal noise (they all have small nonzero resistances). Shot noise occurs due to the presence of *p*-*n* junctions [40]. Only carriers with sufficient energy and velocity towards the junction can surmount the junction barrier caused by the reverse electric field [40]. Carriers which fit this description arrive randomly at the junction such that instead of having continuous flow the steady state current is really made up of a bunch of random independent current

pulses [40]. Flicker noise is found in all active devices [40]. In BJTs, it is caused predominantly by traps in the emitter-base depletion region [40]. These traps have random capture and release times with time constants that cause them to have the largest effect at low frequency [40]. It has been calculated by Basu *et al.* using the circuit simulator TSpice that the total noise current for these devices is approximately 1 to 2 pA at 1 kHz [41]. Although at this level the M2 ion channel may produce a current (as described above in Section 5.5) too close in magnitude to the noise current, the noise should not be a limiting factor for several of the other ion channels tested which display higher conductance.

5.7 REFERENCES

1. John H. Byrne, Stanley G. Schultz, An Introduction to Membrane Transport and Bioelectricity, 2nd Edition, (Raven Press, Ltd., 1994) pp. 1-112

2. Henk M. Keizer, Brian R. Dorvel, Martin Andersson, Daniel Fine, Rebecca B. Price, Joanna R. Long, Ananth Dodabalapur, Ingo Köper, Wolfgang Knoll, Peter A. V. Anderson, Randolph Duran, "Functional Ion Channels in Tethered Bilayer Membrane Arrays: Implications for Biosensors" *ChemPhysChem* (accepted)

3. B. A. Cornell, V. L. B. Braach-Maksvytis, L. G. King, P. D. J. Osman, B. Raguse, L. Wieczorek, R. J. Pace, "A biosensor that uses ion-channel switches" *Nature* vol. 387 (June 5, 1997) pp. 580-583

4. Hagan Bayley, Charles R. Martin, "Resistive-Pulse Sensing—From Microbes to Molecules" *Chemical Review* vol. 100 (2000) pp. 2575-2594

5. Gillian Woodhouse, Lionel King, Lech Wieczorek, Peter Osman, Bruce Cornell, "The ion channel switch biosensor" *Journal of Molecular Recognition* vol. 12 (1999) pp. 328-334

6. W. Knoll, C. W. Frank, C. Heibel, R. Naumann, A. Offenhäusser, J. Rühe, E. K. Schmidt, W. W. Shen, A. Sinner, "Functional tethered lipid bilayers" *Reviews in Molecular Biotechnology* vol. 74 (2000) pp. 137-158

7. Edward T Castellana, Paul S. Cremer, "Solid supported lipid bilayers: From biophysical studies to sensor design" *Surface Science Reports* vol. 61 (2006) pp. 429-444

8. Hiroaki Suzuki, Kazuhito V. Tabata, Hiroyuki Noji, Shji Takeuchi, "Highly Reproducible Method of Planar Lipid Bilayer Reconstitution in Polymethyl Methacrylate Microfluidic Chip" *Langmuir* vol. 22 (2006) pp. 1937-1942

9. Winfried Römer, Claudia Steinem, "Impedance Analysis and Single-Channel Recordings on Nano-Black Lipid Membranes Based on Porous Alumina" *Biophysical Journal* vol. 86 (February 2004) pp. 955-965

10. B. A. Cornell, G. Krishna, P. D. Osman, R. D. Pace, L. Wieczorek, "Tethered-bilayer lipid membranes as a support for membrane-active peptides" *Biochemical Society Transactions* vol. 29, part 4 (2001) pp. 613-617

11. Thierry Stora, Jeremy H. Lakey, Horst Vogel, "Ion-Channel Gating in Transmembrane Receptor Proteins: Functional Activity in Tethered Lipid Membranes" *Angewandte Chemie-International Edition* vol. 38, no. 3 (1999) pp. 389-392

12. Martin Andersson, Henk M. Keizer, Chenyu Zhu, Daniel Fine, Ananth Dodabalapur, Randolph S. Duran, "Detection of Single Ion Channel Activity on a Chip Using Tethered Bilayer Membranes" *Langmuir* vol. 23 (2007) pp. 2924-2927

13. Martin Andersson, George Okeyo, Danyell Wilson, Paul Moe, Paul Blount Daniel Fine Ananth Dodabalapur, Randolph S. Duran," Voltage Induced Gating of the Mechanosensitive MscL Ion Channel Reconstituted in a Tethered Lipid Bilayer Membrane" (submitted)

14. Carl R. Woese, George E. Fox, "Phylogenetic Structure of the Prokaryotic Domain: The Primary Kingdoms" *Proceedings of the National Academy of Sciences of the United States of America* vol. 74, no. 11 (November 1977) pp. 5088-5090

15. David L. Nelson, Michael M. Cox, Lehninger Principles of Biochemistry, 4th Edition, (W. H. Freeman and Company, 2005) pp. 4-5

16. Stefan M. Schiller, Renate Naumann, Katherine Lovejoy, Horst Kunz, Wolfgang Knoll, "Archaea Analogue Thiolipids for Tethered Bilayer Lipid Membranes on Ultrasmooth Gold Surfaces" *Angewandte Chemie-International Edition* vol. 42, no. 2 (2003) pp. 208-211

17. R. Naumann, E. K. Schmidt, A. Jonczyk, K. Fendler, B. Kadenbach, T. Liebermann, A. Offenhäusser, W. Knoll, "The peptide-tethered lipid membrane as a biomimetic system to incorporate cytochrome c oxidase in a functionally active form" *Biosensors & Bioelectronics* vol. 14 (1999) pp. 651-662

18. S. J. Opella, F. M. Marassi, J. J. Gesell, A. P. Valente, Y. Kim, M. Oblatt-Montal, M. Montal, "Structures of the M2 channel-lining segments from nicotinic acetylcholine and NMDA receptors by NMR spectroscopy" *Nature Structural Biology* vol. 6, no. 4 (April 1999) pp. 374-379

19. Declan A. Doyle, João Morais Cabral, Richard A. Pfuetzner, Anling Kuo, Jacqueline M. Gulbis, Steven L. Cohen, Brian T. Chait, Roderick MacKinnon, "The Structure of the Potassium Channel: Molecular Basis of K^+ Conduction and Selectivity" *Science* vol. 280 (April 3, 1998) pp. 69-77

20. Youxing Jiang, Alice Lee, Jiayun Chen, Martine Cadene, Brian T. Chait, Roderick MacKinnon, "Crystal structure and mechanism of a calcium-gated potassium channel" *Nature* vol. 417 (May 30, 2002) pp. 515-522

21. R. R. Ketchem, W. Hu, T. A. Cross, "High-Resolution Conformation of Gramicidin A in a Lipid Bilayer by Solid-State NMR" *Science* vol. 261 (September 10, 1993) pp. 1457-1460

22. Geoffrey Chang, Robert H. Spencer, Allen T. Lee, Margaret T. Barclay, Douglas C. Rees, "Structure of the MscL Homolog form *Mycobacterium tuberculosis*: A gated Mechanosensitive Ion Channel" *Science* vol. 282 (December 18, 1998) pp. 2220-2226

23. Natalia Levina, Sabine Totemeyer, Neil R. Stokes, Petra Louis, Michael A. Jones, Ian R. Booth, "Protection of *Escherichia coli* cells against extreme turgor by activation of MscS and MscL mechanosensitive channels: identification of genes required for MscS activity" *The European Molecular Biology Organization Journal* vol. 18, no. 7 (1999) pp. 1730-1737

24. Roberto Coronado, Ramon Latorre, "Phospholipid Bilayers Made from Monolayers on Patch-Clamp Pipettes" *Biophysics Journal* vol. 43, iss. 2 (1983) pp. 231-236

25. Shin-Ho Chung, Olaf S. Andersen, Vikram Krishnamurthy, Biological Membrane Ion Channels: Dynamics, Structure, and Applications, (Springer Science + Business Media, LLC, 2007) pp. 576-588

26. Bernardo Rudy, Linda E. Iverson, Methods in Enzymology: Volume 207: Ion Channels, (Academic Press, Inc., 1992) pp. 28-53

27. Scanning Electron Microscopy, Inc., Conference Proceedings, AMF O'Hare, IL (1980)

28. R. Lipowsky, E. Sackmann, Structure and Dynamics of Membranes: Generic and Specific Interactions, Volume 1B, (Elsevier Science B. V., 1995) pp.605-640

29. Tanner EDA and Customer Support, T-Spice™ User Guide and Reference, (Tanner Research, Inc., 1998)

30. W. Shockley, M. Sparks, G. K. Teal, "p-n Junction Transistors" *Physical Review* vol. 83, no. 1 (July 1, 1951)

31. Thomas Kind, Matthias Issing, Rüdiger Arnold, Bernt Müller, "Electrical Coupling of Single Cardiac Rat Myocytes to Filed-Effect and Bipolar Transistors" *IEEE Transactions on Biomedical Engineering* vol. 49, no. 12 (December 12, 2002) pp. 1600-1609

32. S. M. Sze, Kwok K. Ng, Physics of Semiconductor Devices, 3rd Edition, (John Wiley & Sons, Inc., 2007) pp. 243 - 288

33. Gerold W. Neudeck, Volume III: The Bipolar Junction Transistor, 2nd Edition: Modular Series on Solid State Devices, (Addision-Wesley Publishing Company, 1989)

34. Technology Modeling Associates, Medici: Two-Dimensional Simulation Program, Version 4.0: Users Manual, (Technology Modeling Associates, Inc., 1997)

35. Ben G. Streetman, Sanjay Banerjee, Solid State Electronic Devices, 5th Edition, (Prentice-Hall of India, Inc., 2004) pp. 17-25 and pp. 434-436

36. L. Li, H. Bender, T. Trenkler, P. W. Mertens, M. Meuris, W. Vandervorst, M. M. Heyns, "Surface passivation and microroughness of (100) silicon etched in aqueous hydrogen halide (HF, HCl, HBr, HI) solutions" *Journal of Applied Physics* vol. 77, no. 3 (February 1, 1995) pp. 1323-1325

37. David A. Hodges, "Darlington's Contributions to Transistor Circuit Design" *IEEE Transactions on Circuits and Systems—I: Fundamental Theory and Applications* vol. 46, no. 1 (January 1, 1999) pp.102-104

38. Elliott Philofsky, "Intermetallic formation in gold-aluminum systems" *Solid-State Electronics* vol. 13, iss. 10 (October 1970) pp. 1391-1394

39. http://www.femto.de/

40. Giuseppe Massobrio, Paolo Antognetti, Semiconductor Device Modeling with SPICE, 2nd Edition, (McGraw-Hill, Inc., 1993) pp. 299-305

41. Debarshi Basu, Ananth Dodabalapur (unpublished)

CHAPTER 6 CONCLUSION

This thesis attempts to make a case for pursuing the development of two different sensing platforms, organic thin-film transistors and ion channels immobilized in tethered bilayer lipid membranes. The benefits to be realized from both of these techniques include flexibility, cost, and portability, in addition to selectivity and sensitivity. Both transduce analyte responses directly to electrical signals, potentially reducing the time necessary to measure a response. Cost benefits for each platform could be realized by reduced fabrication complexity which would arise from the ability to process these systems using standard silicon processing or the potentially lower cost fabrication associated with organic devices (e.g., inject printed circuits). The tBLM systems are very attractive as many of their elements self assemble.

Organic devices offer a lot of flexibility in terms of device configurations, available semiconductors, and chemical modifications to those semiconductors. The sensing response in these devices may even add some benefit in understanding device transport and especially contact injection effects. Coupling the devices to silicon transistors has proven to be a very powerful technique, which, when coupled with chemical modification, e.g., receptors, may prove to be even more robust.

Tethered bilayer lipid membrane systems offer a tremendous degree of flexibility. There is a vast array of preexisting ion channels to choose from. In addition, many of these channels can be modified with a variety of receptors. Large arrays of electrodes equipped with tBLMs and ion channels could make it possible to detect a variety of analytes from within the same aqueous sample. These systems may even be able to help

with the discovery of new cellular mechanisms associated with the cell membrane, as they can be used to isolate these systems in a more controlled, repeatable, laboratory environment.

There is significant work still to be accomplished. In the case of organic sensors, better quantitative understanding must be acquired as to the exact interactions between semiconductors and analytes. This must be accompanied by an ability to measure many responses rapidly while being able to refresh the device. A new analyte delivery system is being built which should be able to accomplish this goal by using mass flow controllers to introduce very controlled concentrations of analyte to the OTFT sensor. It would also be beneficial to be able to perform various types of microscopy and spectroscopy, such as scanning-probe potentiometry and IR spectroscopy, while an analyte response is being measured. This might shed more light on how charges in the channel affect the semiconductor/analyte interaction.

In the case of tBLM systems, now that the basic capability of successfully incorporating and measuring ion channels in a tethered membrane has been shown, it must be successfully integrated with a small scale integrated circuit. This work suggested one device, a bipolar junction transistor, should be able to accomplish this task. If the BJT is successful, further gains in signal to noise ratio can be achieved by the use of small amplifying circuits like the differential amplifier. Long term membrane stability also has a long way to go before these devices will be ready for real world applications. The membranes currently last for hours, but to be viable, they probably need to last for days. It is conceivable that any final sensing solution using tBLMs builds has a system to

build the tBLMs just prior to a sensing measurement, after which the bilayer is rinsed away. The monolayer tethers have been shown to have very long lifetimes.

It is thus the opinion of this author that these sensing platforms are worth pursuing. The development of these sensing systems should also greatly benefit from increases in the general understanding of, and improvements in, the performance of organic semiconductor devices, ion channels (including synthetic ion channels), and bilayer lipid membrane architectures. Should these systems meet their potential, the benefits to environmental and medical monitoring would be significant.

Bibliography

Brian R. Eggins, Chemical Sensors and Biosensors, (John Wiley & Sons, Ltd., 2002) pp. 1-9

APOPO, an organization devoted to the detection of land mines in Africa http://www.apopo.org/newsite/content/index.htm

Dimitra G. Georganopoulou, Lei Chang, Jwa-Min Nam, C. Shad Thaxton, Elliot J. Mufson, William L. Klein, Chad A. Mirkin, "Nanoparticle-based detection in cerebral spinal fluid of a soluble pathogenic biomarker for Alzheimer's disease." *Proceedings of the National Academy of Sciences* Vol. 102, No. 7 (February 15, 2005) pp. 2273-2276

J. Throck Watson, H. Wohltjen, Introduction to Mass Spectrometry, 3rd Edition, (Lippincott-Raven Publishers, 1997)

F. Baldini, A. N. Chester, J. Homola, S. Martellucci, Optical Chemical Sensors, (Springer, 2006)

James M. Miller, Chromatography: Concepts and Contrasts, (John Wiley & Sons, Inc., 2005)

David L. Nelson, Michael M. Cox, Lehninger Principles of Biochemistry, 4th Edition, (W. H. Freeman and Company, 2005) pp. 175-182

Federation of American Scientists Anthrax Fact Sheet http://www.fas.org/biosecurity/resource/agents.htm

The National Cancer Institute Fact Sheet. The Prostate-Specific Antigen (PSA) Test: Questions and Answers http://www.cancer.gov/cancertopics/factsheet/Detection/PSA

"Endocrine Disruptors", National Institute of Environmental Health Sciences, U.S. Department of Health and Human Services, National Institutes of Health (June 2006) http://www.niehs.nih.gov/oc/factsheets/pdf/endocrine.pdf

Michael J. Serby, Karen L. Chobor, Science of Olfaction, (Springer-Verlag, Inc., 1992), pp. 31-119

Carol Turkington, Bonnie Lee Ashby, The Encyclopedia of Infectious Diseases, 3rd edition, (Facts on File, Inc., April 30, 2007)

Julian W. Gardner, Philip N. Bartlett, Electronic Noses: Principles and Applications, (Oxford University Press, Inc., 1999) pp. 1-6

F. Baldini, A.n. Chester, J. Homola, S. Martellucci, Optical Chemical Sensors, (Springer, 2006)

D. S. Ballantine, Jr., R. M. White, S. J. Martin, A. J. Ricco, G. C. Frye, E. T. Zellers, H. Wohltjen, Acoustic Wave Sensors: Theory, Design, and Physico – Chemical Applications, (Academic Press, Inc., 1997)

Mark Derr, "With Training, a Dog's Nose Almost Always Knows." The New York Times 29 May 2001:

http://www-psych.stanford.edu/~bigopp/Behaviorism.html

David Philipps, "Buried alive, waiting for a cheese hound." The Gazette 2004 (published by Gazette Enterprises, a division of Freedom Colorado Information): http://pets.coloradosprings.com/feature_fullstory.jsp?id=4066

G. Sicard, and A. Holley, "Receptor cell responses to odorants: Similarities and differences among odorants." *Brain Res.* 292(1984) pp. 283-296

Gary S. Settles, “Sniffers: Fluid-Dynamic Sampling for Olfactory Trace Detection in Nature and Homeland Security – The 2004 Freeman Scholar Lecture.” *Journal of Fluids Engineering*. 127(2005) pp. 189-218

Aud Thesen, Johan B. Steen, Kjell B. Døving, “Behavior of Dogs During Olfactory Tracking.” *J. exp. Biol*. 180(1993) pp. 247-251

Michael McCulloch, Tadeusz Jezierski, Michael Broffman, Alan Hubbard, Kirk Turner, Teresa Janecki, “Diagnostic Accuracy of Canine Scent Detection in Early - and Late – Stage Lung and Breast Cancer.” *Integrative Cancer Therapies*. Vol. 5, Iss. 1(2006) pp. 30-39

Julio E. Correa, “The Dog’s Sense of Smell.” UNP-66, (Alabama A&M and Auburn Universities, Alabama Cooperative Extension System July 2005) http://www.aces.edu/pubs/docs/U/UNP-0066/UNP-0066.pdf?PHPSESSID=899e618c0b54b53ec7ab56f0e314cb54

A. Maureen Rouhi, “Detecting Illegal Substances,” Chemical & Engineering News, (the American Chemical Society, September 29, 1997) http://pubs.acs.org/hotartcl/cenear/970929/detect.html

National Human Genome Research Institute, National Institutes of Health http://www.genome.gov//Pages/Hyperion//DIR/VIP/Glossary/Illustration/antibody.cfm referenced from a Wikipedia article on antibodies http://en.wikipedia.org/wiki/Antibodies

Research Collaboratory for Structural Bioinformatics (RCSB), Protein Data Bank http://www.rcsb.org/pdb/explore.do?structureId=1IGT

referenced from Wikipedia

http://en.wikipedia.org/wiki/Image:Antibody_IgG.png

Jwa-Min Nam, C. Shad Thaxton, Chad A. Mirkin, "Nanoparticle-Based Bio-Bar Codes for the Ultrasensitive Detection of Proteins." *Science* 301(26 september 2003) pp. 1884 – 1886

Scott E. Osborne, Ichiro Matsumura, Andrew Ellington, "Aptamers as therapeutic and diagnostic reagents: problems and prospects." *Current Opinion in Chemical Biology* Vol. 1, Iss. 1 (June 1997) pp. 5-9

Mirtha Umaña, Jess Waller, "Protein – Modified Electrodes. The Glucose Oxidase/Polypyrrole System." *Anal. Chem.* 58 (1986) pp. 2979-2883

B. Crone, A. Dodabalapur, A. Gelperin, L. Torsi, H. E. Katz, A. J. Lovinger, Z. Bao, "Electronic sensing of vapors with organic transistors." *Applied Physics Letters*, Vo. 78, No. 15(April 9, 2005) pp. 2229-2231

Q. Zhou, R. D. Gould, "A study of the response rate to nitrogen dioxide exposure in metal phthalocyanine thin film sensors." *Thin Solid Films*, 317(1998) pp. 436-439

Yanming Sun, Yunqi Liu, Daoben Zhu, "Advances in organic field effect transistors." *Journal of Materials Chemistry*, 15(2005) pp. 53-65

Daniel R. Gamota, Paul Brazis, Krishna Kalyanasundaram, Jie Zhang, Printed Organic and Molecular Electronics, (Kluwer Academic Publishers, 2004) pp. 56-75

David Nilsson, Thomas Kugler, Per-Olof Svensson and Magnus Berggren, "An all-organic sensor-transistor based on a novel electrochemical transducer concept printed electrochemical sensors on paper." *Sensors and Actuators B*, vol. 86(2002) pp. 193-197

Frances M. Ashcroft, Ion Channels and Disease, (Academic Press, 2000) pp. 1-3

Adrea Vescovi, Adrea Knoll, Ulrich Koert, "Synthesis and functional studies of THF-gramicidin hybrid ion channels." *Organic & Biomolecular Chemistry*, vol. 1, iss. 16 (August 21 2003) pp. 2983-2997

B. A. Cornell, V. L. B. Braach-Maksvytis, L. G. King, P. D. J. Osman, B. Raguse, L. Wieczorek, R. J. Pace, "A biosensor that uses ion-channel switches." *Nature* 387(June 5 1997) pp. 580-583

Hagan Bayley, Charles R. Martin, "Resistive-Pulse Sensing—From Microbes to Molecules." *Chemical Reviews* vol. 100, iss. 7 (July 2000) pp. 2575-2594

Daniel R. Gamota, Paul Brazis, Krishna Kalyanasundaram, Jie Zhang, Printed Organic and Molecular Electronics, (Kluwer Academic Publishers, 2004) pp. 1-36

R. Farchioni, G. Grosso, Organic Electronic Materials,(Springer-Verlag, 2001) pp. 215-219

P. F. Baude, D. A. Ender, T. W. Keller, M. A. Haase, D. V. Muyres, S. D. Theiss, "Organic semiconductor RFID transponders." *Electron Deivces Meeting, 2003, IEDM '03 Technical Digest, IEEE International* (December 8-10, 2003) pp. 8.11-8.14

Yoshinori Fukuda, Teruichi Watanabe, Takeo Wakimoto, Satoshi Miyaguchi, Masami Tsuchida, "An organic LED display exhibiting pure RGB colors." *Synthetic Metals* vol. 111-112 (2000) pp. 1-6

Lisong Zhou, Sungkyu Park, Bo Bai, Jie Sun, Sheng-Chu Wu, Thomas N. Jackson, Shelby Nelson, Diane Freeman, Yongtaek Hong, "Pentacene TFT Driven AM OLED Displays." *IEEE Electron Device Letters* vol. 26 no. 9 (September 9, 2005) pp. 640-642

Jefrey T. Mabeck, George G. Malliaras, "Chemical and biological sensors based on organic thin-film transistors." *Analytical and Bioanalytical Chemistry* vol. 384 (2006) pp. 343-353

John A. Rogers, Zhenan Bao, Kirk Baldwin, Ananth Dodabalapur, Brian Crone, V. R. Raju, Valerie Kuck, Howard Katz, Karl Amundson, Jay Ewing, Paul Drzaic, "Paper-like electronic displays: Large-area rubber-stamped plastic sheets of electronics and microencapsulated electrophoretic inks." *Proceedings of the National Academy of Science* vol. 98 no. 9 (April 24, 2001) pp. 4835-4840

Organic Electronics Conference and Exhibition 2007, "Organic semiconductors: What's it all about?" Display Technology Investor (October 2005) http://www.oec-europe.com/persp_overview.htm

David L. Margulius, "WHAT'S NEXT; With an Organic Sensor, a Food Wrapper Sniffs Out Trouble." The New York Times 4 April 2002: http://query.nytimes.com/gst/fullpage.html?res=9907E6D8103AF937A35757C0A9649C8B63

Noel S. Hush, "An Overview of the First Half-Century of Molecular Electronics." *Molecular Electronics III, Annals of the New York Academy of Sciences* vol. 1006 (December 2003) pp. 1-20

H. Shirakawa, C. K. Chiang, C. R. Fincher, Jr., Y. W. Park, E. J. Louis, S. C. Gau, A. J. Heeger, Alan G. MacDiarmid, "Electrical Conductivity in Doped Polyacetylene." *Physical Review Letters* vol. 39, no. 17(October 24, 1977) pp. 1098-1101

Bengt Nordén, Eva Krutmeijer, Nobel Prize Advanced Information, "The Nobel Prize in Chemistry, 2000: Conductive Polymers" Kungl. Vetenskapsakademien The Royal Swedish Academy of Sciences

http://nobelprize.org/nobel_prizes/chemistry/laureates/2000/chemadv.pdf

Wolfgang Brütting, Physics of Organic Semiconductors, (WILEY-VCH Verlag GmbH & Co. KGaA, 2005) pp.1-13, 273-276, 396-400

Norman R. Mowrer, "Polysiloxanes." *Ameron International Performance Coatings and Finishes* (November 2003) pp. 1-11

http://www.ameronpsx.com/docs/presentation_polysiloxanes.pdf

A. Tsumura, H. Koezuka, T. Ando, "Macromolecular electronic device: Field-effect transistor with a polythiophene thin film." *Applied Physics Letters* vol. 49, iss. 18 (November 3, 1986) pp. 1210-1212

Zhenan Bao, Ananth Dodabalapur, Andrew J. Lovinger, "Soluble and processable regioregular poly(3-hexylthiophene) for thin film field-effect transistor applications with high mobility." *Applied Physics Letters* vol. 69, iss. 26(December 23, 1996) pp. 4108-4110

C. W. Tang, "Two-layer organic photovoltaic cell." *Applied Physics Letters* vol. 48, no. 2(January 13, 1986) pp. 183-185

The Encyclopedia of Alternative Energy and Sustainable Living, A resource of *The Worlds of David Darling*

http://www.daviddarling.info/encyclopedia/F/AE_fill_factor.html

Holger Spanggard, Frederik C. Krebs, “A brief history of the development of organic and polymeric photovoltaics.” *Solar Energy Materials & Solar Cells* vol. 83(2004) pp. 125-146

C. W. Tang, S. A. VanSlyke, “Organic electroluminescent diodes.” *Applied Physics Letters* vol. 51, no. 12(September 21 1987) pp. 913-915

C. Clarisse, M. T. Riou, M. Gauneau, M. Le. Contellec, “Field-Effect Transistor with Diphthalocyanine Thin Film.” *Electronic Letters* vol. 24, no. 11(May 26, 1988) pp. 674-675

Ana C. Arias, Joaquim R. de Lima, Ivo A. Hümmelgen, “Tin Oxide as a Cathode in Organic Light-Emitting Diodes.” *Advanced Materials* vol. 10, no. 5(1998) pp. 392-394

J. H. Burroughes, D. D. C. Bradley, A. R. Brown, R. N. Marks, K. Mackay, R. H. Friend, P. L. Burns, & A. B. Holmes, “Light-emitting diodes based on conjugated polymers.” *Nature* vol. 347(October 11 1990) pp. 539-541

Hedi Mattoussi, Hideyuki Murata, Charles Merritt, Yasuhiro Iizumi, Junji Kido, Zakya H. Kafafi, “Photoluminescence quantum yield of pure and molecularly doped organic solid films.” *Journal of Applied Physics* vol. 86, no. 5 (September 1, 1999) pp. 2642-2650

S. F. Nelson, Y. Y. Lin, D. J. Gundlach, T. N. Jackson, “Temperature-independent transport in high-mobility pentacene transistors.” *Applied Physics Letters* vol. 72 no. 15 (April 13, 1998) pp. 1854-1856

D. J. Gundlach, Y. Y. Lin, T. N. Jackson, S. F. Nelson, D. G. Schlom, "Pentacene Organic Thin-Film Transistors—Molecular Ordering and Mobility." *IEEE Electron Device Letters* vol. 18, no. 3(March 1997) pp. 87-89

Sung Kyu Park, Chung-Chen Kuo, J. E. Anthony, T. N. Jackson, "High mobility solution-processed OTFTs." *Electron Devices Meeting, 2005 IEDM Technical Digest, IEEE International* (December 5-7, 2005) pp. 4-7

Joyce G. Laquindanum, Howard E. Katz, Ananth Dodabalapur, Andrew J. Lovinger, "n-Channel Organic Transistor Materials Based on Napthalene Frameworks." *Journal of the American Chemical Society* vol. 118(1996) pp. 11331-11332

J. Kastner, J. Paloheimo, H. Kuzmany, in Solid State Sciences, edited by H. Kuzmany, M. Mehring, J. Fink (Springer, New York, 1993) pp. 512-515

R.C. Haddon, A. S. Perel, R. C. Morris, T. T. M. Palstra, A. F. Hebard, R. M. Fleming, "C_{60} thin film transistors." *Applied Physics Letters* vol.67, iss. 1(July 3, 1995) pp 121-123

Antonio Facchetti, "Semiconductors for organic transistors." *Materials Today* vol. 10, no. 3 (March 2007) pp. 28-37

A. R. Brown, D. M. deLeeuw, E. J. Lous, E. E. Havinga, :Organic n-type field-effect transistor.", *Synthetic Metals* vol. 66, iss. 3 (October 1994) pp. 257-261

Zhenan Bao, Andrew J. Lovinger, Janelle Brown, "New Air-Stable n-Channel Organic Thin Film Transistors." *Journal of the American Chemical Society* vol. 120 (1998) pp. 207-208

C. Hosokawa, M. Eida, M. Matsuura, K. Fukuoka, H. Nakamura, T. Kusumoto, "Organic multi-color electroluminescence display with fine pixels." *Synthetic Metals* vol. 91(1997) pp. 3-7

Liang Wang, Daniel Fine, Debarshi Basu, Ananth Dodabalapur, "Electric-field-dependent charge transport in organic thin-film transistors." *Journal of Applied Physics* vol. 101, article #054515(2007) pp. 1-8

Reji Hattori, Tsutomu Tsukamizu, Ryusuke Tsuchiya, Kazunori Miyake, Yi He, Jerzy Kanicki, "Current-Writing Active-Matrix Circuit for Organic Light-Emitting Diode Display using a-Si:H Thin-Film-Transistors." *IEICE Trans. Electron* vol. E83-C, no. 5 (May 2000) pp. 779-782

H. Sirringhaus, T. Kawase, R. H. Friend, T. Shimoda, M. Inbasekaran, W. Wu, E. P. Woo, "High-Resolution Inkjet Printing of All-Polymer Transistor Circuits." *Science* vol. 290 (December 15, 2000) pp. 2123-2126

Yanming Sun, Yunqi Liu, Daoben Zhu, "Advances in organic field effect transistors." *Journal of Materials Chemistry*, 15(2005) pp. 53-65

B. Crone, A. Dodabalapur, A. Gelperin, L. Torsi, H. E. Katz, A. J. Lovinger, "Electronic sensing of vapors with organic transistors." *Applied Physics Letters* vol. 78, no. 15 (April 9, 2001) pp. 2229-2231

B. Bott, T. A. Jones, "High sensitivity NO sub(2) sensor based on electrical conductivity changes in phthalocyanine films." *Sensors and Actuators* vol. 5, no. 1 (1984) pp. 43-53

R. Zhou, F. Josse, W. Göpel, Z. Z. Öztürk, Ö. Bekaro lu, "Phthalocyanines as Sensitive Materials for Chemical Sensors." *Applied Organometallic Chemistry* vol. 10 (1996) pp. 557-577

A. Oprea, U. Weimar, E. Simon, M. Fleischer, H. P. Frerichs, Ch. Wilbertz, M. Lehmann, "Copper phthalocyanine suspended gate field effect transistors for NO_2 detection." *Sensors and Actuators B* vol. 118 (2006) pp. 249-254

Luisa Torsi, Ananth Dodabalapur, "Organic Thin-Film Transistors as Plastic Analytical Sensors." *Analytical Chemistry* vol. 77, iss. 19 (October 1, 2005) pp. 380A-387A

L. Torsi, A. Dodabalapur, L. Sabbatini, P. G. Zambonin, "Multi-parameter gas sensors based on organic thin-film-transistors." *Sensors and Actuators B* vol. 67 (2000) pp. 312-316

Jeffrey T. Mabeck, George G. Malliaras, "Chemical and biological sensors based on organic thin-film transistors." *Analytical and Bioanalytical Chemistry* vol. 384(2006) pp. 343-353

Daniel A. Brenards, Gilman E. S. Toombes, George G. Malliaras, Sol M. Gruner, "Gating of an organic transistor through a bilayer lipid membrane with ion channels." *Applied Physics Letters* vol. 89 article no. 053505 (2006) pp. 1-3

William H. Brown, Christopher S. Foote, Organic Chemistry, 2nd Edition, (Saunders College Publishing, 1998) pp.30-40

David W. Oxtoby, H. P. Gillis, Norman H. Nachtrieb, Principles of Modern Chemistry, 4th Edition, (Saunders College Publishing, 1999) pp. 581-600

Jihmei Luo, Harold Hart, “Linear Acene Derivatives. New Routes to Pentacene and Naphthacene and the First Synthesis of a Triptycene with Two Anthracene Moieties.” *The Journal of Organic Chemistry* vol. 52, no. 22 (October 30, 1987) pp. 4833-4836

William J. Bailey, Milton Madoff, “Cyclic Dienes. II. A New Synthesis of Pentacene.” *New Synthesis of Pentacene* [Contribution from the Department of Chemistry, Wayne University] (November 20, 1953) p. 5603

B. I. Kharisov, U. Ortiz, Méndez, L. A. Garza-Rodríguez, H. M. Leija Gutiérrez, A. Medina Medina, S. S. Berdonosov, “Use of various activated forms of elemental nickel and copper for the synthesis of phthalocyanine at low temperature.” *Journal of Coordination Chemistry* vol. 59, iss. 15(October 15, 2006) pp. 1657-1666

Tian-An Chen, Xiaoming Wu, Reuben D. Rieke, “Regiocontrolled synthesis of Poly(3alkylthiophenes) Mediated by Rieke Zinc: Their Characterization and Solid-State Properties.” *Journal of the American Chemical Society* vol. 117 (1995) pp. 233-244

Maria Cristina Tanese, Daniel Fine, Ananth Dodabalapur, Nicola Cioffi, Luisa Torsi, “High Performance Organic Thin Film Transistor Sensors.” Organic Field-Effect Transisoros III *Proceedings of SPIE* vol. 5522 (October, 2004) pp.22-26

Liang Wang, Daniel Fine, Taeho Jung, Debarshi Basu, Heinz von Seggern, Ananth Dodabalapur, “Pentacene field-effect transistors with sub-10-nm channel lengths.” *Applied Physics Letters* vol. 85, no. 10 (September 6, 2004) pp. 1772-1774

Zhenan Bao, Valerie Kuck, John A. Rogers, Mark A. Paczkowski, “Silsesquioxane Resins as High-Performance Solution Processible Dielectric Materials for Organic

Transistor Applications." *Advanced Functional Materials* vol. 12, no. 8(August 2002) pp 526-531

Lei Diao, Dominic D. Schroepfer, C. Daniel Frisbie, P. Paul Ruden, "Electrical characterization of metal/pentacene contacts." *Journal of Applied Physics* vol. 101, article #014510 (2007) pp. 1-8

Product Data Sheet, "AZ 5214 E Image Reversal Photoresist" Clariant Corporation http://groups.mrl.uiuc.edu/dvh/pdf/AZ5214E.pdf

JEOL Ltd. Instruction manual (IEB6FSE-GS-1 (1720)), JBX-6000FS/E: General Statement, (JEOL, Ltd., 2002)

V. Jaubert, P. Lucas, L. Mollard, S. Tedesco, B. Dal'zotto, S. Landis, "Characterization of charging effect on 8" wafer during e-beam lithography exposure." *Microelectronic Engineering* vol. 67-68(2003) pp 149-156

J. Laconte, F. Iker, S. Jorez, N. André, J. Proost, T. Pardoen, D. Flandre, J. P. Raskin, "Thin films stress extraction using micromachined structures and wafer curvature measurements." *Microelectronic Engineering* vol. 76(2004) pp. 219-226

V. Y. Bulko, X. Chi, D. V. Lang, A. P. Ramirez, "Field-effect transistor on pentacene single crystal." *Applied Physics Letters* vol. 83, no. 23 (December 8, 2003) pp. 4773-4775

D. Knipp, R. A. Street, A. VöLkel, J. Ho, "Pentacene thin film transistors on organic dielectrics: Morphology, structural properties, and electronic transport." *Journal of Appied Physics* vol. 93, no. 1(January 1, 2003) pp. 347-355

Byungwook Yoo, Brooks A. Jones Taeho Jung, Debarshi Basu, Antonio Facchetti, Michael R. Wasielewski, Tobin Marks, Ananth Dodabalapur, "High-mobility bottom-contact *n*-channel organic transistors and their use in complementary ring oscillators." *Applied Physics Letters* vol. 88, article # 082104 (2006) pp. 1-3

J. L. Brédas, J. P. Calbert, D. A. Da Silva Filho, J. Cornil, "Organic semiconductors: A theoretical characterization of the basic parameters governing charge transport." *Proceeding of the National Academy of Sciences* vol. 99, no. 9(April 30, 2002) pp. 5804-5809

Siddharth Mohapatra, Michelle Grigas, Robert Wenz, Robert Rotzoll, Viorel Olariu, Oleg Shchekin, Klaus Dimmler, Ananth Dodabalapur, "High Mobility Pentacene Field Effect Transistors on Plastic." *Materials Research Society Symposium Proceedings* vol. 870E (Materials Research Society, 2005) pp. H3.2.1-H3.2.6

Christine C. Mattheus, Gilles A. de Wijs, Robert A. de Groot, Thomas T. M. Palstra, "Modeling the Polymorphism of Pentacene." *Journal of the American Chemical Society* vol. 125, no. 20 (2003) pp. 6323-6330

A. Dodabalapur, L. Torsi, H. E. Katz, "Organic Transistors: Two-Dimensional Transport and Improved Electrical Characteristics" *Science* vol. 268 (April 14, 1995) pp. 270-271

Zhenan Bao, Andrew J. Lovinger, Ananth Dodabalapur, "Organic field-effect transistors with high mobility based on copper phthalocyanine." *Applied Physics Letter* vol. 69, iss. 20(November 11, 1996) pp. 3066-3068

Yen-Yi Lin, David J. Gundlach, Shelby F. Nelson, Thomas N. Jackson, "Pentacene-Based Organic Thin-film Transistors." *IEEE Transactions on Electron Devices* vol. 44, no. 8(August 1997) pp. 1325-1331

Martin Pope, Charles E. Swenberg, Electronic Processes in Organic Crystals and Polymers, (Oxford University Press, 1999) pp. 202-369

David Emin, "Correlated Small-Polaron Hopping Motion" *Physical Review Letters* vol. 25, no. 26 (December 28, 1970) pp.1751-1755

J. L. Brédas, J. P. Calbert, D. A. Da Silva Filho, J. Cornil, "Organic semiconductors: A theoretical characterization of the basic parameters governing charge transport" *Proceedings of the National Academy of Sciences* vol. 99, no. 9 (April 30, 2002) pp. 5804-5809

S. Jeyadev, J. R. Schrieffer, "Interchain polaron tunneling in *trans*-polyacetylene" *Physical Review B* vol. 30, no. 7 (October 1, 1984) pp. 3620-3624

Liang Wang, Daniel Fine, Debarshi Basu, Ananth Dodabalapur, "Electric-field-dependent charge transport in organic thin-film transistors." *Journal of Applied Physics* vol. 101, article # 054515 (2007)

W. D. Gill, "Drift mobilities in amorphous charge-transfer complexes of trinitrofluorenone and poly-*n*-vinylcarbazole" *Journal of Applied Physics* vol. 43, no. 12 (December 12, 1972) pp. 5033-5040

Yulong Shen, Ahmad R. Hosseini, Man Hoi Wong, George G. Malliaras, "How To Make Ohmic Contacts to Organic Semiconductors" *ChemPhysChem* vol. 5 (2004) pp. 16-25

David J. Gundlach, Thomas N. Jackson, "Pentacene TFT With Improved Linear Region Characteristics Using Chemically Modified Source and Drain Electrodes" *IEEE Electron Device Letters* vol. 22, no. 12 (December 2001) pp. 571-573

L. Bürgi, T. J. Richards, R. H. Friend, H. Sirringhaus, "Close look at charge carrier injection in polymer field-effect transistors" *Journal of Applied Physics* vol. 94, no. 9 (November 1, 2003) pp. 6129-6137

F. Amy, C. Chan, A. Kahn, "Polarization at the gold/pentacene interface" *Organic Electronics* vol. 6 (2005) pp. 85-91

Lei Diao, Dominic D. Schroepfer, P. Paul Ruden, C. Daniel Frisbie, "Electrical characterization of metal/pentacene contacts" *Journal of Applied Physics* vol. 101, article# 014510 (2007) pp. 1-8

Liang Wang, Daniel Fine, Debarshi Basu, Ananth Dodabalapur (unpublished)

A. Oprea, U. Weimar, E. Simon, M. Fleischer, H. P. Frerichs, Ch. Wilbertz, M. Lehmann, "Copper phthalocyanine suspended gate field effect transistors for NO_2 detection." *Sensors and Actuators B* vol. 118 (2006) pp. 249-254

Marcel Bouvet, "Phthalocyanine-based field-effect transistors as gas sensors" *Analytical and Bioanalytical Chemistry* vol. 384 (2006) pp. 366-373

B. Crone, A. Dodabalapur, A. Gelperin, L. Torsi, H. E. Katz, A. J. Lovinger, "Electronic sensing of vapors with organic transistors." *Applied Physics Letters* vol. 78, no. 15 (April 9, 2001) pp. 2229-2231

Molecular formulas are listed at the Sigma-Aldrich online chemical catalog http://www.sigmaaldrich.com/Area_of_Interest/The_Americas/United_States.html

L. Torsi, A. Tafuri, N. Cioffi, M. C. Gallazzi, A. Sassella, L. Sabbatini, P. G. Zambonin, "Regioregular polythiophene field-effect transistors employed as chemical sensors" *Sensors and Actuators B* vol. 93 (2003) pp. 257-262

M. C. Tanese, L. Torsi, N. Cioffi, L. A. Zotti, D. Colangiuli, G. M. Farinola, F. Babudri, F. Naso, M. M. Giangregorio, L. Sabbatini, P. G. Zambonin, "Poly(phenyleneethynylene) polymers bearing glucose substituents as promising active layers in enantioselective chemiresistors" *Sensors and Actuators B* vol. 100 (2004) pp. 17-21

L. Torsi, A. Dodabalapur, N. Cioffi, L. Sabbatini, P. G. Zambonin, "NTCDA organic thin-film-transistor as humidity sensor: weaknesses and strengths" *Sensors and Actuators B* vol. 77 (2001) pp. 7-11

Zheng-Tao Zhu, Jeffrey T. Mason, Rüdiger Dieckmann, George G. Malliaras, "Humidity sensors based on pentacene thin-film transistors" *Applied Physics Letters* vol. 81, no. 24 (December 9, 2002) pp. 4643-4645

Deepak Sharma, "Combining silicon and organic/polymer semiconductors in a new class of sensor devices" *Masters Thesis* (December 2005) p 22

Cynthia Burham, Daniel Fine, Ananth Dodabalapur, unpublished

Daniel Fine, Liang Wang, Debarshi Basu, Ananth Dodabalapur, unpublished

Liang Wang, Daniel Fine, Ananth Dodabalapur, "Nanoscale chemical sensor based on organic thin-film transistors" *Applied Physics Letters* vol. 85, no. 26 (December 27, 2004) pp. 6386-6388

Deepak Sharma, Ananth Dodabalapur, unpublished

Maryadele J. O'Neil, Ann Smith, Patricia E. Heckelman, John R. Obenchain, Jo Ann R. Gallipeau, Mary Ann D'Arecca, Susan Budavari, The Merck Index, (Merck & Co., Inc., 1996) p. 5985

William H. Brown, Christopher S. Foote, Organic Chemistry, 2nd Edition, (Saunders College Publishing, 1998) p. 25

L. Torsi, A. J. Lovinger, B. Crone, T. Someya, A. Dodabalapur, H. E. Katz, A. Gelperin, "Correlation between Oligothiophene Thin Film Transistor Morphology and Vapor Responses" *Journal of Physical Chemistry B* vol. 106, (2002) pp. 12563-12568

Luisa Torsi, Ananth Dodabalapur, "Organic thin-film transistors as plastic analytical sensors" *Analytical Chemistry* vol. 77, no. 19 (October 1, 2005) pp. 380A-387A

Takao Someya, Howard E. Katz, Alan Gelperin, Andrew J. Lovinger, Ananth Dodabalapur, "Vapor sensing with , -dihexylquarterthiophene field-effect transistors: The role of grain boundaries" *Applied Physics Letters* vol. 81, no. 16 (October 14, 2002) pp. 3079-3081

Deepak Sharma, Ananth Dodabalapur, (unpublished)

Hisao Ishii, Kazuhiko Seki, "Energy Level Alignment at Organic/Metal Interfaces Studied by UV Photoemission: Breakdown of Traditional Assumption of a Common Vacuum Level at the Interface" *IEEE Transactions on Electron Devices* vol. 44, no. 8 (August 1997) pp. 1295-1301

F. Amy, C. Chan, A. Kahn, "Polarization at the gold/pentacene interface" *Organic Electronics* vol. 6 (2005) pp. 85-91

L. Bürgi, T. J. Richards, R. H. Friend, H. Sirringhaus, "Close look at charge carrier injection in polymer field-effect transistors" *Journal of Applied Physics* vol. 94, no. 9 (November 1, 2003) pp. 6129-6137

Martin Pope, Charles E. Swenberg, Electronic Processes in Organic Crystals and Polymers, (Oxford University Press, 1999) pp. 202-369

Deepak Sharma, Liang Wang, Cynthia Burham, Daniel Fine, Ananth Dodabalapur, "Organic and Hybrid Organic/Inorganic, Transistors for Chemical and Bio Sensing" *Electron Devices Meeting, 2005, IEDM Technical Digest, IEEE International* ISBN # 0-7803-9268-x (December 5-7, 2005)

Ben G. Streetman, Sanjay Banerjee, Solid State Electronic Devices, 5th Edition, (Prentice-Hall of India, Inc., 2004) p. 302

Deepak Sharma, Daniel Fine, Ananth Dodabalapur, (unpublished)

David W. Oxtoby, H. P. Gillis, Norman H. Nachtrieb, Principles of Modern Chemistry, 4th Edition, (Saunders College Publishing, 1999) pp. 147-148

Laura Pirondini, Francesca Bertolini, Barbara Cantadori, Franco Ugozzoli, Chiara Massera, Enrico Dalcanale, "Design and self-assembly of wide and robust coordination cages" *Proceedings of the National Academy of Sciences* vol. 99 no. 8 (April 16, 2002) pp. 4911-4915

Adrian Bachtold, Peter Hadley, Takeshi Nakanishi, and Cees Dekker, "Logic Circuits with Carbon Nanotube Transistors" *Science* vol. 294, (November 9, 2001) pp. 1371-1320

Xavier Batlle, Bart Jan Hattink, and Amílcar Labarta, "Quantitative x-ray photoelectron spectroscopy study of Al/AlOx bilayers" *Journal of Applied Physics* vol. 91, (June 15, 2002) pp. 10163-10168

ELNA CO., LTD. “Introduction to Aluminum Electrolytic Capacitors: How Capacitors Work” (ELNA CO., LTD., 2001-2007)

http://www.elna.co.jp/en/ct/c31_inde.htm

David Mitzi, “Solution-processed inorganic semiconductors” *Journal of Materials Chemistry* vol. 14, no. 15 (2004) pp. 2355-2365

Daniel Fine, Liang Wang, Deepak Sharma, Ananth Dodabalapur, “Planar nanoscale architecture for organic thin-film field-effect transistors” Applied Physics Letters vol. 89, article # 203118 (2006) pp. 1-3

David J. Gundlach, LiLi Jia, Thomas N. Jackson, “Pentacene TFT With Improved Linear Region Characteristics Using Chemically Modified Source and Drain Electrodes” *IEEE Electron Device Letters* vol. 22, no. 12 (December 2001) pp. 571-573

Liang Wang, Daniel Fine, Taeho Jung, Debarshi Basu, Heinz von Seggern, and Ananth Dodabalapur, “Pentacene field-effect transistors with sub-10-nm channel lengths” *Applied Physics Letters* vol. 85, no. 10 (September 6, 2004) pp. 1772-1774

D. Knipp, R. A. Street, A. Völkel, J. Ho, “Pentacene thin film transistors on inorganic dielectrics: Morphology, structural properties, and electronic transport” *Journal of Applied Physics* vol. 93, no. 1 (January 1, 2003) pp. 347-355

Anna B. Chwang, C. Daniel Frisbie, “Field Effect Transport Measurements on Single Grains of Sexithiophene: Role of the Contacts” *Journal of Physical Chemistry B* vol. 140 (2000) pp. 12202-12209

L. Bürgi, T. J. Richards, R. H. Friend, H. Friend, “Close look at charge carrier injection in polymer field-effect transistors” *Journal of Applied Physics* vol. 94, no. 9 (November 1, 2003) pp. 6129-6137

Yulong Shen, Ahmad R. Hosseini, Man Hoi Wong, George G. Malliaras, "How to Make Ohmic Contacts to Organic Semiconductors" *ChemPhysChem* vol. 5, (2004) pp. 16-25

F. Amy, C. Chan, A. Kahn, "Polarization at the gold/pentacene interface" *Organic Electronics* vol. 6 (2005) pp. 85-91

B. G. Streetman, Solid State Electronic Devices, 4th Edition, (prentice-Hall, Inc., 1995)

Peter Mark, Wolfgang Helfrich, "Space-Charge-Limited Currents in Organic Crystals" *Journal of Applied Physics* vol. 33, no. 1 (January, 1962) pp. 205-215

P. W. M. Blom, M. J. M. De Jong, J. J. M. Vleggaar, "Electron and hole transport in poly(*p*-phenylene vinylene) devices" *Applied Physics Letters* vol. 68, no. 23 (June 3, 1996) pp. 3308-3310

Josephine B, Lee, Paul C. Chang, Alexander Liddle, and Vivek Subramanian, "10-nm Channel Length Pentacene Transistors" *IEEE Transactions on Electron Devices*, vol. 52, no. 8 (August 2005) pp. 1874-1879

John H. Byrne, Stanley G. Schultz, An Introduction to Membrane Transport and Bioelectricity, 2nd Edition, (Raven Press, Ltd., 1994) pp. 1-112

Henk M. Keizer, Brian R. Dorvel, Martin Andersson, Daniel Fine, Rebecca B. Price, Joanna R. Long, Ananth Dodabalapur, Ingo Köper, Wolfgang Knoll, Peter A. V. Anderson, Randolph Duran, "Functional Ion Channels in Tethered Bilayer Membrane Arrays: Implications for Biosensors" *ChemPhysChem* (accepted)

B. A. Cornell, V. L. B. Braach-Maksvytis, L. G. King, P. D. J. Osman, B. Raguse, L. Wieczorek, R. J. Pace, "A biosensor that uses ion-channel switches" *Nature* vol. 387 (June 5, 1997) pp. 580-583

Hagan Bayley, Charles R. Martin, "Resistive-Pulse Sensing—From Microbes to Molecules" *Chemical Review* vol. 100 (2000) pp. 2575-2594

Gillian Woodhouse, Lionel King, Lech Wieczorek, Peter Osman, Bruce Cornell, "The ion channel switch biosensor" *Journal of Molecular Recognition* vol. 12 (1999) pp. 328-334

W. Knoll, C. W. Frank, C. Heibel, R. Naumann, A. Offenhäusser, J. Rühe, E. K. Schmidt, W. W. Shen, A. Sinner, "Functional tethered lipid bilayers" *Reviews in Molecular Biotechnology* vol. 74 (2000) pp. 137-158

Edward T Castellana, Paul S. Cremer, "Solid supported lipid bilayers: From biophysical studies to sensor design" *Surface Science Reports* vol. 61 (2006) pp. 429-444

Hiroaki Suzuki, Kazuhito V. Tabata, Hiroyuki Noji, Shji Takeuchi, "Highly Reproducible Method of Planar Lipid Bilayer Reconstitution in Polymethyl Methacrylate Microfluidic Chip" *Langmuir* vol. 22 (2006) pp. 1937-1942

Winfried Römer, Claudia Steinem, "Impedance Analysis and Single-Channel Recordings on Nano-Black Lipid Membranes Based on Porous Alumina" *Biophysical Journal* vol. 86 (February 2004) pp. 955-965

B. A. Cornell, G. Krishna, P. D. Osman, R. D. Pace, L. Wieczorek, "Tethered-bilayer lipid membranes as a support for membrane-active peptides" *Biochemical Society Transactions* vol. 29, part 4 (2001) pp. 613-617

Thierry Stora, Jeremy H. Lakey, Horst Vogel, "Ion-Channel Gating in Transmembrane Receptor Proteins: Functional Activity in Tethered Lipid Membranes" *Angewandte Chemie-International Edition* vol. 38, no. 3 (1999) pp. 389-392

Martin Andersson, Henk M. Keizer, Chenyu Zhu, Daniel Fine, Ananth Dodabalapur, Randolph S. Duran, "Detection of Single Ion Channel Activity on a Chip Using Tethered Bilayer Membranes" *Langmuir* vol. 23 (2007) pp. 2924-2927

Martin Andersson, George Okeyo, Danyell Wilson, Paul Moe, Paul Blount Daniel Fine Ananth Dodabalapur, Randolph S. Duran," Voltage Induced Gating of the Mechanosensitive MscL Ion Channel Reconstituted in a Tethered Lipid Bilayer Membrane" (submitted)

Carl R. Woese, George E. Fox, "Phylogenetic Structure of the Prokaryotic Domain: The Primary Kingdoms" *Proceedings of the National Academy of Sciences of the United States of America* vol. 74, no. 11 (November 1977) pp. 5088-5090

David L. Nelson, Michael M. Cox, Lehninger Principles of Biochemistry, 4th Edition, (W. H. Freeman and Company, 2005) pp. 4-5

Stefan M. Schiller, Renate Naumann, Katherine Lovejoy, Horst Kunz, Wolfgang Knoll, "Archaea Analogue Thiolipids for Tethered Bilayer Lipid Membranes on Ultrasmooth Gold Surfaces" *Angewandte Chemie-International Edition* vol. 42, no. 2 (2003) pp. 208-211

R. Naumann, E. K. Schmidt, A. Jonczyk, K. Fendler, B. Kadenbach, T. Liebermann, A. Offenhäusser, W. Knoll, "The peptide-tethered lipid membrane as a biomimetic system to incorporate cytochrome c oxidase in a functionally active form" *Biosensors & Bioelectronics* vol. 14 (1999) pp. 651-662

S. J. Opella, F. M. Marassi, J. J. Gesell, A. P. Valente, Y. Kim, M. Oblatt-Montal, M. Montal, "Structures of the M2 channel-lining segments from nicotinic acetylcholine and NMDA receptors by NMR spectroscopy" *Nature Structural Biology* vol. 6, no. 4 (April 1999) pp. 374-379

Declan A. Doyle, João Morais Cabral, Richard A. Pfuetzner, Anling Kuo, Jacqueline M. Gulbis, Steven L. Cohen, Brian T. Chait, Roderick MacKinnon, "The Structure of the Potassium Channel: Molecular Basis of K^+ Conduction and Selectivity" *Science* vol. 280 (April 3, 1998) pp. 69-77

Youxing Jiang, Alice Lee, Jiayun Chen, Martine Cadene, Brian T. Chait, Roderick MacKinnon, "Crystal structure and mechanism of a calcium-gated potassium channel" *Nature* vol. 417 (May 30, 2002) pp. 515-522

R. R. Ketchem, W. Hu, T. A. Cross, "High-Resolution Conformation of Gramicidin A in a Lipid Bilayer by Solid-State NMR" *Science* vol. 261 (September 10, 1993) pp. 1457-1460

Geoffrey Chang, Robert H. Spencer, Allen T. Lee, Margaret T. Barclay, Douglas C. Rees, "Structure of the MscL Homolog form *Mycobacterium tuberculosis*: A gated Mechanosensitive Ion Channel" *Science* vol. 282 (December 18, 1998) pp. 2220-2226

Natalia Levina, Sabine Totemeyer, Neil R. Stokes, Petra Louis, Michael A. Jones, Ian R. Booth, "Protection of *Escherichia coli* cells against extreme turgor by activation of MscS and MscL mechanosensitive channels: identification of genes required for MscS activity" *The European Molecular Biology Organization Journal* vol. 18, no. 7 (1999) pp. 1730-1737

Roberto Coronado, Ramon Latorre, "Phospholipid Bilayers Made from Monolayers on Patch-Clamp Pipettes" *Biophysics Journal* vol. 43, iss. 2 (1983) pp. 231-236

Shin-Ho Chung, Olaf S. Andersen, Vikram Krishnamurthy, Biological Membrane Ion Channels: Dynamics, Structure, and Applications, (Springer Science + Business Media, LLC, 2007) pp. 576-588

Bernardo Rudy, Linda E. Iverson, Methods in Enzymology: Volume 207: Ion Channels, (Academic Press, Inc., 1992) pp. 28-53

Scanning Electron Microscopy, Inc., Conference Proceedings, AMF O'Hare, IL (1980)

R. Lipowsky, E. Sackmann, Structure and Dynamics of Membranes: Generic and Specific Interactions, Volume 1B, (Elsevier Science B. V., 1995) pp.605-640

Tanner EDA and Customer Support, T-Spice™ User Guide and Reference, (Tanner Research, Inc., 1998)

W. Shockley, M. Sparks, G. K. Teal, "p-n Junction Transistors" *Physical Review* vol. 83, no. 1 (July 1, 1951)

Thomas Kind, Matthias Issing, Rüdiger Arnold, Bernt Müller, "Electrical Coupling of Single Cardiac Rat Myocytes to Filed-Effect and Bipolar Transistors" *IEEE Transactions on Biomedical Engineering* vol. 49, no. 12 (December 12, 2002) pp. 1600-1609

S. M. Sze, Kwok K. Ng, Physics of Semiconductor Devices, 3rd Edition, (John Wiley & Sons, Inc., 2007) pp. 243 - 288

Gerold W. Neudeck, Volume III: The Bipolar Junction Transistor, 2nd Edition: Modular Series on Solid State Devices, (Addision-Wesley Publishing Company, 1989)

Technology Modeling Associates, Medici: Two-Dimensional Simulation Program, Version 4.0: Users Manual, (Technology Modeling Associates, Inc., 1997)

Ben G. Streetman, Sanjay Banerjee, Solid State Electronic Devices, 5th Edition, (Prentice-Hall of India, Inc., 2004) pp. 17-25 and pp. 434-436

L. Li, H. Bender, T. Trenkler, P. W. Mertens, M. Meuris, W. Vandervorst, M. M. Heyns, "Surface passivation and microroughness of (100) silicon etched in aqueous hydrogen halide (HF, HCl, HBr, HI) solutions" *Journal of Applied Physics* vol. 77, no. 3 (February 1, 1995) pp. 1323-1325

David A. Hodges, "Darlington's Contributions to Transistor Circuit Design" *IEEE Transactions on Circuits and Systems—I: Fundamental Theory and Applications* vol. 46, no. 1 (January 1, 1999) pp.102-104

Elliott Philofsky, "Intermetallic formation in gold-aluminum systems" *Solid-State Electronics* vol. 13, iss. 10 (October 1970) pp. 1391-1394

http://www.femto.de/

Giuseppe Massobrio, Paolo Antognetti, Semiconductor Device Modeling with SPICE, 2nd Edition, (McGraw-Hill, Inc., 1993) pp. 299-305

Debarshi Basu, Ananth Dodabalapur (unpublished)

Vita

Daniel Hayes Fine was born in San Antonio, Texas, on March 18, 1978, the eldest of two children, a son and a daughter, to Ronald and Molly Fine. He attended high school at Thomas Jefferson High School for Science and Technology, graduating in 1996. He then matriculated at Cornell University where he earned a Bachelor's of Science in the field of electrical engineering. While there, he participated in several internships at Digital Equipment Corporation, which later was sold and became part of Compaq Computer Corporation, as a circuit designer and tester in a group working on the Alpha processor architecture. He entered the Graduate School at the University of Texas at Austin in the fall of 2000, completing his Masters of Science in Engineering in 2002. He then joined Professor Ananth Dodabalapur's organic semiconductor research group in the spring of 2002 to pursue his doctorate.

Permanent address: 8115-B Ceberry Drive,
Austin, Texas 78759

This dissertation was typed by the author.